2-26-2019

Evaluation of Unmanned Aircraft Flying Qualities Using a Stitched Learjet Model

Patrick M. Callaghan

Evaluation of Unmanned Aircraft Flying
Qualities Using a Stitched Learjet Model

THESIS

Patrick M. Callaghan, Captain, USAF

AFIT-ENY-MS-19-M-206

DEPARTMENT OF THE AIR FORCE
AIR UNIVERSITY

AIR FORCE INSTITUTE OF TECHNOLOGY

Wright-Patterson Air Force Base, Ohio

AFIT-ENY-MS-19-M-206

EVALUATION OF UNMANNED AIRCRAFT FLYING QUALITIES USING A STITCHED LEARJET MODEL

THESIS

Presented to the Faculty

Department of Aeronautical Engineering

Graduate School of Engineering and Management

Air Force Institute of Technology

Air University

Air Education and Training Command

in Partial Fulfillment of the Requirements for the

Degree of Master of Science in Aeronautical Engineering

Patrick M. Callaghan, B.S.A.E.

Captain, USAF

February 26, 2019

AFIT-ENY-MS-19-M-206

EVALUATION OF UNMANNED AIRCRAFT FLYING QUALITIES USING A

STITCHED LEARJET MODEL

THESIS

Patrick M. Callaghan, B.S.A.E.
Captain, USAF

Committee Membership:

D. L. Kunz, PhD
Chair

R. G. Cobb, PhD
Member

M. F. Reeder, PhD
Member

AFIT-ENY-MS-19-M-206

Abstract

In recent years, military UAVs have taken over missions that were too dull, dirty, or dangerous for manned aircraft. The increased demand has led to a build-fly-fix-fly development mentality, plaguing the early lifecycle with staggering mishap rates. Currently, MIL-STD-1797 lists flying qualities for UAVs as TBD, and the standards for manned fixed wing are inadequate when applied to UAVs. In an effort to expand the database of UAV flying qualities, an analysis was completed on a Simulink model of an LJ-25D developed from Calspans Variable Stability System aircraft at the United States Test Pilot School. Three maneuvers were simulated: (1) a non-precision, non-aggressive climbing spiral, (2) a precision, non-aggressive side step landing, and (3) a precision, non-aggressive aerial refueling task. These maneuvers were chosen to evaluate the performance and workload of the aircraft as four stability and control parameters were scaled. The data were utilized in identifying trends between the scaled stability and control parameters and resulting workload and performance metrics. Thumbprint plots were generated to identify Level 1, Level 2, and Level 3 flying qualities and compared to MIL-STD-1797 plots. Results point to utilizing a combination of classical aircraft literal factors, such as ζ_{sp} and CAP, with newly developed mathematical techniques, such as L_2 norm and TIC, to assess the workload of the flight controller and performance during the maneuver.

Table of Contents

List of Figures

viii

List of Tables

. List of Symbols

α angle of attack

β sideslip angle

δ_a aileron deflection

δ_e elevator deflection

δ_r rudder deflection

δ_t throttle position

θ pitch angle

ζ_d Dutch damping ratio

ζ_p phugoid damping ratio

ζ_{sp} short period damping ratio

τ pilot delay

ϕ roll angle

ψ yaw angle

ω_{BW} bandwidth

ω_d Dutch natural frequency

ω_p phugoid natural frequency

ω_{sp} short period natural frequency

h altitude

L_p Rolling moment due to roll

$L_{\delta a}$ Roll moment due to aileron deflection

M_q Pitching moment due to pitch

$M_{\delta e}$ Pitching moment due to elevator deflection

p roll rate

q pitch rate

r yaw rate

T_R roll mode time constant

T_S minimum doubling time for spiral mode

v_t true velocity

x state vector

$\dot{x}$ derivative state vector

. List of Acronyms

ADS Aeronautical Design Standard

CAP Control Anticipation Parameter

CG Center of Gravity

DoD Department of Defense

FAA Federal Aviation Administration

FC Flight Condition

FDM Flight Dynamics Model

FPM Foot per Minute

GUI Graphical User Interface

ISR Intelligence Surveillance Reconnaissance

HOS High-Order System

JSBSim Jon S. Berndt Simulation

kts Knots

KCAS Knots Calibrated Airspeed

KIAS Knots Indicated Airspeed

KTAS Knots True Airspeed

LHP Left Half Plane

LOES Low-Order Equivalent System

MATLAB Matrix Laboratory

MIL-STD Military Standard

MTE Mission Task Element

NACA National Advisory Committee on Aeronautics

NASA National Aeronautics and Space Administration

NRC National Research Council

PIO Pilot Induced Oscillation

PID Proportional Integral Derivative

ROC Rate of Climb

RHP Right Half Plane

RPV Remotely Piloted Vehicle

SIO System Induced Oscillation

TIC Theil's Inequality Coefficient

TPS Test Pilot School

UA Unmanned Aircraft

UAS Unmanned Aerial System

UAV Unmanned Aerial Vehicle

USAF United States Air Force

V/STOL Vertical and/or Short Takeoff and Landing

VISTA Variable In-flight Test Simulator

VSS Variable Stability System

EVALUATION OF UNMANNED AIRCRAFT FLYING QUALITIES USING A
STITCHED LEARJET MODEL

I. Introduction

As man entered into the world of flight, early aviation pioneers recognized the
importance of the interface between man and machine. Over decades, engineers and
aviators built and tested thousands of aircraft, steadily converging on the properties
of aircraft that improved mans control of the aerial machine. These properties, called
flying qualities, are defined by the United States Air Force (USAF) Test Pilot School
(TPS) handbook as "those stability and control characteristics which influence the
ease of safely flying an aircraft during steady and maneuvering flight in the execution
of the total mission" [4]. As technology advances, unmanned aerial vehicles (UAVs)
have become a commonplace in both the civilian and military world. Despite the
progress in both fixed wing and rotorcraft flying qualities over the past 100 years, UAV
flying qualities have remained largely unexplored. The technical specifications for
neither fixed wing nor rotorcraft make direct translations to adequate flying qualities
of an unmanned vehicle, and the current "build-fly-fix-fly" remains an inefficient and
mishap prone methodology. The focus of this research is to continue the advancement
of unmanned flying qualities by identifying key characteristics of UAVs that result in
satisfactory workload and performance for various mission task elements (MTE).

1.1 Background

After the 2011 raid on Osama Bin Laden's compound, a note was found in his
handwriting stating "Brothers said they were frankly exhausted from the enemies air

bombardments" [49]. The bombardments were due in part to the relentless use of UAVs in the fight against the Taliban. Their ability to stay aloft for 20+ hours at a time, out of reach of ground fire, provides the military with a unique asset in the war on terror. Maintaining a constant "eye in the sky," they also have been instrumental in reducing the number of fratricide events: "U.S. troops are three times safer from friendly fire attacks when deployed in war zones covered by drones compared with traditional warfare" [49]. As a result, the number of UAV missions has increased significantly and is projected to increase even further. Figure 1 shows the exponential increase of UAV missions conducted by the US government.
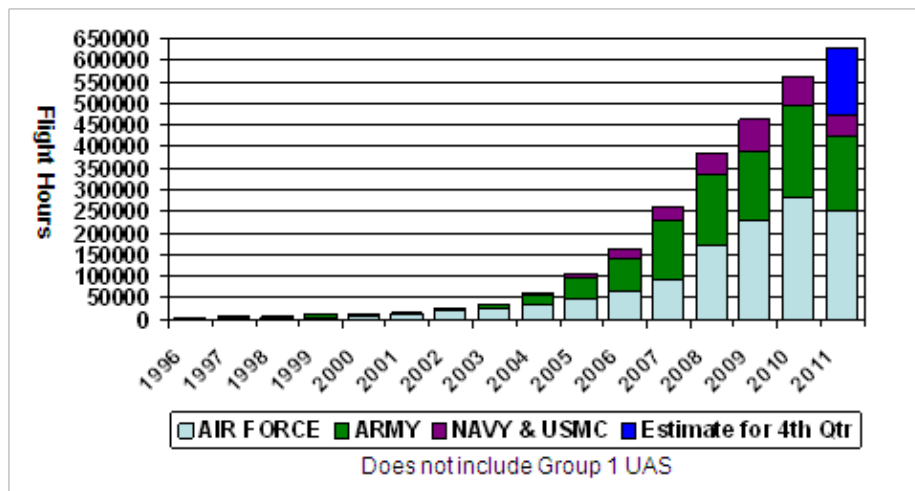
Figure 1. Flight Hours for Unmanned Systems between 1996 and 2011 [51]

Not only have drones been effective in saving soldiers on the battlefield, but they have also been used in the civilian world to save lives in several capacities. In 2017, DJI, a Chinese manufacturer of drones, reported that drones have saved at least 59 people since 2013. Drones have been used to find lost hikers in a snowy field, drop ropes and life vests to drowning swimmers, and find lost kayakers in remote areas [42]. Their small size and high maneuverability allows them to fly at low altitudes and in tight spaces where manned aircraft cannot operate. UAVs do not require the on board life support systems needed for manned flight. In turn, they weigh less,

allowing for a larger payload, and are smaller, making them cheaper. Thus, their lower costs make them less of a liability when an asset is lost.

In recent years, military UAVs have taken over missions that were too 'dull, dirty, or dangerous' for manned aircraft [24]. Although they have been effective at completing these missions, their mishap rates have been nearly 10-20 times as high as their manned counterparts have incurred [15]. Figure 2 shows the staggering rate of UAV mishaps over the lifecycle of each aircraft.
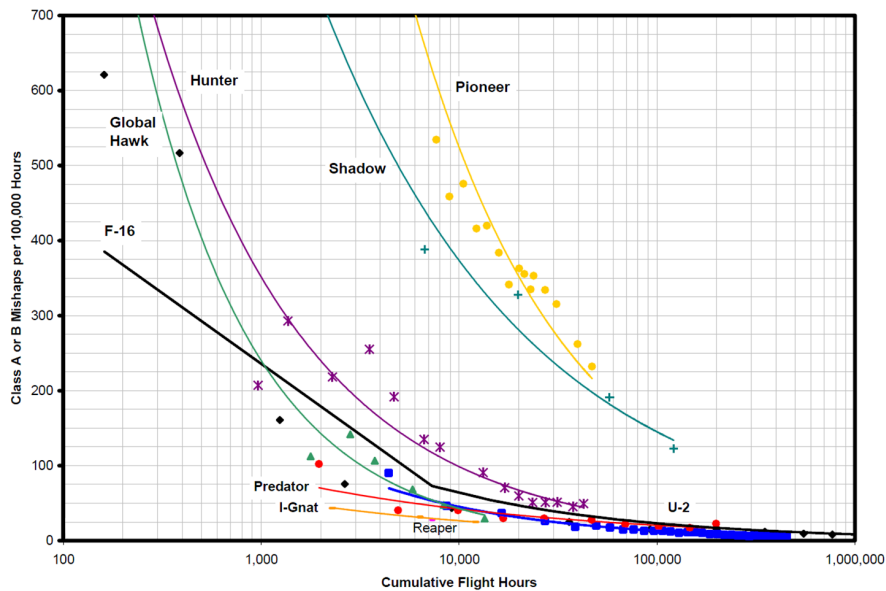
Figure 2. U.S. Military Aircraft and UAS Class A Mishap Rates, 1986-2006 [15]

The data shows that as flight hours accumulate, mishap rates decrease exponentially. But from the mishap data early in the development of the UAVs, it is clear a "build-fly-fix-fly" mentality drove the development of the Global Hawk, Hunter, Shadow, and Pioneer [24]. Instead of using a "hunt and peck" method of design, a database of UAV flying handling qualities design knowledge based on historical data could prevent some of the mishaps early in the lifecycle of a UAV. Lowering the mishap rate will decrease both the cost and risk of developing UAVs.

1.2 Research Problem Motivation and Description

As UAVs become commonplace in both military and civilian applications, an overarching governing document is required to ensure the airworthiness of each UAV. A piece of that qualification includes assessing the flying qualities of the aircraft. Cooper and Harper stated that flying qualities refer to "those qualities or characteristics of an aircraft that govern the ease and precision with which a pilot is able to perform the tasks required in support of an aircraft role" [16]. Several standards have been developed for military fixed-wing, military rotary-wing, and civilian aircraft, but none accurately classify the varying size and missions UAVs assume.

The Air Force's fixed-wing document governing flying and handling qualities is MIL-STD-1797. Its purpose is "to assure flying qualities for adequate mission performance and flight safety regardless of the design implementation or flight control system augmentation" [5]. Currently, no requirement has yet to be developed to fit UAVs into MIL-STD-1797, and the section for UAVs reads TBD. The current MIL-STD-1797 which governs the flying qualities of Air Force aircraft has four classes of aircraft based on maximum gross weight and maximum g-load [5]. Each of these categories corresponds to an aircraft type which also coincide with the mission set the aircraft accomplishing [5]. For example, an F-16 has high g-loading and a medium maximum takeoff weight, classifying it as a Class IV aircraft, typical of fighters. A C-17 with high gross and low g-loading would be a Class III aircraft, typical of heavy transport aircraft. But because fixed-wing UAVs can vary widely in weight and operating altitude yet accomplish the same intelligence, reconnaissance, and surveillance (ISR) mission, they do not easily fit into the existing manned fixed-wing categories in MIL-STD-1797. One UAV may operate in Class A airspace with a payload of over 3000 lbs, while another may operate below 1000 feet and weigh a mere 30 lbs. The two UAVs may have vastly different weights and operating altitudes, but have the

same maneuverability and accomplish the same mission.

ADS-33E addresses the flying qualities of rotary aircraft based on mission task performance. The goal of the document is to "assure that no limitations on flight safety or on the capability to perform intended missions will result from deficiencies in flying qualities" [19]. ADS-33E requires the aircraft fly various mission task elements representative of an operational flight envelope, while specifying varying performance standards that must be met. Certain performance standards are further broken down by aircraft primary mission to provide tighter tolerances for more maneuverable aircraft such as scout/attack and relaxed tolerances for less maneuverable aircraft such as cargo/utility and slung load. Because ADS-33E is focused solely on rotorcraft, its direct applicability to fixed-wing UAV flying qualities is minimal. But, the philosophy of utilizing mission task elements and maneuverability to evaluate flying qualities could prove useful in evaluating UAVs in both precision and non-precision maneuvers.

The Federal Aviation Administration (FAA) must also deem an aircraft airworthy, but their standards are less stringent than MIL-STD-1797. Their primary concern is safety and meeting certain standards in performance, structural design, and several other categories [22]. They ensure the safety of the passengers on board with little concern for the commercial success of an aircraft. On the other hand, the success of a military aircraft can be life or death on the battlefield, and therefore advanced flying qualities parameters are paramount in determining the effectiveness of an aircraft before it is built.

Despite the airworthiness requirements set by MIL-STD-1797, ADS-33E, and the FAA, UAV flying qualities still lack an overarching document that specifies the design principles necessary for satisfactory mission performance. The development of both fixed-wing and rotary-wing aircraft is aided through the use of a database of design knowledge compiled over decades of testing. Without a similar UAV design database

to build future UAVs, the Department of Defense (DoD) risks the success of a UAV program even before its inception.

By exploring new parameters based on workload and performance during mission oriented maneuvers, a knowledge base about what parameters correlate with certain flying handling qualities can be determined. These workload and performance values from known aircraft with satisfactory handling qualities, such as the LJ-25D, provides a basis for engineers to design future UAVs.

1.3 Research Objectives

The primary goal of this research is to further the database of available UAV handling qualities knowledge and provide new metrics to accurately correlate subjective flying qualities with UAV engineering design principles. To do this, a stitched model of the CALSPAN Variable Stability System (VSS) LJ-25D, shown in Figure 3, will be used to simulate various flight maneuvers and post process results from the simulation.

Figure 3. Learjet LJ25 Variable Stability System [8]

The stitched model refers to a "full flight-envelope, real-time simulation model composed of individual linear models and trim data for discrete flight conditions" [8]. It was developed at the Air Force Test Pilot School using flight data collected on the LJ-25D VSS. The model was built in Matrix Laboratory's (MATLAB) Simulink, a

proprietary, graphical block diagramming software effective for simulating complex dynamic systems [34]. The results of this research can be compared to data from future flight tests on the LJ-25D. This research builds upon the work of Lt Col. Kara Greene's *Toward a Flying Qualities Standard for Unmanned Aircraft* [24], Lt Joshua Kim's *Evaluation of Unmanned Aircraft Flying Qualities Using JSBSIM* [30], and Capt Ali Hamidani's *Evaluating the Autonomous Flying Qualities of a Simulated Variable Stability Aircraft* [26], with the following objectives:

1. Evaluate the flying qualities of an unmanned LJ-25D through various precision and non-precision maneuvers.

2. Identify trends between stability and control parameter scaling, workload and performance metrics, and classical control literal factors.

1.4 Thesis Overview

Chapter I described the background and motivation behind developing flying handling qualities metrics for UAVS. Chapter II, the literature review, includes a concise summary of the development of manned flying qualities and previous efforts on advancing unmanned aircraft (UA) flying qualities. Next, Chapter III, research methodology, is presented, which includes a detailed description of the LJ-25D stitched model and the performance metrics that will be calculated for the maneuvers. Chapter IV then presents the results of the research, including the evaluation of each maneuver using previously researched performance and workload metrics. Finally, Chapter V provides the conclusions of the research and future recommendations for research.

II. Literature Review

This chapter first provides an introduction to the history and development of modern day flying handling qualities metrics. Next, the flying qualities standards for manned fixed wing and manned rotary wing are explained. Finally, previous research accomplished in the area of UAV flying qualities is presented.

2.1   Early Development of Flying Qualities

Even before the Wright Brothers' first flight, an Englishman by the name of G.H. Bryan had developed the theoretical groundwork of stability [12]. Stability refers to the response of an aircraft in a trimmed state to a perturbation [13]. Bryan termed the initial response to a perturbation as the static response and the oscillatory response as the dynamic response. He correctly identified that aircraft of the time needed to be both statically and dynamically stable in the longitudinal axis and lateral-directional axis. He even identified the two primary modes of longitudinal oscillation: the phugoid mode and the short-period mode. His work continued to the lateral-directional modes, distinguishing the spiral mode, roll mode, and Dutch roll mode [40]. Although the calculations developed from Bryan's work were often too computationally intensive to be utilized by aircraft designers, Bryan had laid the theoretical foundation for future investigations in flying qualities.

Since the first Wright Flyer, a cornerstone of flight has been the interface between man and machine. On one of their first flights, Wilbur noted, "the machine seemed to steer all right laterally, but after attaining high speed began to undulate somewhat and suddenly turned downward" [35]. Although it is only a crude description of the phenomenon taking place, it is one of the first descriptions of "flying and handling qualities." The Wright Brothers continuously modified their designs, seeking one

that, in the pilot's opinion, met acceptable flying and handling characteristics. But only so much progress could be made with little understanding of aerodynamics and a lack of correlation between pilot opinion and engineering design.

As the Wright brothers continued to refine their design, the US Army Signal Corps took interest in new "heavier-than-air" flying machines. In 1907, they released a request for proposal for a heavier-than-air machine, along with a list of specifications. Although most specifications were performance related, buried within the request is the first US military flying qualities requirement. It read:

> Before acceptance, a trial endurance flight will be required of at least one hour during which time the flying machine must remain continuously in the air without landing. It shall return to the starting point and land without any damage that would prevent it immediately starting upon another flight. During this trial flight of one hour it must be steered in all directions without difficulty and at all times under perfect control and equilibrium.
>
> – Advertisement and Specification for a Heavier-than-Air Flying Machine, Signal Corps Specification No. 486, December 1907 [7]

Early aviators knew that if the machine was difficult to control in flight, it would be increasingly demanding or even impossible to accomplish the mission at hand. But simply stating "steered in all directions without difficulty" leaves the specification up for interpretation based on the pilot's opinion. A standardized system was needed for both the subjective flying qualities determined by the pilot's opinion and the objective qualities based on engineering theory.

As WWI broke out, trench warfare dominated the battlefield, and the airplane added another dimension. Although airplanes were still underdeveloped, their merits were undeniable. They were primarily used in the form of reconnaissance for artillery strikes and aerial photography [48]. Soon after, both the fighter airplane and the bomber airplane were developed. Clearly, the unnamed British general who had

9

stated "the airplane is useless for the purposes of war" [48] had been proven wrong by the rapid advancement in technology.

Across the Atlantic Ocean, the United States established National Advisory Committee for Aeronautics (NACA) in 1915, with goal of advancement in aeronautics [46]. NACA made its home at Langley Field, Virginia, and by 1922, flight test research had begun on several aircraft from both U.S. and foreign services. The dozen man team was initially tasked to "supervise and direct the scientific study of the problem of flight, with a view to their practical solution, and to determine the problems which should be experimentally attacked" [10]. The Navy Bureau of Aeronautics contacted NACA to utilize these aircraft in studying the design features that correlated to stability, controllability, and maneuverability. The research first focused on obtaining accurate data to understand stall characteristics, takeoff speeds, and landing speeds. Down the road, NACA began developing instrumentation needed to measure data in flight, which enabled the study of pressure distributions along wings. With this new instrumentation, a series of flight tests which previously lasted months could be shortened to a single day [10]. The pressure data allowed aircraft design parameters to be correlated to stability and control characteristics.

In the 1930s, commercial aviation became a profitable venture due to the increased size and performance of aircraft. In the commercial world, a new emphasis was put on safety and operational efficiency. Edward Warner, both the chief scientist for NACA and a consultant for the Douglas Aircraft Company with a vested interest in the success of the new DC-4, convinced NACA to investigate flying qualities in an attempt to find those qualities desired by pilots [10]. Warner tasked Hartley Soulè to conduct a study on writing a set of requirements which resulted in satisfactory flying qualities [40].

As a result, a report titled *Preliminary Investigation of the Flying Qualities of*

Figure 4. The Stinson Reliant played an important role in developing early flying qualities metrics [1]

Airplanes suggested further refinement of flying qualities requirements and recommended further testing on assorted aircraft [44]. Flying a Stinson Reliant aircraft similar to Figure 4, the test team made measurable control inputs which were then correlated to aircraft design specifications. Tests continued on a total of 12 aircraft, creating a small design database focused on flying qualities for aircraft of various sizes [10]. The data was used to forge crude numeric formulas to be used as rules of thumb for future designs. The database benefited aircraft designers through the 1940s, especially in the development of combat aircraft [10].

In the 1950s, aircraft had become bigger, faster, and more maneuverable than ever before. Designers also became more experimental, creating variable stability aircraft to vary aircraft parameters via an in flight control system. The first of these aircraft was the NT-33A, pictured in Figure 5. The NT-33A was programmed to create the feel of an aircraft with different flying qualities characteristics than its own

[6]. As a result, further research could be done in determining what aircraft design characteristics resulted in satisfactory flying qualities without having to physically design and build the geometry's of an aircraft with those characteristics.

Figure 5. The NT-33A aided in the development of the X-15, A-10, F-15, F-16, F-18, F-117, and F-22 [6]

The NT-33A provided the Air Force with nearly 40 years of service and was instrumental in developing the flying qualities standards used today [6]. Far before the end of its service life, it was clear that a replacement was needed to continue research and development via variable stability aircraft [14]. The solution was to modify an F-16D to create the NF-16D Variable Stability In-flight Test Simulator (VISTA), shown in Figure 6. The first major project that employed the NF-16D was to demonstrate the effectiveness of thrust vectoring on the F-16's maneuverability in flight [33]. At the conclusion of the program, the aircraft was refitted to the original VISTA configuration and assigned to the United States Test Pilot School where it is operated today [33].

Over time, aircraft designers refined their skills and created higher performance

Figure 6. The F-16 VISTA [36]

planes with improved flying qualities. New rotating wing aircraft called helicopters drove the separation of flying qualities standards for fixed wing and rotary-wing aircraft. These standards will be discussed separately in the subsections 2.2 and 2.3.

2.2 Manned Fixed-Wing Flying Qualities

By 1969, a standalone document titled *Flying Qualities of Piloted Airplanes* represented the Army, Air Force, and Navy's requirements for fixed wing aircraft. Also termed MIL-F-8785(ASG), the goal of the military specification was to "assure flying qualities that provide adequate mission performance and flight safety regardless of design implementation or flight control system mechanization" [3]. Within the specification, aircraft were further broken down into classes based on weight and maneuverability and were assessed in three different flight phases, termed categories, based on aircraft mission. This allowed designers to access aircraft design parameters for aircraft of varying sizes and mission sets [3]. MIL-F-8785B was further revised to MIL-F-8785C in 1980 and although MIL-F-8785C is now obsolete, it set the stage for MIL-STD-1797B, today's gold standard in flying qualities specifications.

MIL-STD-1797 was first published 31 March 1987 for use in developing USAF

aircraft [5]. MIL-STD-1797 and its subsequent versions added to MIL-F-8785C by incorporating more design criteria from research conducted in the 1970s and 1980s [37]. MIL-STD-1797 also added in subjective criteria based on Cooper-Harper ratings, which was not included in MIL-F-8785C. The current version, MIL-STD-1797B, was published in 2006 and continues to be used for assessing fixed wing flying qualities standards. The subsequent subsections discuss the various subjective and objective criteria of MIL-STD-1797B used to assess fixed wing aircraft.

2.2.1 Subjective Criteria.

In the 1960s, pilot rating scales became a prominent technique to assess the handling qualities of aircraft. These scales provided pilots and engineers a method to assess vehicle performance and pilot workload in the completion of specific mission tasks [16]. But without a single standardized scale to be used across airframes and test programs, the job of comparing pilot ratings from one aircraft to another became increasingly difficult. In 1969, George Cooper and Robert Harper published a paper titled *The Use of Pilot Rating in the Evaluation of Aircraft Handling Qualities* which sought to standardize the pilot rating scale not only across the US armed services, but also the world [16].

2.2.1.1 Cooper-Harper Rating Scale.

The resulting Cooper-Harper Pilot Rating Scale, shown in Figure 7, utilizes a decision tree to guide the pilot to a numbered rating based on the demands of the pilot in the selected task or required operation. The scale ranges ten values with the worst rating being a 10 and the best being a 1. The decision tree is a series of three questions asking:

1. Is the vehicle controllable?

2. Is adequate performance attainable with a tolerable pilot workload?

3. Is it satisfactory without improvement?
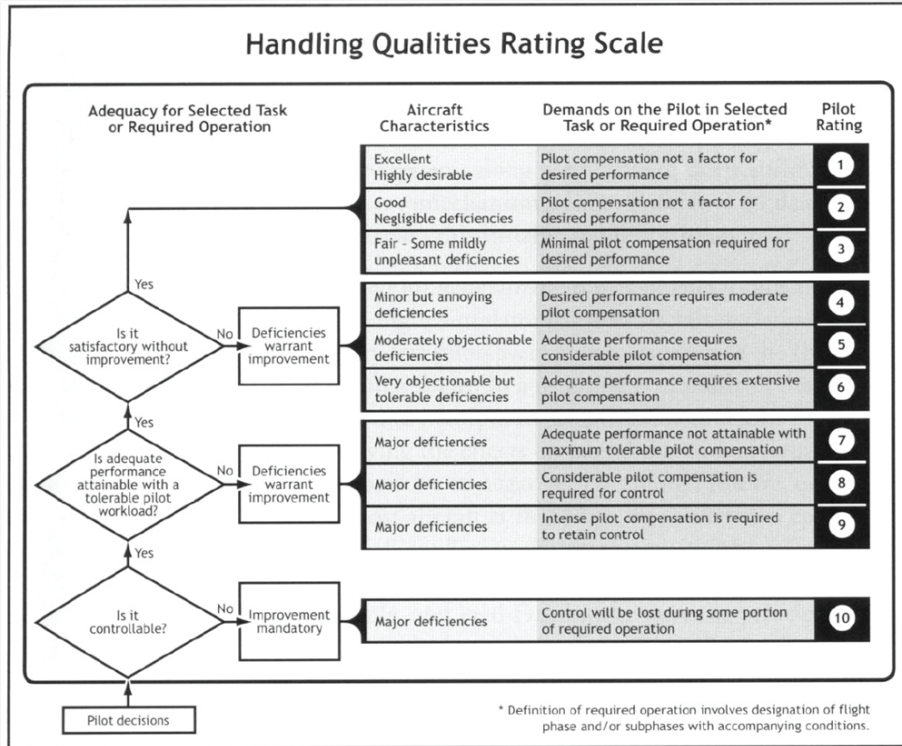
Figure 7. Cooper-Harper Pilot Rating Scale [5]

The Cooper-Harper rating scale utilizes these questions to guide the pilot to an objective handling qualities rating between 1 and 10 to the aircraft. A Cooper-Harper rating between 1 and 3 indicates Level 1 flying qualities, termed satisfactory. A rating between 4 and 6 indicates Level 2 flying qualities, termed acceptable. Finally, a rating between 7 and 9 indicates Level 3 flying qualities, termed controllable [5].

The rating scale can be used in a wide variety of operational tasks, such as takeoff, landing, and in-flight refueling. The scale seeks to identify when the pilot workload is excessive and his mission performance begins to degrade. As Cooper and Harper state in their paper, "In a specific task, he is capable of attaining essentially the same performance for a wide range of vehicle characteristics, at the expense of significant

15

reductions in his capacity to assume other duties and to plan subsequent operations"
[16]. In this particular instance, Cooper and Harper observed that the test pilots could maintain the same performance in poorer handling qualities vehicles, but at the expense of accomplishing basic mission tasks.

The evaluation thus seeks to assess the pilot-vehicle operation in the accomplishment of the mission. If pilot workload is excessive in accomplishing the mission task, then he will rate it poorly on the scale. Conversely, if the mission task was less difficult to accomplish and the pilot maintained his capacity to complete operational tasks, he will rate it highly on the scale.

The Cooper-Harper rating scale has become the standard in the assessment of fixed wing aircraft. Because the scale is dichotomous, it lends itself to repeatability by guiding the pilot in evaluations via a series questions regarding performance and workload [27]. It is also included in MIL-STD-1797, which states, "we use it as the principal way to relate flying qualities requirements to operational needs" [5]. Down the road, the rating scale would be modified for rotary aircraft and even a UAV derivative of the scale was created, which will be presented later in Section 2.5 of this chapter.

2.2.2 Objective Criteria.

As flying qualities research advanced via programs such as the NT-33A and NF-16D, large databases of pilot ratings and subsequent aircraft parameters were amassed. Engineers worked to create thumbprint plots, such as the one in Figure 8, to correlate pilot ratings on the Cooper-Harper scale to objective aircraft parameters. Aircraft design parameters such as the short-period natural frequency times the pitch rate transfer function zero associated with the short-period mode, $\omega_{sp}T_{\theta_2}$, and the equivalent short-period damping ratio, ζ_{sp}, are good indicators of fixed wing aircraft

mission performance in the longitudinal axis [45].

The short-period mode is dominates a pilot's opinion of longitudinal flying qualities. The magnitude of short-period damping is ζ_{sp}, which is representative of how much the short-period mode oscillation is damped. A low ζ_{sp} will cause the aircraft to be too sensitive and difficult to control in higher precision and aggression tasks. A high ζ_{sp} will be too sluggish and again difficult to control in certain tasks. During early research to develop plots such as Figure 8, a 'sweet spot' was determined to be around a ζ_{sp} of 0.7 [45], which correlated to good pilot opinion of the aircraft. $\omega_{sp}T_{\theta_2}$ was chosen to be used in several MIL-STD-1797 flying qualities graphs due to its correlation to n_α, the aircraft load factor response to angle of attack [45]. Once again, an optimum value was determined for $\omega_{sp}T_{\theta_2}$ from flight test, around 2.25, which correlated to good pilot opinion.

With a large sample sizes of data, engineers were able to draw lines around the areas where pilots reported satisfactory, adequate, and controllable flying qualities. The areas were then deemed Level 1, Level 2, and Level 3 flying qualities, respectively, producing a "thumbprint" outline for varying design values. Without building aircraft, manned fixed wing designers can predict aircraft flying qualities based on objective aircraft designer parameters.

2.2.2.1 Literal Factors.

From the correlation of large sample sizes of data to Cooper-Harper ratings came several literal factors which predict aircraft flying qualities. From these correlations, engineers were able to produce thumb print charts bounding Level 1, Level 2, and Level 3 flying qualities ratings. One of the most important literal factors is the Control Anticipation Parameter (CAP). CAP is the ratio of the instantaneous pitch acceleration, $\dot{q}_0$, to the change in steady-state load factor, Δn_{ss} [27].
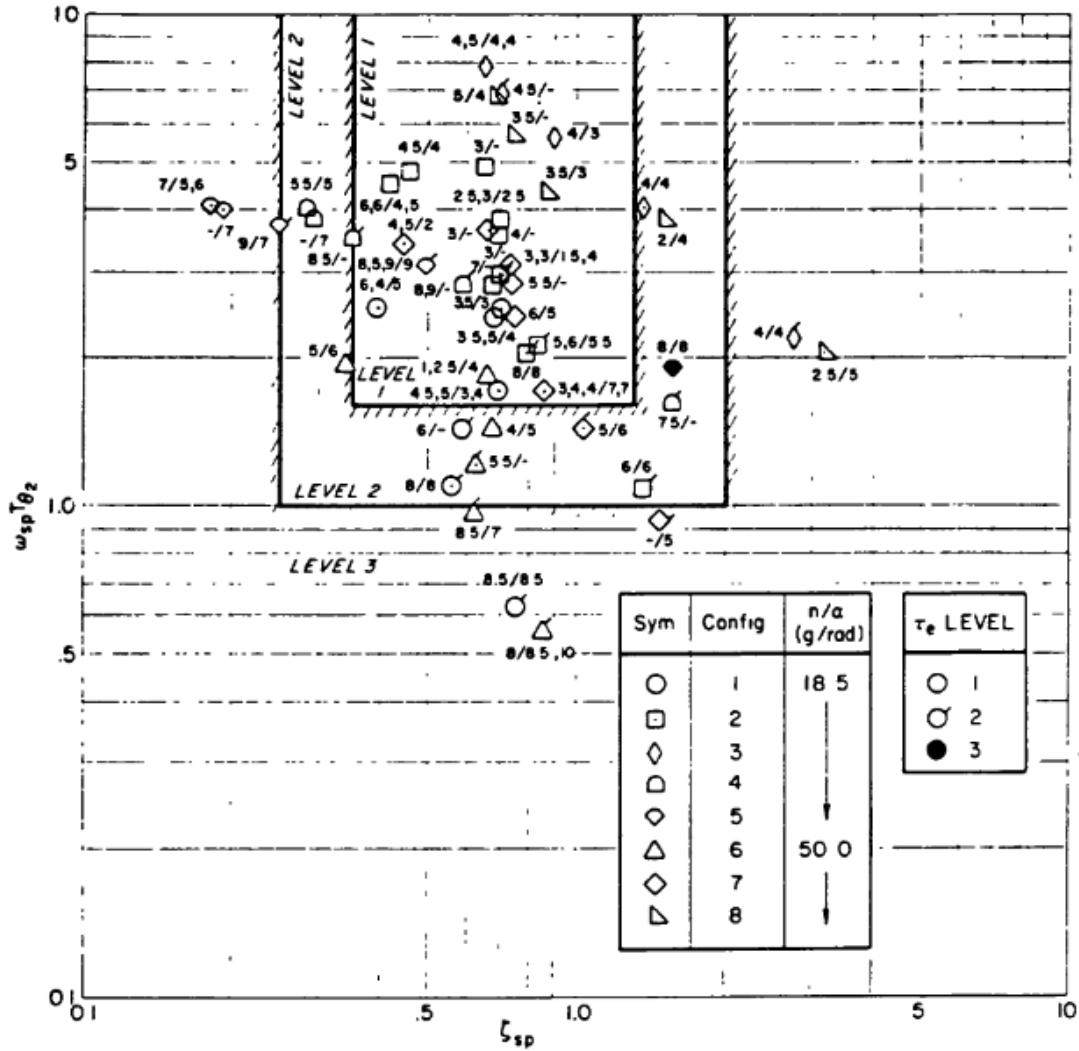
Figure 8. $\omega_{sp}T_{\theta_2}$ vs ζ_{sp} **plot depicting how Cooper-Harper ratings drove objective criteria** [**5**]

CAP is a literal factor that describes the pilot's perception threshold of angular pitching acceleration which accompanies any minor changes to the aircraft's flight path [9]. The control anticipation parameter correlates well with pilot opinion because aircraft that are deemed difficult to control often require either too much precise path adjustment and are considered "sensitive," or not enough precise path adjustment and are considered "sluggish." Figure 9 from MIL-STD-1797B depicts how CAP and short-period damping are used to set Level 1, Level 2, and Level 3 boundaries on

18

short-period dynamic requirements.
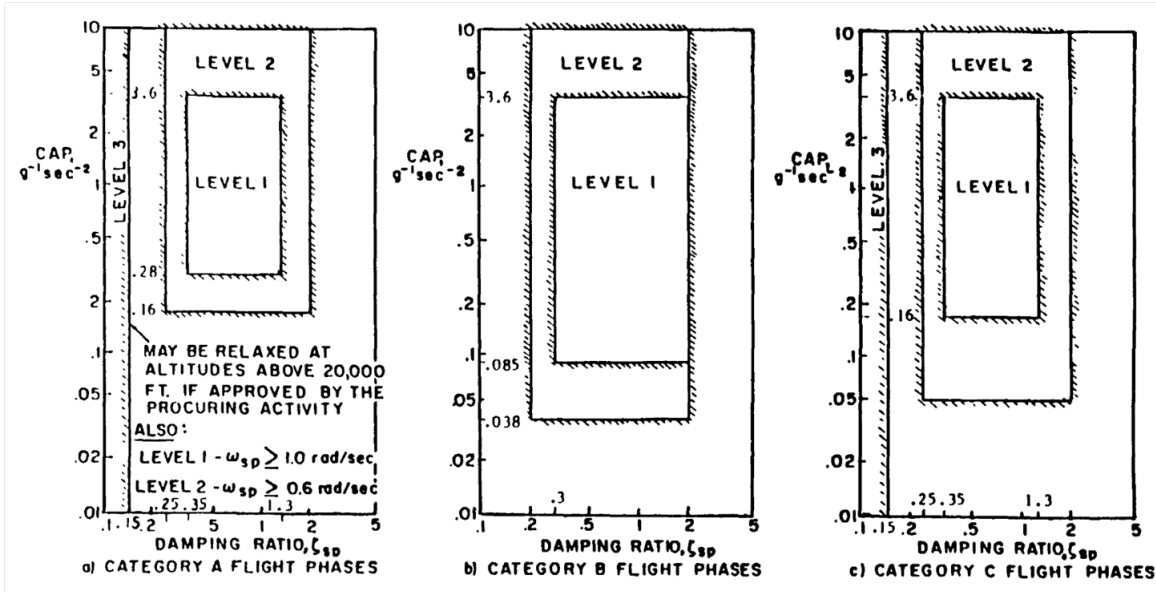
Figure 9. Short-period Dynamic Requirements [5]

It should be noted that this definition of CAP was developed from data on classical aircraft without highly augmented control systems [11]. Further research has since been conducted by Bischoff in his report, *The Control Anticipation Parameter for Augmented Aircraft*, to create a modified CAP that more accurately represents the higher-order dynamics of augmented aircraft [11].

Another literal factor that accurately predicts longitudinal flying qualities is $\omega_{sp}T_{\theta 2}$. In addition to being related to n_{α}, $\omega_{sp}T_{\theta 2}$ is also representative of the time response between aircraft pitch attitude and flight path [5]. As a result, $\omega_{sp}T_{\theta 2}$ is proportional to CAP and can be used in creating thumbprint plots describing the short-period pitch response. Figure 9 and Figure 10 show similar shaped outlines as ζ_{sp} is varied with changing CAP and $\omega_{sp}T_{\theta 2}$, respectively.

In addition to frequency domain analysis of literal factors, a time domain analysis of literal factors also correlates to pilot ratings. By working directly from the pitch rate response of the aircraft, aircraft designers can create satisfactory systems without

19
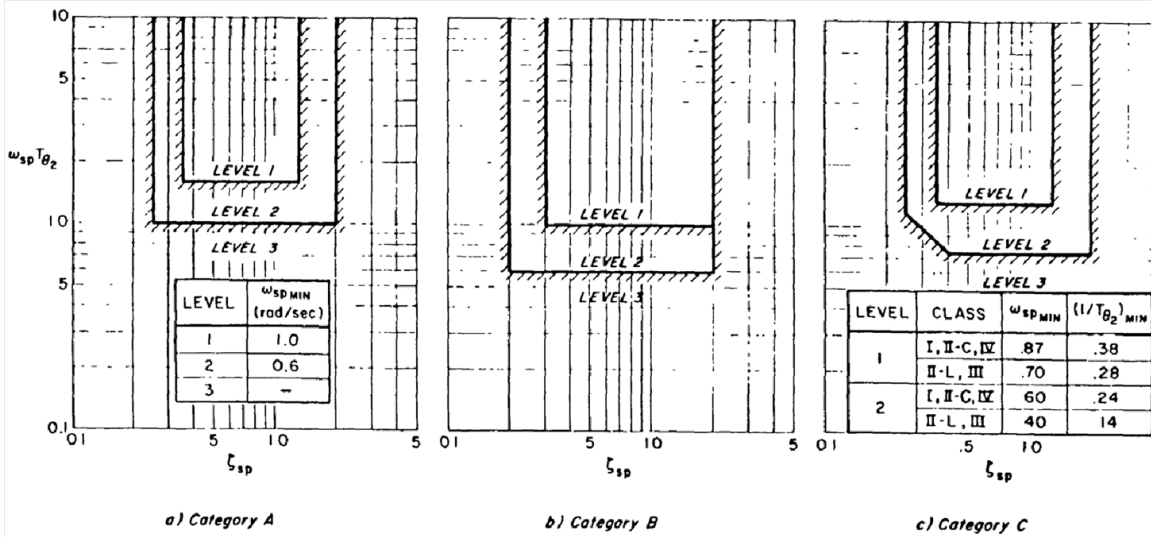
Figure 10. Short-period Pitch Response to Pitch Controller [5]

direct designation of dominant system poles and zeros [5]. Figure 11 shows the pitch rate response of an aircraft to a pilot step input.
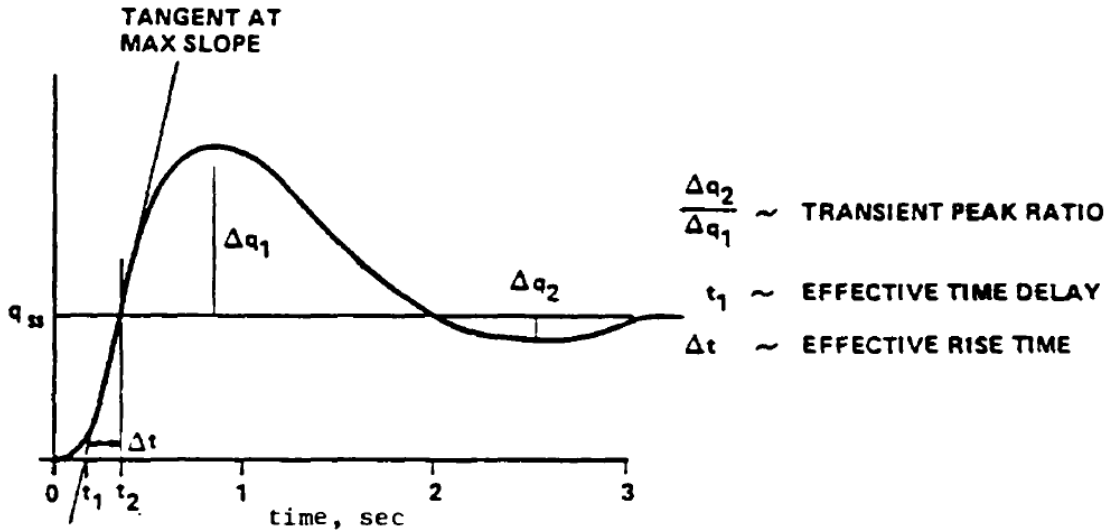
Figure 11. Time Domain Transient Response Parameters [5]

Several aircraft performance specifications arose from these transient literal factors to aid in identifying Level 1, 2, or 3 aircraft. Equivalent time delay (t_1) requirements, the analog to τ_θ in the frequency domain, are specified in Table 1. Transient peak ratio ($\frac{\Delta q_2}{\Delta q_1}$) requirements, correspondent to short-period damping factor in the frequency

20

domain, are listed in Table 1 as well. Finally, effective rise time requirements, which are analogous to CAP in the frequency domain, are spelled out in Table 2.

Table 1. Equivalent Time Delay and Transient Peak Ratio Requirements[5]

Level	Equivalent Time Delay t_1	Transient Peak Ratio $\frac{\Delta q_2}{\Delta q_1}$
1	$t_1 \leq .12$ sec	$\frac{\Delta q_2}{\Delta q_1} \leq .30$
2	$t_1 \leq .17$ sec	$\frac{\Delta q_2}{\Delta q_1} \leq .60$
3	$t_1 \leq .21$ sec	$\frac{\Delta q_2}{\Delta q_1} \leq .85$

Table 2. Rise Time Values[5]

	Non-terminal Flight Phases		Terminal Flight Phases	
Level	Min Δt	Max Δt	Min Δt	Max Δt
1	$9/V_t$	$500/V_t$	$9/V_t$	$200/V_t$
2	$3.2/V_t$	$1600/V_t$	$3.2/V_t$	$645/V_t$

2.2.2.2 Classification Category.

Several mission sets exist within manned fixed-wing aircraft which require vastly different aircraft to accomplish them. In turn, pilots have different desired flying qualities based on the mission set of the aircraft. For example, a cargo aircraft would be ill suited for carrying sensitive payloads if it were highly maneuverable, while a fighter would be a poor dogfighting aircraft if it had sluggish maneuverability. MIL-STD-1797B incorporated a classification category to aid in designing an aircraft tailored to a specific mission set. The document breaks down aircraft into four primary Classes: Class I is small light aircraft, Class II is medium weight with low to medium maneuverability, Class III is heavy, low maneuverability, and Class IV is high maneuverability [5]. Table 3 shows the full aircraft classification guide from MIL-STD-1797B.

Aircraft were separated into classes by using two primary design factors: maximum g-load (n) and gross weight [5]. G-load separates high and low maneuverability

Class I – Small light aircraft such as:	Light utility Primary trainer Light observation
Class II – Medium weight, low-to-medium maneuverability aircraft such as:	Heavy utility/search and rescue Light or medium transport/cargo/tanker Early warning/electronic countermeasures/airborne command,control, or communications relay Antisubmarine Assault transport Reconnaissance Tactical bomber Heavy attack Trainer for Class II
Class III – Large, heavy, low-to-medium maneuverability aircraft such as:	Heavy transport/cargo/tanker Heavy bomber Patrol/early warning/electronic countermeasures/airborne command, control, or communications relay Trainer for Class III
Class IV – High-maneuverability aircraft such as:	Fighter-interceptor Attack Tactical reconnaissance Observation Trainer for Class IV

Table 3. Aircraft Classification in MIL-STD-1797B [5]

aircraft, while maximum gross weight primarily isolates the heavier transport aircraft from all others. Plotting maximum g-load vs. gross weight yields Figure 12. Once again based on historical data of past aircraft, lines are drawn to aid in delineating one class from another, although exceptions may exist [5]. MIL-STD-1797B incorporates these class categories by relaxing or tightening certain aircraft performance parameters based on aircraft class.

2.2.2.3 Modified Neal-Smith Criteria.

The Modified Neal-Smith Criteria, often referred to as the Neal-Smith criteria, is a design method that utilizes a specified pilot model in a pilot-aircraft pitch attitude control system with unity feedback [5]. With this model, varying adjustments can be made to pilot delay, pilot gain, and develop lead or lag compensation [5]. The open-loop response of the system is plotted on a Nichols Chart, where the closed-loop dynamics can be ascertained. The closed-loop droop bounds the minimum gain while the closed-loop resonance sets the maximum allowable pilot gain to meet certain
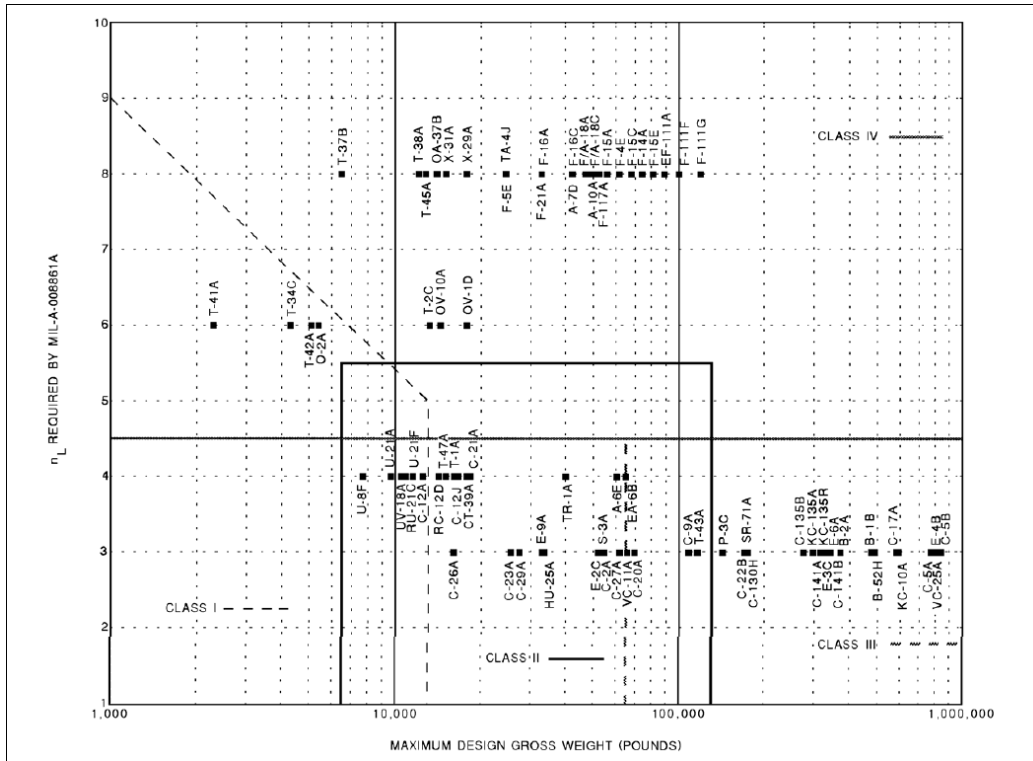
Figure 12. Aircraft Classification in MIL-STD-1797B [5]

flying qualities levels. Figure 13 pictures a sample Nichols chart for determining pilot-in-the-loop pitch dynamics.

The overarching usefulness of the Neal-Smith Criteria is in determining the bandwidth of the closed-loop systems with the pilot in the loop. From where the open-loop plot intersects the closed-loop phase of -90 degrees is the bandwidth. Table 4 depicts the minimum bandwidth required by the Neal-Smith Criteria for various categories of flight.

Table 4. Neal-Smith Criteria for Bandwidth [5]

Flight Phase	Bandwidth
Category A	3.5 rad/s
Category B	1.5 rad/s
Landing	2.5 rad/s
Other Category C	1.5 rad/s
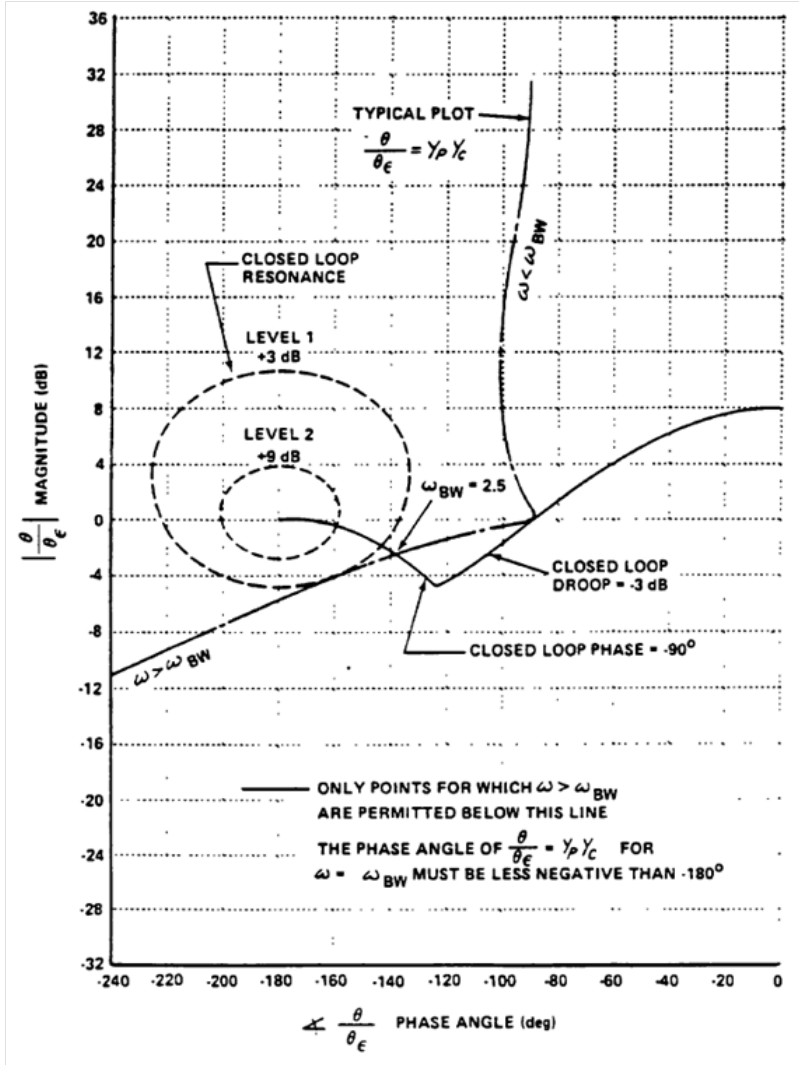
Figure 13. Modified Neal-Smith Design Criteria for Pitch Dynamics [5]

2.3 Manned Rotary-Wing Standards

Fixed-wing flying qualities were much further developed by the 1950s as opposed to rotary-wing flying qualities. As a result, MIL-F-83300, titled *Flying Qualities of Piloted V/STOL Aircraft*, was not released until December of 1970 [2]. One of the primary goals of MIL-F-83300 was for the development of V/STOL (Vertical and/or Short Takeoff and Landing) flying qualities criteria via first developing techniques to analyze and evaluate V/STOL flying qualities and second generate flying quali-

ties requirements and design criteria [29]. The program utilized the XV-4B variable stability test vehicle to develop baseline flying qualities data [29], much in the way the NT-33 was utilized in fixed-wing flying qualities. Part of the research program included in-depth reviews of draft specifications by 10+ industry entities and several government entities across the Air Force, Army and Navy [29]. Despite the work towards improving design requirements, helicopter mission performance continued to lack [23].

In the mid 1980s, Aeronautical Design Standard (ADS) 33 replaced the previous flying qualities documents governing vertical lift aircraft. ADS-33 sought to focus on the mission of the aircraft, and therefore separated aircraft into four primary missions categories regardless of weight: attack, scout, utility, and cargo. During evaluation, aircraft complete certain MTEs representative of the operational mission [19]. Examples of MTEs are takeoff, lateral reposition, and side step; each MTE has criteria to meet desired performance and adequate performance [19]. The advantage to this standard is the performance criterion for each MTE can be based on both aircraft precision and quickness without reference aircraft gross weight [23]. In other words, ADS-33 assesses MTE and operational environment to determine the class to evaluate the rotorcraft [23]. ADS-33 went through several revisions until becoming ADS-33E in 2000 and remains the standard for rotary-wing aircraft flying qualities today.

2.4 Unmanned Aerial Vehicle Standards

Air Force Maj. Gen. David Baker stated in 1956 that "We can readily see that except for certain types of missions, the manned combat aircraft will become technically obsolete in the future" [21]. In the 1960s, the mission of unmanned aerial vehicles had expanded from primarily being expendable target drones to carrying

surveillance equipment and completing aerial reconnaissance missions [21]. The intelligence community quickly identified unmanned drones as an asset to be utilized in gathering critical information over hostile territory without risking American lives. Still, no design criterion existed to assess the flying qualities and its effects on mission performance.

In 1976, AFFDL-TR-76-125, *Remotely Piloted Vehicle Flying Qualities Design Criteria*, became the first attempt at creating flying qualities standards for unmanned vehicles [25]. The report was the second part of a four part program for developing a remotely piloted vehicle (RPV) flying qualities specification [41]. The document takes a top down approach in developing requirements: "performance-oriented criteria are developed in hierarchical fashion from mission requirements, through total system requirements, to subsystem requirements. The criteria encompass automatic and manual controls, command and data link, controls and displays as well as vehicle stability and control" [41]. The final goal of phase II was to develop flying qualities requirements that could later be validated by simulation and analysis [30]. As the final phases were never completed, the document stands as a technical report, not a mandatory standard.

The primary issue in applying AFFDL-TR-76-125 to modern aircraft lies in the document's definition of RPV: "unmanned air vehicle which has the capability of being controlled by a remote operator during some flight phase of an operational mission" [41]. AFFDL-TR-76-125 was developed at a time when completion of the RPV mission relied on human interaction with the system. Today, UAVs are expected to achieve satisfactory mission performance without the intervention of human operators, thus reducing the skill requirements of operators and increase system reliability [50]. Since AFFDL-TR-76-125 was published in 1976, it has yet to be updated in any form to reflect the shift of focus in requirement development from pilot-aircraft

interface to full aircraft autonomy.

One of the challenges still being addressed by UAV researchers is the classification of UAVs [30]. AFFDL-TR-76-125 utilized the four class criteria from MIL-F-8785C based on gross weight and maneuverability. That criterion works well with manned fixed-wing aircraft and is used in MIL-STD-1797B, but fails in accurately describing the mission and performance for UAVs. Flying qualities design challenges vary greatly depending on the size of the UAV; a small disturbance to a 5000 lb UAV is a large disturbance to a 20 lb UAV. The longitudinal, lateral, and directional sensitivities associated with the controls also vary depending on the size of a UAV [50], and therefore the relationships between small and large UAVs cannot be assumed to be linear. Williams also alludes to the lack of pilot comments, writing, "the challenges relate to the absence of control stick force feedback, an absence of vibration and buffet response" [50]. The challenges faced in developing UAV flying qualities have led to the lack of a leading standard in the UAV community [23].

In addition to the military extensively researching flying qualities, National Air and Space Administration's (NASA) had continued the flying qualities work that NACA had pioneered in the 1920s. A 2004 study conducted by the National Research Council (NRC) assessed the overall scientific and technical quality of NASA's Pioneering Revolutionary Technology Program [38]. In evaluation of NASA's UAV research, the NRC highlighted that the existing flying quality standards utilized for manned aircraft may be too restrictive in development of UAVs, and "further evolution of the base work done by NASA to include unmanned systems is essential to creating a competitive advantage for U.S. products as this market becomes more price-driven" [38]. The NRC identified the vested interest for not only the military but the civilian sector in the development of a flying qualities standard for UAVs.

2.5   Previous UAV Flying Qualities Research

One of the overarching issues with developing an unmanned flying qualities standard is determining how to classify the aircraft. AFFDL-TR-76-125 used the maneuverability and gross weight metrics from manned aircraft to classify RPVs, as those frequently aligned with the general mission of the manned aircraft. This scale fails when applied to UAVs because recent advances in technology allow an ultra-light, highly maneuverable quad-copter to accomplish the same reconnaissance mission as a heavy, sluggish *Predator* drone.

Recently, several researchers have devised new UAV specific classes which seek to resolve the dilemma. For example, Williams classified UAVs via control system and reuseability. Figure 14 pictures how Williams utilizes autonomy to separate RPVs from UAVs and reusablility to exclude single mission UAVs such as missiles and target drones from multi-mission UAVs such as *Predator*, *Global Hawk*, and *Pioneer* [50].
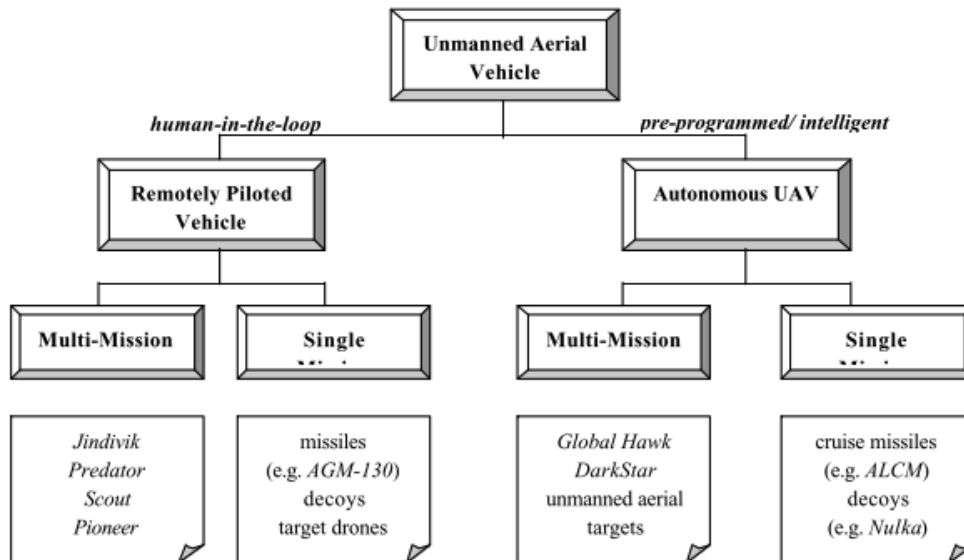

Figure 14. Williams's UAV Class System [50]

Cotting proposed an alternate class system for UAVs shown in Figure 15, based on Reynolds Number and aircraft weight [17]. With this scale, lighter, slower UAVs

which operate at lower Reynolds Numbers are classed together, just as heavier, faster UAVs at higher Reynolds Numbers are grouped. The Unmanned Systems Integrated Roadmap: FY 2011-2036 offered a UAV class system based off operational altitude, weight, and airspeed. Figure 16 shows the five classes of UAVs: penetrating, persistent, tactical, small tactical, and micro/mini tactical. Despite these innovative class alternatives to maneuverability and gross weight, Greene points out that basing UAV classes on physical and performance metrics of the UAV may be flawed all together: "the correlation between class and mission tends to break down for unmanned aircraft, because unmanned aircraft of very different sizes often perform the same missions" [23]. But, without sufficient UAV flying qualities research or a database of flight test data, an alternative mission-based classification approach cannot be validated either [23].
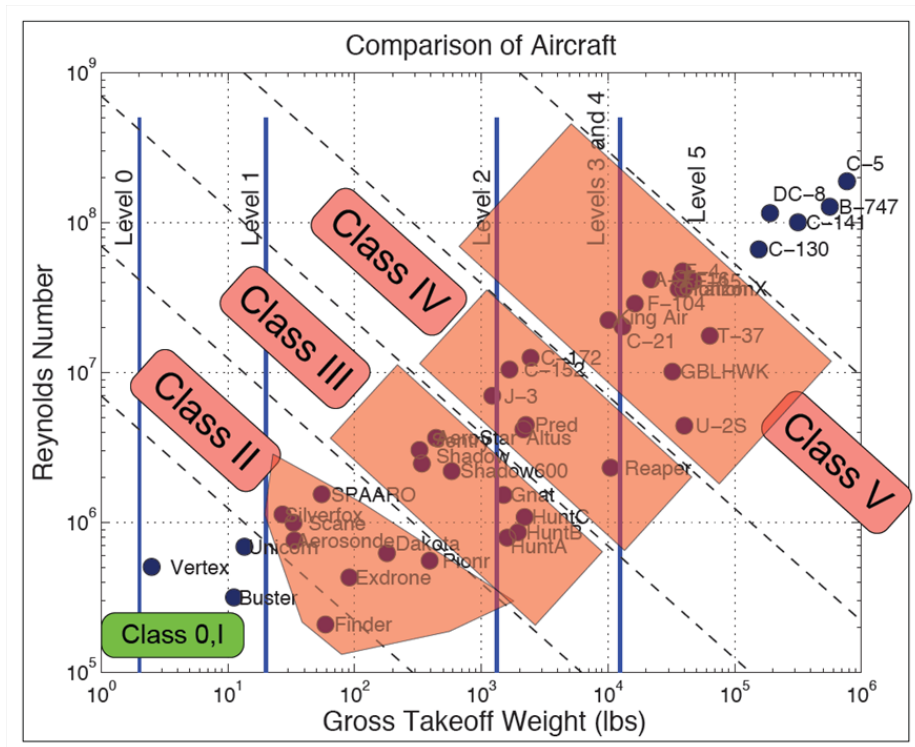

Figure 15. UAV Grouping by Reynolds Number and Aircraft Weight [17]

In addition to UAV classification changes, several adapted Cooper-Harper rating
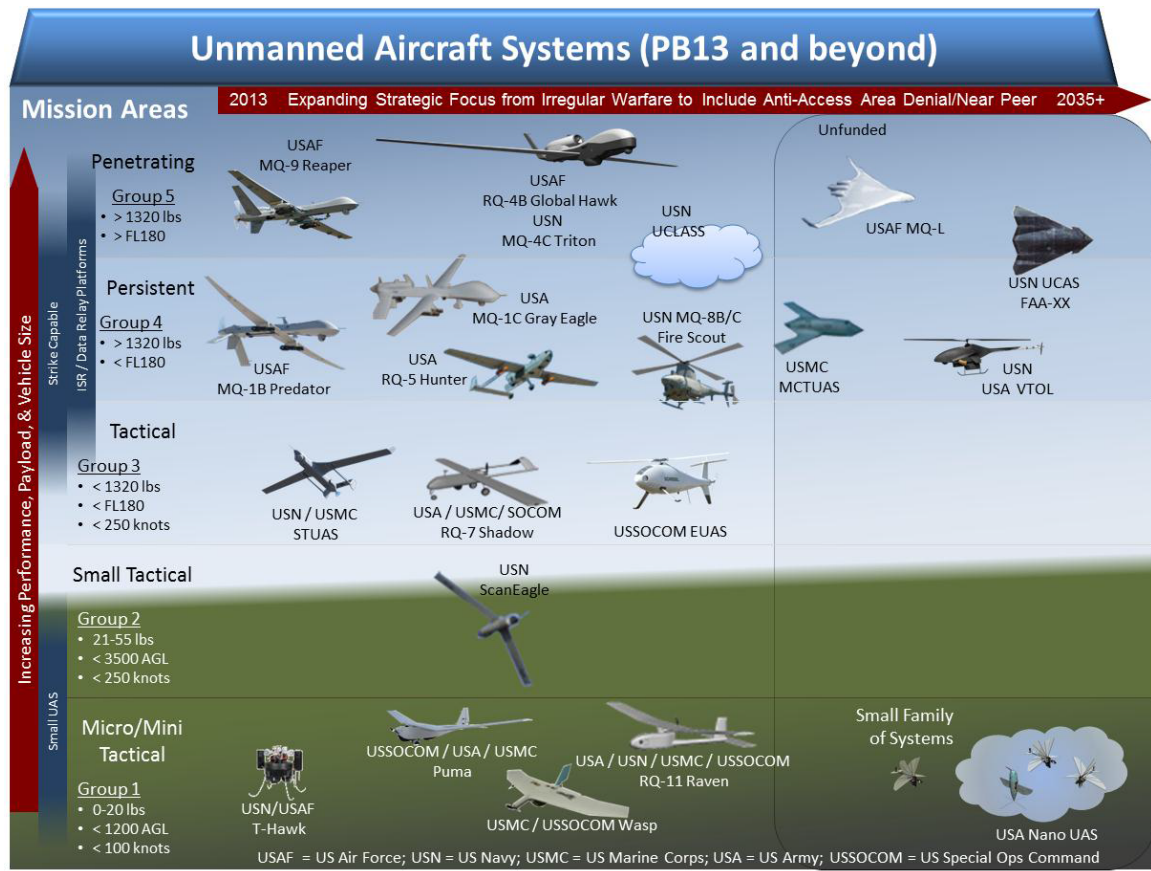
Figure 16. UAV Grouping by Operational Altitude, Weight, and Airspeed [51]

scales have been contrived as an alternative to the original. Cotting proposed a modi-
fied version of the Cooper-Harper Piloted Rating Scale for unmanned systems, shown
in Figure 17. He defined UAV flying qualities as "those qualities or characteristics
of an aircraft and sensor system that govern the ease and precision with which an
operator is able to perform the tasks required in support of its *mission* role" [18].
Cotting's scale focuses on the operator's ability to perform the tasks necessary to
complete the mission. A rating scale of 1 to 10, where 10 is worst and 1 is best, is
utilized by the evaluator to give an ordinal rating with several logic gates similar to
the original Cooper-Harper Rating Scale [18]. Although Cotting successfully adapts
the scale for UAVs, there still remains disagreement amongst the UAV community
on what "good" UAV performance entails [23]

Cotting's focus was similar to ADS-33E in that a specific MTE would be evaluated using the modified Cooper-Harper Scale. Each task reflects the mission, thereby evaluating the aircraft and sensor integrated systems necessary for mission success [18]. He breaks down the MTEs into task categories, sorted by aggressiveness and precision. Figure 18 illustrates how aircraft roles relate to MTEs and various task categories representative of the aircraft mission. Cotting recognized that validation of the scale precludes its widespread adoption by the flying qualities community, as well as a standard set of MTEs for evaluation [18].
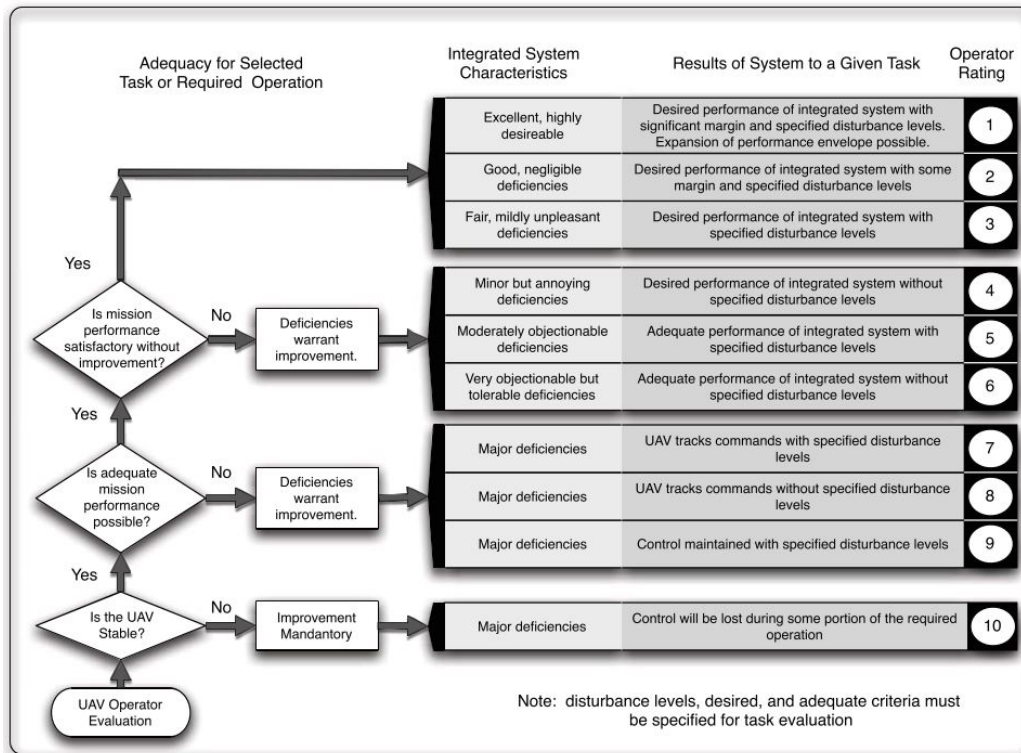

Figure 17. Cotting's Modified Cooper-Harper Rating Scale for UAVs [18]

Several research endeavors involving UAV flying and handling qualities have been completed at the Air Force Institute of Technology. This thesis builds on the foundation that Greene first laid for developing an unmanned flying qualities standard. In Greene's dissertation *Toward a Flying Qualities Standard for Unmanned Aircraft*, she stated the end goal of her research was to kick-start a process utilized in the air-
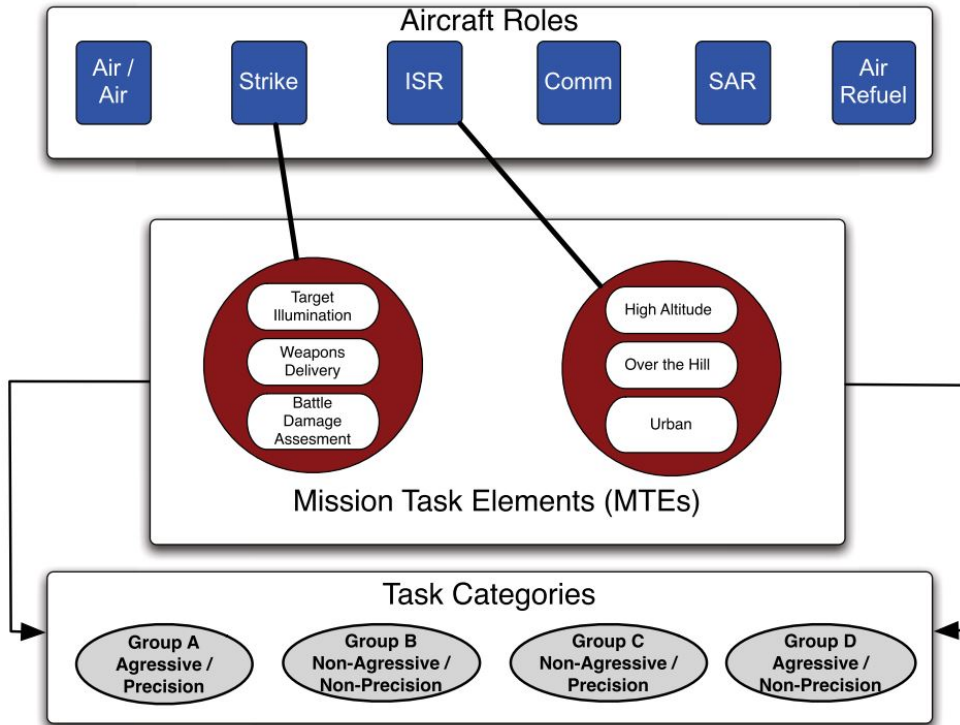
Figure 18. Notional Relation between UAV Roles, Mission Task Elements, and Task Categories [18]

craft design and model validation that increases the overall success rate of UAVs [23]. Using the j2 Universal Tool-Kit software, she evaluated three UAV models through four maneuvers: the non-precision non-aggressive climbing spiral, the non-precision aggressive air-to-ground tracking, the precision non-aggressive offset landing, and the precision aggressive pitch and roll discrete tracking [23]. From these maneuvers, flying qualities criteria such as pitch quickness, bandwidth, and time delay were calculated and recorded. From her analysis, she found that weight is a poor classifier for UAVs [23].

As expected, Greene recommended incorporating verified models into the analysis, which Kim did in his follow-on research. Kim investigated a Cessna 172 (C172) climbing spiral maneuver using Jon S. Berndt Simulation (JSBsim) [30]. The C172, a validated model based on publicly available data, was analyzed using workload and

performance metrics with varying levels of aggressiveness during the spiral maneuver. He also assessed the effects of varying both longitudinal and lateral-directional stability and control derivatives to mimic the research techniques of variable stability aircraft. His findings stated that how much the autopilot works in completing a maneuver is not as much of a concern as the actuator position limits and rate limits degrading aircraft performance [30].

Subsequent research by Hamidani investigated workload and performance metrics during two precision aggressive tasks: pitch attitude tracking and altitude tracking. Using an F-16 model in JSBsim, he also varied longitudinal stability and control derivatives and assessed the tracking ability of the aircraft [26]. Hamidani also recommended further investigation into the relationship between control surface deflection and aircraft performance [26].

2.6   Summary

A history of the development of modern day flying qualities was presented, starting from the first pioneers discovering the concepts of static stability to modern day criteria used to assess aircraft flying qualities. Large databases of flight test data were utilized in the development of documents such as MIL-STD-1797B and ADS-33E. These standards drive contemporary flying qualities criteria, yet these criteria are inadequate for UAVs. Several alternate classifications have been proposed to aid in developing new flying qualities criteria, but without actual flight test data, they remain unproven hypotheses. Previous research leveraged simulations of UAVs as a cost-effective alternative to flight test. Chapter III details the methodology of using such simulations to assess workload and performance of an LJ-25D.

III. Research Methodology

The overarching goal of this research is to contribute to a database of UAV flying handling qualities. A stitched model of an LJ-25D is utilized in various maneuvers and analyzed using workload and performance metrics. Ideally, correlations can be drawn from the data indicating design parameters that equate to satisfactory flying qualities.

3.1 Simulink Model of LJ-25D Aircraft

As previously stated, the LJ-25D model is a stitched, quasi-linear, parameter-varying model developed at the USAF Test Pilot School [8]. For the LJ-25D aircraft under consideration, a full flight envelope simulation model was created utilizing actual flight data from five different flight and loading conditions [8]. The model was then implemented in Simulink and validated at various flight conditions. Reference 5 details the exact procedures to create such a stitched model.

3.1.1 Model Development.

After taking the flight test data, the model was stitched primarily using the x-body axis velocity state U as a scheduling parameter [8]. Density ratio scaling permitted state and trim data to be interpolated between available point model data [8]. The stitched model can also scale forces and moments based on changes in aircraft weight, moment of inertia, and center of gravity (CG) location [8]. In summary, "model stitching is accomplished by implementing lookup tables of the aircraft state trim values, control input trim values, and stability and control derivatives based on point models and trim data" [8]. Figure 19 shows a detailed block diagram of how the scheduling parameter U interfaces with the lookup tables and subsequent pilot commands,

34

aircraft states, and nonlinear equations of motion to output the next aircraft state.
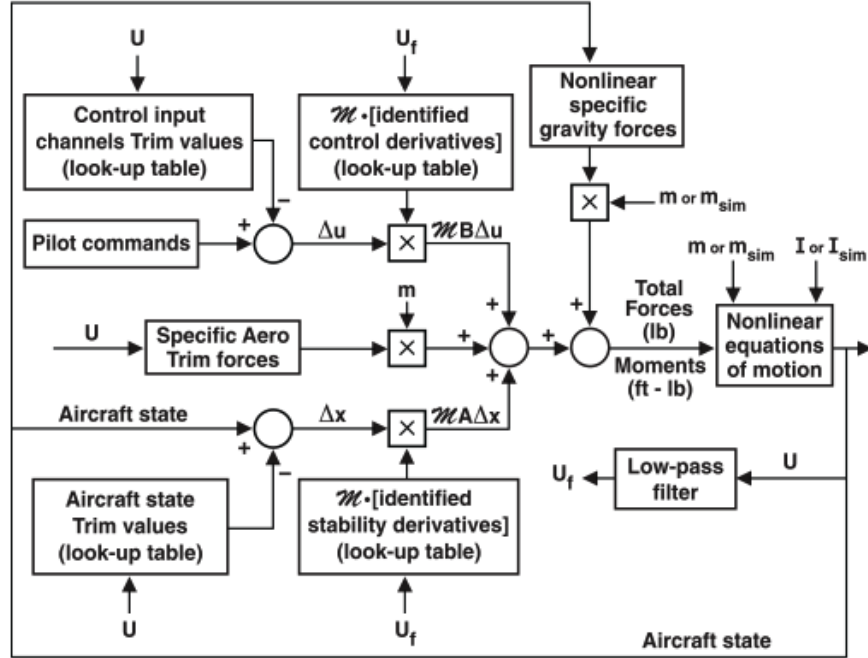
Variable	Description
U	Total longitudinal body axis velocity
U_f	Filtered velocity
$\triangle u$	Control perturbations (e.g., δ_e)
$\triangle x$	State perturbations [e.g., $w \equiv (W - W_0)$]
$\mathcal{M}$	Mass and inertia matrix
A	Dimensional stability derivatives
B	Dimensional control derivatives
m	Aircraft mass
I	Aircraft inertia matrix

Figure 19. LJ-25D Model stitching block diagram [8]

An important aspect of the model is control surface actuator saturation. Saturation occurs if either the position of the actuator reaches a limit or the rate of actuator movement reaches its limit. Saturation can cause undesirable flying qualities [5] and will be one of the primary focuses of performance and workload metrics in analysis of aircraft maneuvers. Table 5 shows the LJ-25D control surface deflection limits and Table 6 shows the LJ-25D control surface rate limits.

Table 5. LJ-25D Control Surface Deflection Limits

Elevator Deflection	min	-15°
	max	15°
Aileron Deflection	min	-40°
	max	40°
Rudder Deflection	min	-30°
	max	30°

Table 6. LJ-25D Control Surface Rate Limits

Elevator Rate	min	-100°/s
	max	100°/s
Aileron Rate	min	-150°/s
	max	150°/s
Rudder Rate	min	-100°/s
	max	100°/s

3.1.2 Stability Parameter Scaling.

Within the LJ-25D model are two lookup table data structures: an A matrix for the stability parameters and a B matrix for the control parameters. The stitched model is composed of 8 point models, with 4 of them at flaps-up and 4 at flaps 20 degrees. Each of the flap settings are at approximately 185 kts, 220 kts, 250 kts, and 300 kts. Reference 5 plots the flaps up derivatives as they change with airspeed.

As part of this research, four stability and control parameters will be scaled as a method of altering the bare airframe dynamics of the LJ-25D. The two stability parameters are M_q, the pitching moment due to pitch rate, and L_p, the rolling moment due to roll rate. The two control parameters are $M_{\delta e}$, the pitching moment due to elevator deflection, and $L_{\delta a}$, the rolling moment due to aileron deflection. Table 7 depicts the four stability and control parameters.

Previous research by Kim [30] and Hamidani [26] scaled the stability and control derivatives C_{mq}, C_{lp}, $C_{m\delta_e}$, and $C_{l\delta_a}$ instead of the stability and control parameters. Due to limitations in the design of the LJ-25D Simulink model, only the stability and control parameters could be scaled. Because there is a proportional relationship

Table 7. Stability and Control Parameters [52]

Stability Parameter	Definition	Units
M_q	$\frac{\bar{q}_1 S \bar{c}^2}{2 I_{yy} U_1} C_{mq}$	s^{-1}
$M_{\delta e}$	$\frac{\bar{q}_1 S \bar{c}}{I_{yy}} C_{m\delta_e}$	s^{-2}
L_p	$\frac{\bar{q}_1 S b^2}{2 I_{xx} U_1} C_{lp}$	s^{-1}
$L_{\delta a}$	$\frac{\bar{q}_1 S b}{I_{xx}} C_{l\delta_a}$	s^{-2}

between the stability and control derivatives scaled by Kim and Hamidani and the respective stability and control parameters, the end result will always be a proportionally scaled parameter.

For each maneuver, a single stability and control parameter will be varied. The scaling factor was generally multiplied between 0.25 and 2 of the original bare airframe parameter. Scaling factors varied between stability and control parameters. The reasoning was twofold: first, it was to ensure an accurate model of the new bare airframe was developed, as data from an inaccurate model would be unusable. Second, it allows full completion of each maneuver, as some large changes of stability derivatives alter bare airframe dynamics to a point of instability.

3.1.3 Lower-Order Equivalent System Development.

In order to quantify the literal factors utilized in the objective criteria, MIL-STD-1797 sets out a methodology to simplify the higher-order systems (HOS) into a Lower-Order Equivalent System (LOES). In order to accurately model the HOS, the LOES and HOS must be analyzed by evaluating the difference in gain and phase [5]. The overall goal is to minimize the cost function, described by Equation 1,

$$J = \frac{20}{n} \sum_{\omega_1}^{\omega_n} [(G_{HOS} - G_{LOES})^2 + .02(\phi_{HOS} - \phi_{LOES})^2] \tag{1}$$

where J is the overall cost, n is the number of frequencies, G is the gain in decibels, and ϕ is the phase in degrees. The primary goal is to minimize the cost enough that the difference in magnitude and phase between the HOS and LOES fits within bounds described by MIL-STD-1979. Figure 20 depicts an acceptable LOES, as the differences in both magnitude and phase remain between the black boundaries. Outside of those limits indicates a LOES that may be inaccurate at that frequency, and should be used with caution.
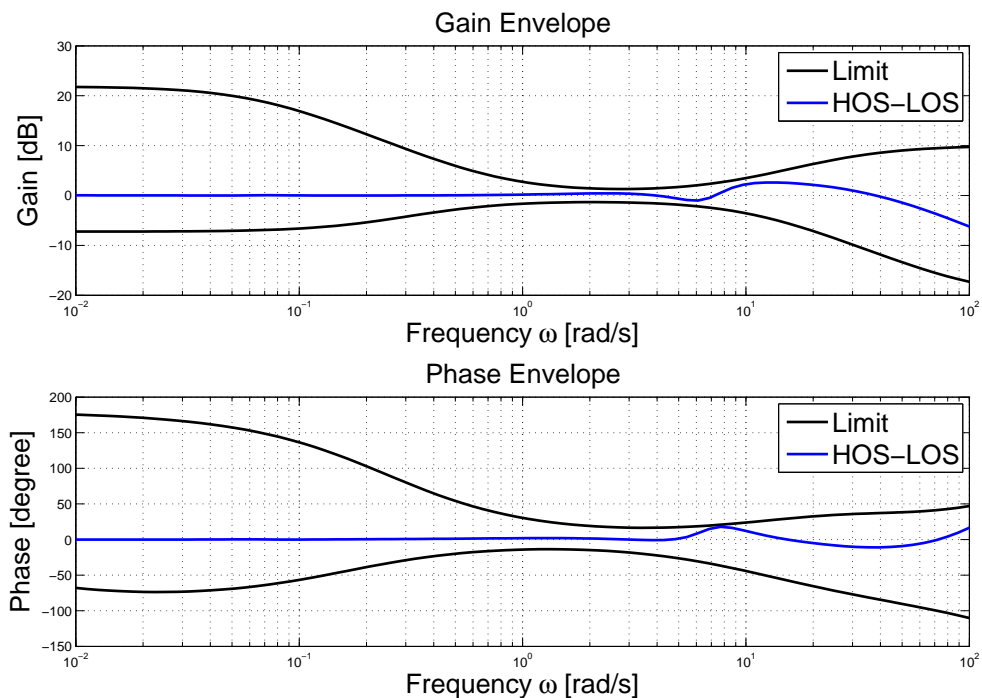
Figure 20. Envelopes of Maximum Unnoticeable Added Dynamics Example

With the simplification of the HOS, a LOES allows the designer to extract important literal factors that drive the aircraft dynamics. For longitudinal aircraft dynamics, the LOES takes the form of Equation 2,

$$\frac{\theta}{\delta_e} = \frac{K_\theta(s + 1/T_{\theta_1})(s + 1/T_{\theta_2})e^{-\tau_e s}}{(s^2 + 2\zeta_p\omega_p s + \omega_p^2)(s^2 + 2\zeta_{sp}\omega_{sp}s + \omega_{sp}^2)} \tag{2}$$

where ζ_p and ζ_{sp} represent the phugoid and short-period modal damping respectively.

Similarly, for lateral aircraft dynamics, the LOES takes the form of Equation 3,

$$\frac{\phi}{\delta_a} = \frac{K_\phi(s^2 + 2\zeta_\phi\omega_\phi s + \omega_\phi^2)e^{-\tau_{e\phi}s}}{(s + 1/T_S)(s + 1/T_R)(s^2 + 2\zeta_d\omega_d s + \omega_d^2)} \tag{3}$$

where ζ_ϕ and ζ_d represent the roll and Dutch roll modal damping respectively. These literal factors described in both Equation 2 and Equation 3 are then used in various graphics to depict where satisfactory, acceptable, and controllable flight levels exist.

In assessing the effects of altering stability and control parameters, a LOES was developed for each scaled parameter. For changes to M_q and $M_{\delta e}$, a longitudinal LOES as described in Equation 2 was developed. For scaling of the parameters L_p, $L_{\delta a}$, a lateral LOES as described in Equation 3 was developed. To ensure an accurate model, MATLAB's *fmincon* function matched a lower-order equivalent system to the bare airframe by minimizing Equation 1. This was done utilizing a Bode plot analysis, as described above.

3.2   Flight Maneuvers

As stated in Chapter II, varying levels of precision and aggressiveness are required for an aircraft to complete a task maneuver. The report WL-TR-97-3100 lists maneuvers based on precision and aggressiveness and are shown in Table 8 [31]. Three flight maneuvers were chosen in the analysis of aircraft workload and performance: a climbing spiral task, an aerial refueling task, and a side step landing maneuver. The climbing spiral maneuver is representative of a non-precision, non-aggressive maneuver while the aerial refueling task and side step landing task are representative of precision, non-aggressive tracking tasks.

No.	Mission Task Element (MTE)	Related Flight Phase (Ref. 1)	MTE Status at Program Completion		
			Evaluated (Flight)	Evaluated (Simulator)	Needs Refinement
Non-Precision, Non-Aggressive Demonstration Maneuvers					
1	Takeoff and Departure Climb	TO	✓	✓	
2	Heading Change	CR, LO	✓	✓	
3	Supersonic Heading Change	CR, LO		✓	
4	Altitude Change	CL, D	✓	✓	
5	Supersonic Altitude Change	CL, D		✓	
6	Waveoff/Go-Around	WO		✓	
7	Landing	L	✓	✓	
Non-Precision, Aggressive Demonstration Maneuvers					
8	Air-to-Air Longitudinal Gross Acquisition	CO			
9	Post-Stall Air-to-Air Longitudinal Gross Acquisition	CO	✓		
10	Air-to-Air Lateral Gross Acquisition	CO			
11	Post-Stall Air-to-Air Lateral Gross Acquisition	CO	✓		
12	Air-to-Ground Gross Acquisition	GA			
13	Loaded Roll Reversal	CO			✓
14	Post-Stall Roll Reversal	CO	✓		
Precision, Non-Aggressive Demonstration Maneuvers					
15	Catapult Takeoff	CT			✓
16	Flightpath Capture and Hold	AR		✓	
17	Altitude Rate Capture and Hold	*	✓	✓	
18	Supersonic Altitude Rate Capture and Hold	*		✓	
19	Pitch Attitude Capture and Hold	*	✓	✓	
20	Supersonic Pitch Attitude Capture and Hold	*		✓	
21	Post-Stall Pitch Attitude Capture and Hold	*	✓		
22	Bank Angle Capture and Hold	*	✓	✓	
23	Supersonic Bank Angle Capture and Hold	*		✓	
24	Close Formation	FF			✓
25	Probe-and-Drogue Refueling	RR	✓		
26	Tanker Boom Tracking	RR			
27	Simulated Aerial Refueling	RR	✓		
28	Precision Low-Altitude Flight	LAPES			✓
29	Precision ILS Capture and Track	PA	✓	✓	
30	Precision Offset Landing	L	✓	✓	
31	STOL Precision Offset Landing	L			✓
Precision, Aggressive Demonstration Maneuvers					
32	Air-To-Air Fine Tracking	CO			
33	Post-Stall Air-To-Air Fine Tracking	CO	✓		
34	Air-To-Ground Tracking	GA			
35	Pitch and Roll Discrete Tracking	CO	✓		
36	Pitch and Roll Sum of Sines Tracking	CO	✓		

Table 8. Mission Task Elements [31]

3.2.1 Climbing Spiral.

The climbing spiral maneuver is a non-precision, non-aggressive maneuver representative of a typical ISR task that a UAV would accomplish. The task includes a simultaneous change in both altitude and heading for a specified period of time. The flight controller should have enough control authority to complete the maneuver without saturation issues and achieve satisfactory performance.

3.2.1.1 Control System Design.

In designing the aircraft control systems, the desire was to fully automate the model thereby simulating a fully autonomous UAV. An autonomous UAV "receives goals from humans and translates them into tasks to be performed without human interaction" [51]. By automating control within the LJ-25D model, desired maneuvers can be repeated and subsequent performance evaluated.

Prior to evaluation of the aircraft in completion of the maneuver, a longitudinal controller was developed using classical control concepts. The longitudinal controller, shown in Figure 21, incorporates three feedback loops and a Proportional, Integral, Derivative (PID) controller. First, a pitch-attitude tracking autopilot was developed closing the loop on pitch rate, q, and then pitch angle, θ. With satisfactory tracking of pitch, altitude rate of climb, denoted by 'z dot' in the block diagram, can be fed back and subtracted from a target rate of climb (ROC). The difference between the target ROC and aircraft ROC is the error e, which is then sent to the PID controller. The controller, modeled by Figure 22, was tuned to provide satisfactory rise time, settling time, and overshoot. By varying K_p, K_i, and K_d, the proportional, integral, and derivative gains, respectively, satisfactory aircraft ROC performance was achieved.
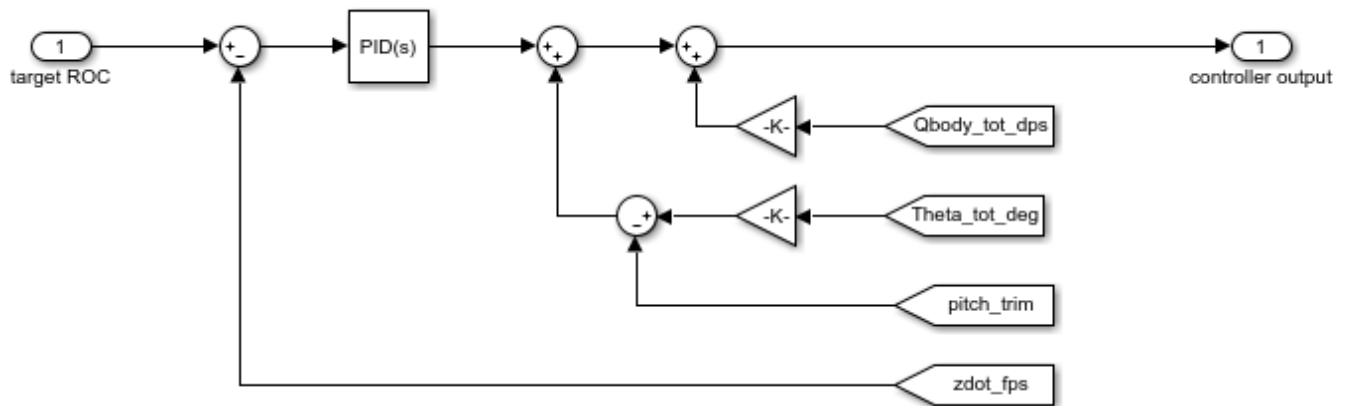
Figure 21. Block Diagram of Spiral Maneuver Longitudinal Controller

41
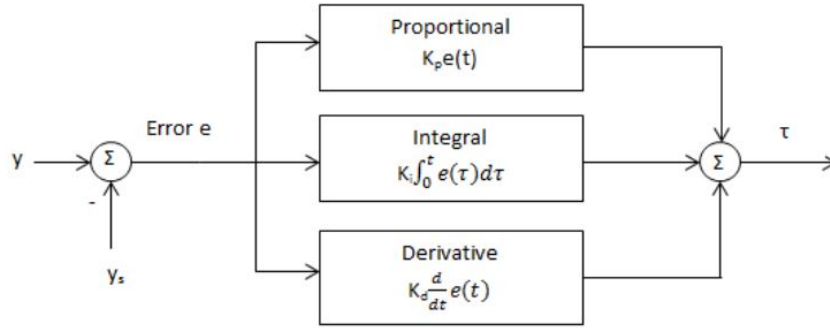
Figure 22. Block Diagram of a PID Controller [28]

The PID controller then outputs an error command, e_c, which is added to θ_e, the difference between the aircraft pitch angle and trimmed pitch angle. The result of that is subtracted from q, which is now the controller output. The command output enters an elevator actuator block modeled as a second-order system with position and rate limits. Finally, that is sent to the bare airframe system which then outputs the various aircraft parameters.

Next a lateral controller was developed to track a roll command. Figure 23 depicts a block diagram of the proportional feedback controller used during the spiral command. A similar design to the pitch attitude tracker was utilized. First by feeding back roll rate, p, in an inner loop then by closing an outer loop with roll angle ϕ and subtracting that from the desired roll angle. The error is then again fed into a second-order elevator actuator which outputs into the bare airframe dynamics. The feedback gains for ϕ and p were tuned to provide satisfactory tracking performance aircraft roll angles.

To ensure a coordinated turn, a directional controller was implemented to track a zero degree sideslip angle, β. Figure 24 shows the proportional feedback controller utilized to coordinate turns during the climbing spiral maneuver.

Finally, a throttle controller was designed to ensure a steady velocity during the maneuver. Figure 25 depicts the throttle controller. It first feeds back aircraft ve-
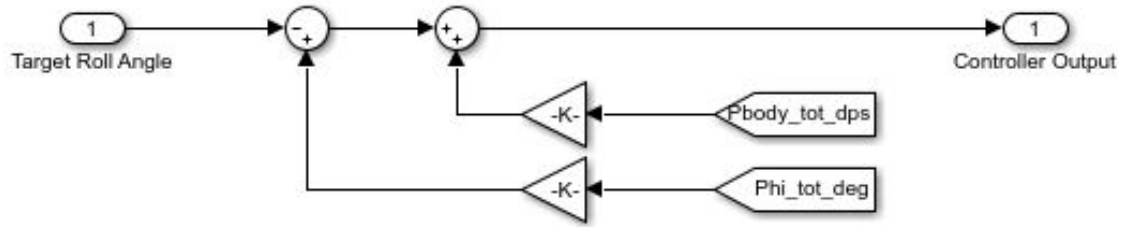
Figure 23. Block Diagram of Spiral Maneuver Lateral Controller
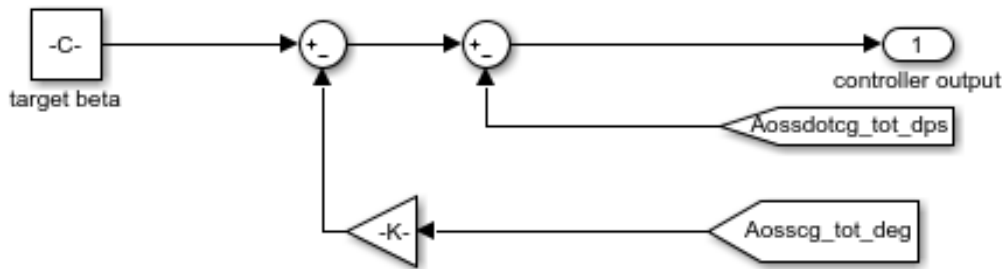
Figure 24. Block Diagram of Spiral Maneuver Sideslip Controller

locity in KCAS, which is subtracted from the trim velocity and fed into a phase-lead compensator. The output of that is added to the throttle trim position and then fed into an engine model that limits both throttle position and throttle rate. The result is sent to an engine scaling model utilizing table lookup data which outputs the thrust to the bare airframe. Table 9 summarizes the gains used in the controllers developed for the climbing spiral maneuver.

3.2.1.2 Target Inputs.

Two separate inputs were made for the climbing spiral maneuver. First, a ROC input is sent to the longitudinal controller to trigger a climb at a certain point in time. At that same time, a target roll angle is sent to the lateral controller, initiating the turning portion of the climbing spiral. The trim speed is fed into the throttle controller, prompting it to add throttle to maintain trim speed during the maneuver.
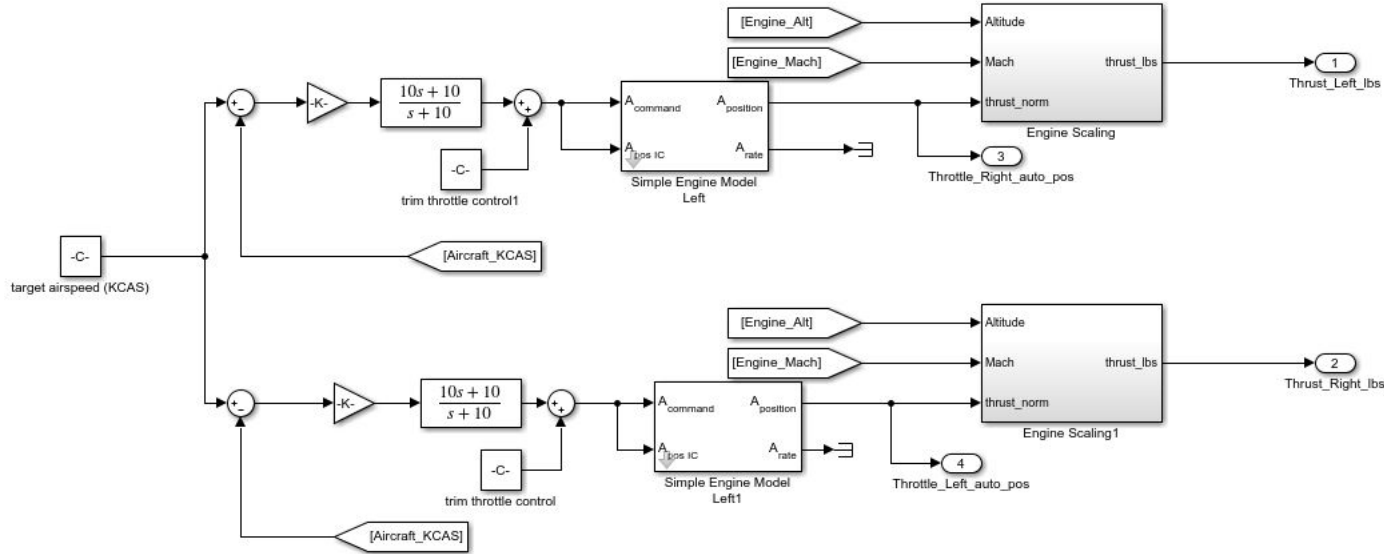
Figure 25. Block Diagram of Spiral Maneuver Throttle Controller

Table 9. Gains for Climbing Spiral Autopilots

Autopilot System	Gain Parameter	Control Parameter	Value
Longitudinal	K_p	Proportional	1.5
	K_i	Integral	1
	K_d	Derivative	0.3
	K_q	Pitch Rate	0.952
	K_θ	Pitch Angle	1
Lateral	K_p	Roll Rate	0.28
	K_ϕ	Roll Angle	1.02
Directional	K_β	Sideslip	4.0
Throttle	K_T	Throttle	1

The sideslip controller continually minimizes the sideslip angle to zero throughout the maneuver, ensuring a coordinated turn.

3.2.2 Side Step Maneuver.

Under report WL-TR-97-3100, the side step landing maneuver can be considered 'Precision Offset Landing' and thus is a precision, non-aggressive maneuver [31]. The maneuver investigates lateral-directional control as well as longitudinal control, as it requires the aircraft to roll while maintaining heading and flaring to maintain altitude.

3.2.2.1 Control System Design.

In accomplishment of the side step maneuver, several controllers needed to be employed to accurately control the pitch, roll, and yaw of the aircraft during the maneuver. In order to track the correct ROC, the same controller used in the climbing turn was again used in the side step. The climbing turn throttle controller also provides adequate performance and was employed again for the side step maneuver. A more complicated controller was developed for tracking y_{cg}, or side step distance, via aileron control. First, P, ϕ, $\dot{y}$, and y_{cg} were closed via feedback loops, with the target side step distance at the input. A lead compensator added control to the high frequency areas of the response. Figure 26 depicts the block diagram of the controller.
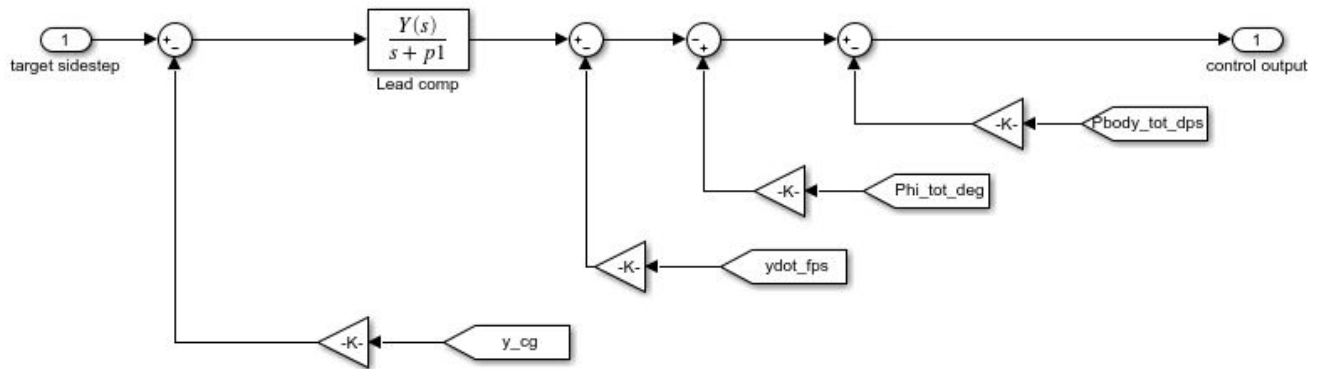
Figure 26. Block Diagram of Side Step Maneuver Lateral Controller

A slightly different rudder controller was used to track heading instead of sideslip. By tracking a heading of zero, this ensures that the aircraft's nose remained as parallel as possible in relation to the runway, as opposed to the relative wind in the lateral axis. The heading controller fed back R and ψ. The addition of a lead compensator ensured satisfactory control at higher frequencies. Figure 27 depicts the block diagram of the controller.

Several gains, poles, and zeros were iterated in the design to obtain a satisfactory

45
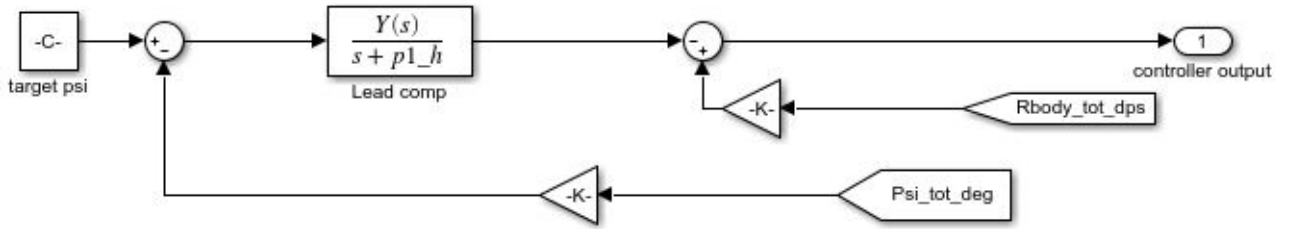
Figure 27. Block Diagram of Side Step Maneuver Heading Controller

response from the system. Table 10 summarizes the gains used in the controllers developed for the side step maneuver. Note the two lead compensators use the same poles and zeros, but different gains.

Table 10. Gains for Side Step Autopilots

Autopilot System	Parameter	Control Parameter	Value
Longitudinal	K_p	Proportional Gain	1.5
	K_i	Integral Gain	1
	K_d	Derivative Gain	0.3
	K_q	Pitch Rate Gain	0.952
	K_θ	Pitch Angle Gain	1
Lateral	K_p	Roll Rate Gain	0.28
	K_ϕ	Roll Angle Gain	1.02
	$K_{\dot{y}}$	Horizontal Rate Gain	0.275
	K_y	Horizontal Distance Gain	1
	K	Lead Compensator Gain	0.778
	z_1	Lead Compensator Zero	-1.5
	p_1	Lead Compensator Pole	-37.5
Directional	K_R	Yaw Rate Gain	1
	K_ψ	Yaw Angle Gain	1.25
	K	Lead Compensator Gain	5
	z_1	Lead Compensator Zero	-1.5
	p_1	Lead Compensator Pole	-37.5
Throttle	K_T	Throttle Gain	1

3.2.2.2 Target Inputs.

To setup the approach, the aircraft starts in a 750 foot per minute (FPM) descent at 7000 ft MSL. In order to replicate a glide slope of approximately 3 degrees, the

aircraft trim speed was set to 140 knots. The gear was also set down, with flaps at 10 degrees, again to simulate an instrument approach setup. When the plane passes 6750 ft, approximately 10 seconds into the maneuver, the aircraft begins to track the side step to an adjacent runway, which is at a 500 foot horizontal increment from where the aircraft began its descent. The 6750 ft mark is considered the maneuver start point, where all workload and performance data are first analyzed. In the vertical plane, the aircraft tracks a height above touchdown of 50 ft above the imaginary runway at 6250 feet; therefore the controller aims to flare at 6300 feet where a human pilot would take control. Ground effect is not modeled in this simulation. The parameters for the maneuver termination point are a 2% steady-state error in both the z and y axis. When the aircraft is within 2% of the side step distance of 500 ft and within 2% vertical height of 6300, and remains within those bounds for the remaining simulation time, the termination point is marked. All workload and performance data are analyzed from the maneuver start point to the maneuver termination point.

3.3 Evaluation of Maneuver Workload and Performance

Previous research in UAV flying qualities by Hamidani [26] and Kim [30] focused in assessing the UAV's workload and performance during a climbing turn maneuver, a pitch tracking maneuver, and an altitude tracking maneuver. The software utilized in both Hamidani and Kim's research, JSBSim, only output actuator position, and not actuator rate. Therefore, rate limiting had to be inferred from position rate graphs. Previous UAV research [30] recommended investigating the effects of rate limiting on UAV performance and workload. In manned fixed-wing flying qualities, pilot induced oscillation (PIO) has been known to be caused by "nonlinear events such as saturation of control rate or position limits at too low a command" [37]. Rate limiting has been known to be a cause of PIO in manned aircraft for some

time [32]. Although PIOs are not an issue in UAVs, system induced oscillations (SIO) may become problematic during precision aggressive maneuvers [30]. The LJ-25D model allows for the investigation into actuator rate limiting and its effects on aircraft workload and performance during a task.

3.3.1 Aerial Refueling.

Under report WL-TR-97-3100 lists, the aerial refueling maneuver can be considered 'tanker boom tracking' and thus is a precision non-aggressive maneuver [31]. The maneuver elicits precision control by simultaneously tracking altitude, roll angle, and airspeed.

3.3.1.1 Control System Design.

In designing a longitudinal control system, a similar approach to the ROC controller was taken. Again, the pitch-attitude tracking autopilot previously developed was utilized for the two inner loops of the controller. The final outer loop was then modified to feedback aircraft altitude. Instead of a PID compensator, a lead-lag compensator, shown in Equation 4, was chosen to provide a robust design to track altitude.

$$Lead\,Lag\,Compensator\,=K\,\frac{s\,+\,z_1}{s\,+\,p_1}\frac{s\,+\,z_2}{s\,+\,p_2} \qquad (4)$$

Gain K is varied based on task: a large step 1000 foot altitude change requires a lower gain than an aerial refueling tracking task with a margin of $\pm$ 10 feet. Table 11 depicts the values for K, T_1 and T_2 for large and small amplitude altitude tracking tasks.

For roll, sideslip, and throttle control, the previously developed controllers utilized in the climbing spiral provided satisfactory performance in completing an aerial

48

Table 11. Lead Lag Compensator for Altitude Control Design Values

Task	K	z_1	p_1	z_2	p_2
Large Amplitude Tracking	-1	-1.0282	-9.3469	-0.0714	-0.0060
Precise Amplitude Tracking	-4.87	-1.0282	-9.3469	-0.0714	-0.0060

refueling task. Therefore, these controllers were not modified for the aerial refueling task.

3.3.1.2 Target Inputs.

In order to simulate an aerial refueling task, the tracking input for both target altitude and roll angle needed to mimic the randomness of turbulent airflow at altitude. Previous research [26] utilized a multi-sine input for a pitch attitude tracking task and an altitude tracking task. These were accomplished separately as two tasks; this research will employ a multi-sine input to both altitude tracking and roll tracking to adequately model a UAV controller adjusting to maintain refueling tracking tolerances. In addition, the throttle controller will be set to maintain trim speed by making adjustments to thrust. Equation 5 depicts the form of the multi-sine input used for altitude and roll command inputs.

$$h_{CMD} - or - \phi_{CMD} = A_1 sin(\omega_1 t + \phi_1) + A_2 sin(\omega_2 t + \phi_2) + A_3 sin(\omega_3 t + \phi_3) \quad (5)$$

3.3.2 Maneuver Workload Metrics.

The workload is the relationship between resource supply and task demand [43]. Previous research [26, 30] employed the $\mathcal{L}_2$ error norm of the control surface deflection away from the trimmed condition as primary metric of workload. A value of zero indicates the control system did no work during the maneuver, and a value of 1 indicates the control system work was maximized during the maneuver. The $\mathcal{L}_2$ error

norm is shown in Equation 6:

$$\mathcal{L}_2 = \sqrt{\frac{1}{n} \sum_{i=1}^{n} (x_1(i) - x_2(i))^2} \tag{6}$$

In addition to assessing the $\mathcal{L}_2$ error norm for elevator, aileron, and rudder deflection positions during a maneuver, the $\mathcal{L}_2$ error norm for elevator, aileron, and rudder deflection rates will also be assessed.

3.3.3 Maneuver Performance Metrics.

Originally developed for economic forecasting [47], Theil's Inequality Coefficient (TIC) has been adapted to assess time histories of simulation to determine their accuracy. It is primarily used in assessing nonlinear systems such as the LJ-25D model utilized in this thesis, and "culminating in the validation of an aircraft simulation model using flight test data" [20]. TIC is shown in Equation 7.

$$TIC = \frac{\sqrt{\frac{1}{n} \sum_{i=1}^{n} (x_i - \tilde{x}_i)^2}}{\sqrt{\frac{1}{n} \sum_{i=1}^{n} x_i^2} + \sqrt{\frac{1}{n} \sum_{i=1}^{n} \tilde{x}_i^2}} \tag{7}$$

where x is the simulation time history, $\tilde{x}$ is the desired track, and n is the number of data samples. A TIC of less than 0.25 is considered an accurate model. Ideally, correlations can be made between workload metrics from the $\mathcal{L}_2$ error norm of actuator positions, actuator rates, and TIC performance metrics.

3.4 Summary

An explanation of the LJ-25D Simulink model and its development at the USAF Test Pilot School was presented. A discussion of the climbing spiral maneuver, aerial refueling maneuver, and side step maneuver was provided, along with the methodology of developing the controllers for each maneuver. The $\mathcal{L}_2$ error norm and TIC

equations showed how workload and performance are calculated for each mission task. An analysis of the LJ-25D model during each flight maneuver using the evaluation techniques described will be presented in Chapter IV.

IV. Results

4.1 Bare Airframe Analysis

Before altering the stability and control parameters, a bare airframe analysis of the LJ-25D was conducted to establish a baseline of aircraft parameters. First, the aircraft was trimmed, and using previously described techniques in Section 3.1.3, a LOES was developed for both the longitudinal and lateral-directional stability axes. The aircraft was trimmed to a flight path angle of 0 degrees at 200 KCAS and 5000 ft, with zero flaps and gear up. Table 12 shows the longitudinal literal factors in baseline trim condition for the LJ-25D.

Table 12. Longitudinal Trim Results, 200 KCAS 5,000 ft

K_c	$T_{\theta 1}$	$T_{\theta 2}$	τ_θ	ω_p	ω_{sp}	ζ_p	ζ_{sp}	$\omega_{sp}T_{\theta 2}$	CAP	J
-1.27	2.98	2.97	0.01	0.23	0.83	-0.30	0.76	2.48	0.33	12.47

First, the cost function value using Equation 1 of 12 indicates an accurate model. For the purposes of this analysis, an acceptable model has a cost value under 25 and remains within the MIL-STD-1979 $HOS - LOS$ bounds. When examining the poles and zeros, any negative number indicates the pole or zero exists in the right half plane (RHP), indicating it is unstable. A positive number indicates the pole or zero lies in the left half plane (LHP), and thus stable. Table 12 indicates the bare airframe has a satisfactory short-period damping (ζ_{sp}) value of 0.76. The phugoid mode, denoted by ζ_p, has a value of -0.30. The second order transfer function associated with the phugoid mode can be written as Equation 8. The poles of the polynomial in Equation 8 are $0.0695 \pm 0.219i$, indicating that the pair of poles associated with the phugoid mode lie in the RHP and thus are unstable.

$$\frac{1}{(s^2 + 2\zeta_p\omega_p s + \omega_p^2)} = \frac{1}{(s^2 - 0.139s + 0.0529)} \tag{8}$$

The controllers developed for each maneuver mitigate the unstable phugoid mode. Figure 28 shows the Bode plot analysis of the longitudinal LOES developed for the bare airframe. Figure 28a shows the HOS and LOES are nearly identical Bode plots in both magnitude and phase and Figure 28b confirms that with the $HOS - LOS$ envelope plot.

(a) Overlay Bode Plot   (b) Envelope Plot
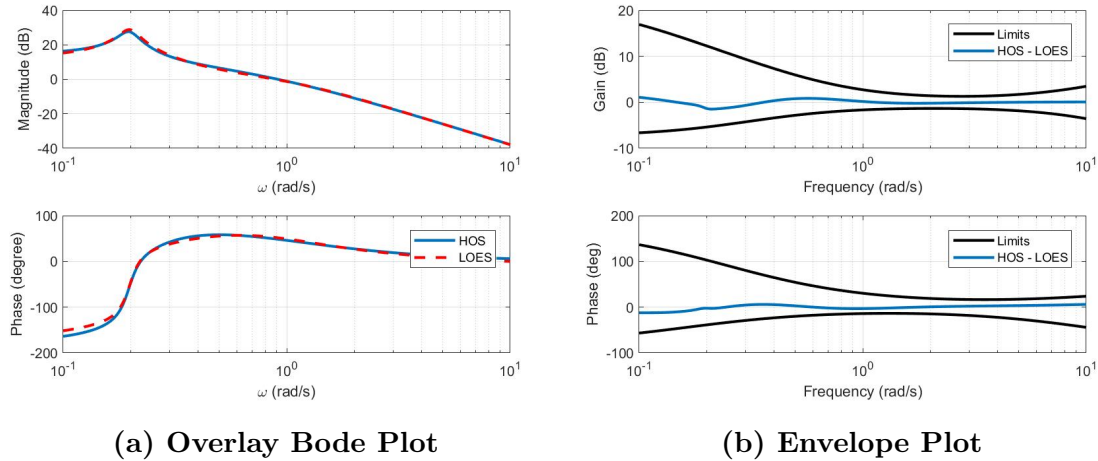
Figure 28. Longitudinal LOES for Baseline Bare Airframe, 200 KCAS 5,000 ft

An analysis of the bare airframe lateral-directional dynamics was also completed. Table 13 shows the lateral-directional literal factors in baseline trim condition for the LJ-25D.

Table 13. Lateral-Directional Trim Results, 200 KCAS 5,000 ft

K_ϕ	ζ_ϕ	ω_ϕ	τ_ϵ	T_r	T_s	ζ_d	ω_d	BW	J
-3.83	6.70	3.26	0.045	-0.016	1.18	-0.25	0.67	2.04	23.89

From the baseline analysis, the Dutch roll mode, denoted by ζ_d, is -0.25. Utilizing the same analysis technique used in Equation 8, it is determined the poles associated with the Dutch roll mode lie in the RHP, indicating instability. The zero T_r representing the roll mode time constant also lies in the RHP. That is not as concerning for an aircraft developer but does indicate that the plane eventually would demonstrate

53

instability for that mode. Figure 29 shows the Bode plot analysis of the lateral-directional LOES developed for the bare airframe. Similar to the longitudinal Bode plots, the lateral-directional Bode plots indicate the LOES is an accurate model.

(a) Overlay Bode Plot   (b) Envelope Plot
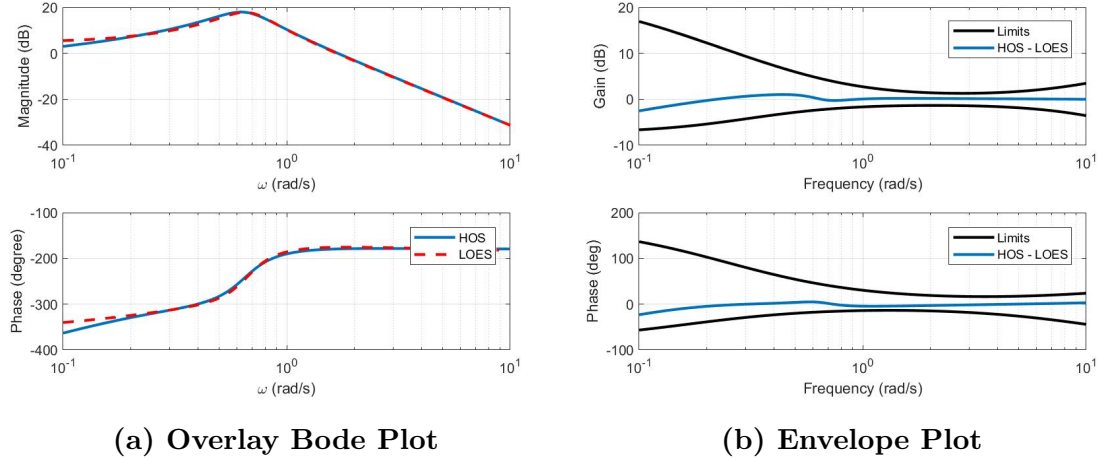
Figure 29. Lateral LOES for Baseline Bare Airframe, 200 KCAS 5,000 ft

4.1.1 Stability Parameter Scaling Analysis.

In order to do an accurate analysis of literal factors, a LOES was developed for every stability parameter at every scaling factor. Cost function was used to determine if the LOES accurately modeled the HOS. The LOES is based on the LJ-25D at 5,000 ft and 200 KCAS, which were the parameters utilized in the climbing turn and aerial refueling maneuver. Separate LOESs were developed for the side step maneuver, which required a different altitude, airspeed, flap setting and gear setting. Those LOES used for the side step maneuver slightly differ from the LOES used in the climbing spiral maneuver and aerial refueling maneuver. The lone outlier is the 1.5 x M_{elev}, which had a significantly different LOES for the side step maneuver as compared to the LOES for climbing turn and aerial refueling. Bode plots of the LOES overlaid on the HOS as well as the MIL-STD-1797 plots of $HOS - LOES$ within gain and phase envelopes can be found in Appendix A.

Table 14. M_q LOES Specifications, 200 KCAS 5,000 ft

Scale	K_c	$T_{\theta 1}$	$T_{\theta 2}$	τ_θ	ω_p	ω_{sp}	ζ_p	ζ_{sp}	$\omega_{sp}T_{\theta 2}$	CAP	J
0.25 x	-1.27	3.12	3.12	0.01	0.26	0.70	-0.51	0.72	2.18	0.24	10.17
1 x	-1.27	2.98	2.98	0.01	0.23	0.83	-0.30	0.76	2.48	0.33	12.47
2 x	-1.27	2.74	2.74	0.01	0.20	1.03	-0.09	0.84	2.82	0.47	15.51
4 x	-1.30	2.60	2.60	0.01	0.17	1.28	0.25	1.08	3.32	0.68	6.70
6 x	-1.34	1.35	1.35	0.01	0.47	0.69	1.63	2.27	0.93	0.10	20.08

Table 14 presents the LOES developed from scaling M_q. M_q was the sole stability parameter capable of being scaled greater than twice its original value without sacrificing the integrity of the LOES. Note that as M_q increases, phugoid damping changes from unstable to stable and short-period becomes more stable, as indicated by the increasing ζ_{sp}.

Next, M_{elev} was scaled and a LOES developed at each point. Table 15 depicts the LOES developed from scaling M_{elev}.

Table 15. M_{elev} LOES Specifications, 200 KCAS 5,000 ft

Change	K_c	$T_{\theta 1}$	$T_{\theta 2}$	τ_θ	ω_p	ω_{sp}	ζ_p	ζ_{sp}	$\omega_{sp}T_{\theta 2}$	CAP	J
0.25 x	-0.35	6.36	6.36	0.01	0.28	0.66	-0.48	0.84	4.19	0.44	2.36
0.75 x	-0.96	3.32	3.32	0.01	0.25	0.82	-0.38	0.76	2.73	0.36	11.44
1 x	-1.27	2.98	2.98	0.01	0.23	0.83	-0.30	0.76	2.48	0.33	12.47
1.25 x	-1.57	2.65	2.65	0.01	0.20	0.84	-0.16	0.78	2.22	0.30	13.11
†1.5 x	-1.89	2.42	2.42	0.01	0.17	0.78	0.18	0.85	1.88	0.23	6.47
*1.5 x	-2.69	4.91	0.01	0.01	0.16	10.90	0.16	6.79	0.11	0.27	10.51

† indicates model used for climbing turn and aerial refueling maneuver
* indicates model used for side step maneuver

M_{elev} did not experience as much of a change in short-period damping, but did yield a steady increase in phugoid damping, again changing from unstable to stable. An important point is the different models used at 1.5 x M_{elev}. The side step maneuver at 1.5 x M_{elev} has vastly different literal factors from the models used during the climbing turn and aerial refueling. The difference is attributed to the changes in altitude, velocity, gear extension, and flap deployment. This is the only instance

where LOES significantly differed across the three maneuvers. Also, past research was criticized for large changes in M_{elev} ($\frac{1}{10}$ x to 10 x) as unrealistically large changes to the sizes of the control surfaces. This research attempts to mitigate that by keeping the changes smaller and thus within the realm of possibility for an aircraft designer.

Next, lateral-directional LOES's were developed at each scaled value of L_p. Table 16 shows the LOES developed from scaling L_p.

Table 16. L_p **LOES Specifications, 200 KCAS 5,000 ft**

Change	K_ϕ	ζ_ϕ	ω_ϕ	τ_ϵ	T_r	T_s	ζ_d	ω_d	BW	J
0.25 x	-18.83	6.61	3.24	0.03	-0.003	1.24	-0.30	0.69	2.04	23.08
0.75 x	-17.82	6.65	3.24	0.03	-0.003	1.21	-0.27	0.68	2.04	23.60
1 x	-3.83	6.70	3.26	0.05	-0.016	1.18	-0.26	0.67	2.04	23.89
1.25 x	-4.51	6.60	3.20	0.04	-0.014	1.17	-0.24	0.66	2.03	24.15
1.5 x	-20.00	6.74	3.26	0.03	-0.003	1.15	-0.22	0.66	2.03	24.40

To note on L_p LOES is the Dutch roll mode damping, as it remains unstable throughout the changes but does move towards the LHP as L_p increases. The roll mode time constant, T_r also remains unstable throughout the scaling. Spiral mode time constant, T_s steadily decreases, indicating an increasing spiral mode time constant and improved lateral handling qualities. That, combined with the steady increase in Dutch roll damping, indicates workload should decrease and performance increase during each maneuver as L_p is scaled up.

Finally, Table 17 presents the LOES developed from scaling L_{ail}.

Table 17. L_{ail} **LOES Specifications, 200 KCAS 5,000 ft**

Change	K_ϕ	ζ_ϕ	ω_ϕ	τ_ϵ	T_r	T_s	ζ_d	ω_d	BW	J
0.5 x	1.37	26.48	0.004	0.01	-15.62	1.37	-0.28	0.65	1.48	1.25
0.75 x	-3.91	6.80	3.62	0.04	-0.01	1.17	-0.25	0.67	1.78	25.59
1 x	-3.83	6.70	3.26	0.05	-0.02	1.18	-0.26	0.67	2.04	23.89
1.25 x	-5.03	7.01	3.23	0.04	-0.01	1.19	-0.26	0.67	2.27	22.78
1.5 x	4.08	0.03	0.10	0.01	-300.00	-1.66	-10.00	0.03	2.40	620.87

The 1.5 x L_{ail} LOES was not used due to its high cost value, over 600, indicating the LOES does not match the HOS. The Bode and envelope plots in Figure 78,

Appendix A verify the inaccuracy graphically as well. The 1.5 x L_{ail} points are included in the analysis for trend identification purposes but should be used cautiously when drawing conclusions.

4.2 Climbing Spiral Analysis

The first maneuver analyzed was the non-precision, non-aggressive climbing spiral maneuver. First, a baseline analysis was completed varying bank angle and climb rate. Bank angle and climb rate were then fixed for the remaining runs which varied the stability and control parameters.

4.2.1 Baseline Climbing Spiral.

Before altering the stability and control parameters of the bare airframe, a short performance analysis was completed on the aircraft with controllers in the loop. Three separate runs were completed, each starting at a trim condition of 200 KCAS and 5,000 ft, for a duration of 180 seconds. The exact flight conditions are shown in Table 18 and the resulting aircraft paths in Figure 30.

Table 18. Baseline Climbing Spiral Flight Conditions, 200 KCAS 5,000 ft

Flight Condition (FC)	Rate of Climb (FPM)	Bank Angle (deg)
1	1000	10
2	1500	20
3	2000	30

Further analysis was completed to determine L_2 norms of actuator rate and position as well as TIC values for rate of climb, roll angle, and velocity. Figure 31a and Figure 31b depicts these values for elevator, aileron, and rudder actuator rates and actuator positions, respectively. Aileron and rudder actuator rates and actuator positions increase slightly with maneuver aggressiveness, while elevator rates and positions remains constant. Throttle sees a steady increase in position as aggressiveness
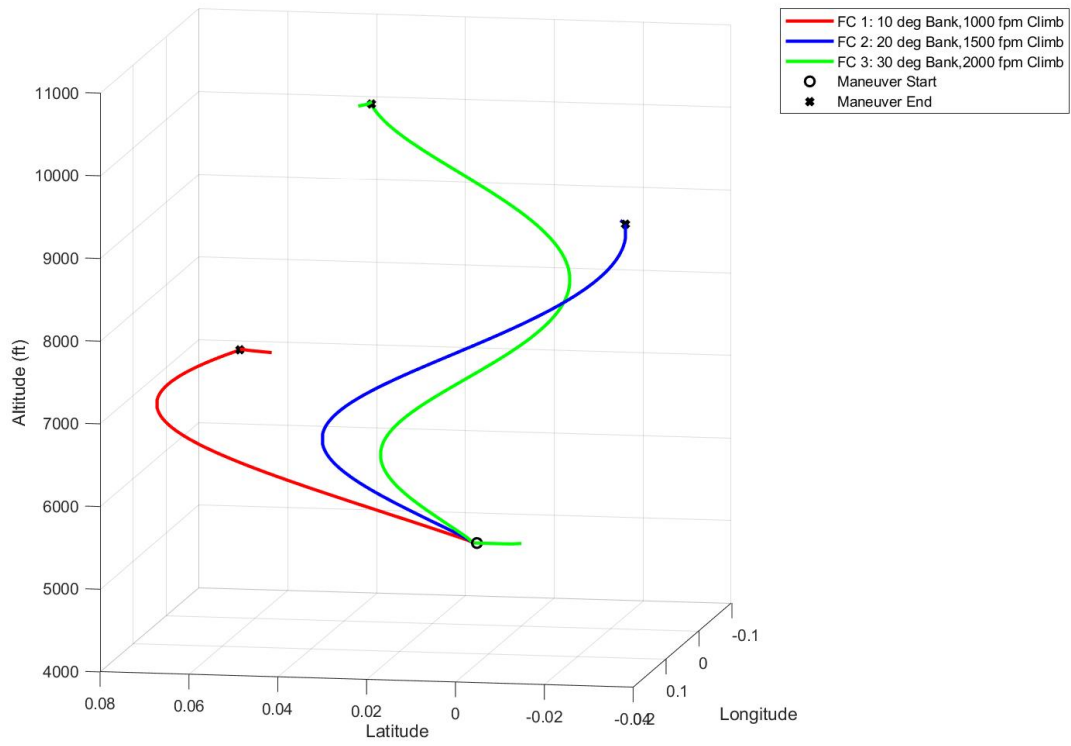
Figure 30. Baseline Climbing Spiral Maneuver

increases.
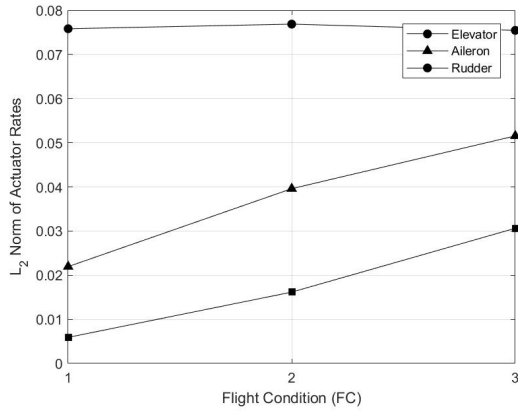
(a) $\mathcal{L}_2$ Norm of Actuator Rate
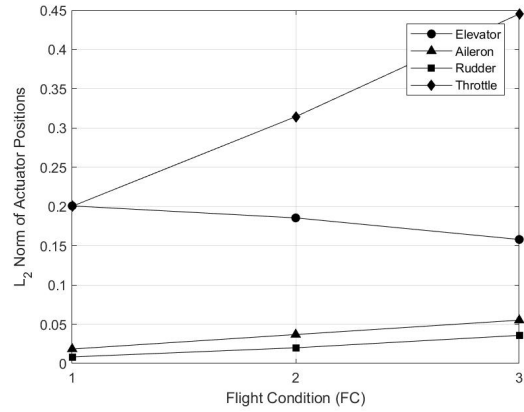
(b) $\mathcal{L}_2$ Norm of Actuator Position
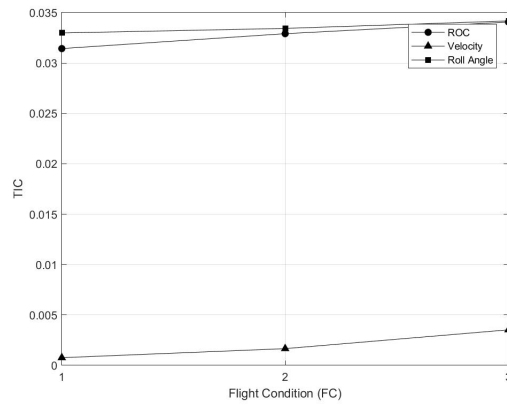
(c) TIC Values

Figure 31. Workload and Performance Metrics of Baseline Climbing Spiral

These actuator position and rate values indicate that performing the most aggressive climbing spiral maneuver, FC 3, takes slightly more work from the aileron and rudder, but primarily more throttle to achieve. Figure 31c shows the TIC values for roll angle, rate of climb, and velocity for the three flight conditions remain nearly constant across flight conditions.

After assessing the data, FC 3 was chosen as the nominals to be utilized moving forward with stability and control parameter scaling runs of the climbing spiral. As evidenced by the nearly identical $\mathcal{L}_2$ norms and TIC values across all flight conditions, FC 3 provides an ample level of aggressiveness in the turning spiral and still maintains

adequate aircraft performance throughout the maneuver.

4.2.2 Stability Parameter Scaling.

In order to assess how the stability and control parameters affect aircraft workload and performance, the four stability and control parameters M_q, $M_{\delta e}$, L_p, and $L_{\delta a}$ were scaled according to their values in Section 4.1.1. Subsequent runs were completed using Flight Condition 3: 2000 FPM climb and 30 degree bank angle.

4.2.2.1 M_q Scaling.

The first parameter M_q represents the pitching moment due to pitch rate, and was scaled by 0.25 x M_q, 1 x M_q, 2 x M_q, 4 x M_q, and 6 x M_q. Figure 32 shows the resulting five aircraft tracks plotted on a single graph. Visual inspection shows each of the tracks is nearly identical, a result of the non-precision, non-aggressive nature of the maneuver. However, important data can be gathered from the actuator positions and rates as well as the literal factors associated with the bare airframe dynamics.

Figure 33a is a view of how the $\mathcal{L}_2$ norm of elevator, aileron, and rudder actuator rates change with M_q scaling. For this particular plot, the elevator rate $\mathcal{L}_2$ norm steadily decreases as M_q is scaled: from 11% of its maximum elevator rate to about 6%. Figure 33b shows elevator, aileron, rudder, and throttle actuator positions stay nearly constant as M_q is scaled. Finally, Figure 33c depicts the TIC values of ROC, bank angle, and velocity as M_q is scaled. TIC of ROC appears to steadily increase as M_q is scaled, but the y-axis scale indicates it is a small amount. TIC of bank angle and TIC of velocity stay nearly constant.

Figure 34 presents a four pane of aircraft analysis graphs. Figure 34a and Figure 34b are two analysis plots from MIL-STD-1797 (Figures 44 and 45 in MIL-STD-1797, respectively). The bare airframe was plotted utilizing the aircraft literal factors
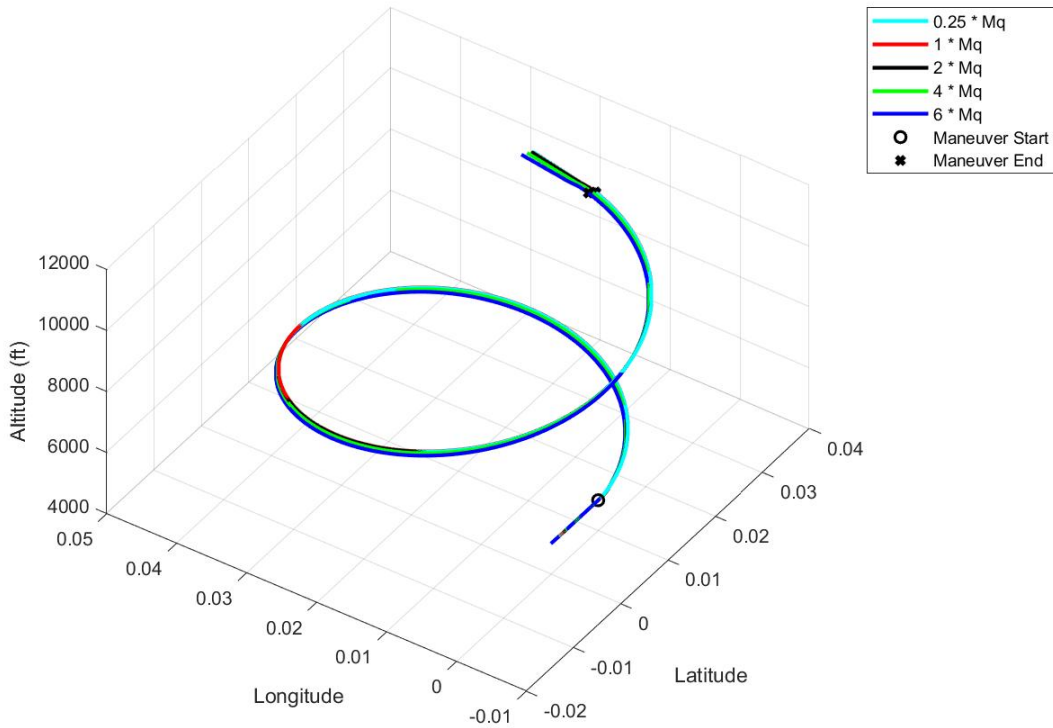
Figure 32. M_q **Scaled Climbing Spiral Maneuver**

derived from the LOES and aircraft level determined via boundaries set in MIL-STD-1797. According to the MIL-STD-1797 graphs, points 0.25 x M_q through 4 x M_q remain within Level 1 flying qualities, but 6 x M_q strays outside that bound. This is driven by the high ζ_{sp} value of 1.63, indicating the aircraft controls are very sluggish causing difficulty for the pilot to control the aircraft.

In addition to assessing the bare airframe dynamics based off of MIL-STD-1797 criteria, additional criteria were created to assess performance. In the case of Figure 34c, TIC is plotted vs ζ_{sp}, with ζ_{sp} boundaries for Level 1, 2, and 3 flying qualities from MIL-STD-1797. In this case, a high ζ_{sp} will cause the aircraft to be overdamped and not have the maneuverability to complete the task. A low ζ_{sp} will cause the aircraft to be borderline unstable, again unsuitable for the task. TIC then accounts
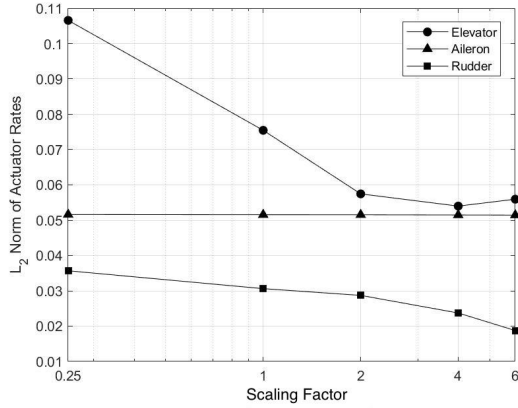
(a) $\mathcal{L}_2$ **Norm of Actuator Rate**
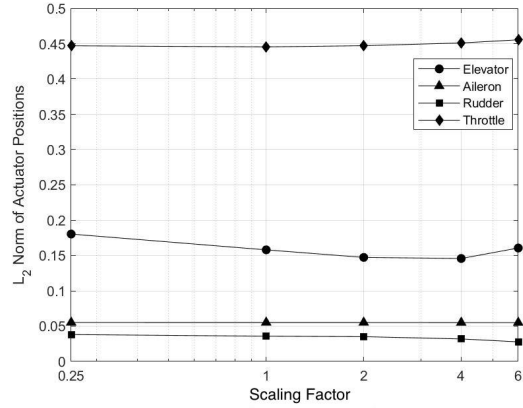
(b) $\mathcal{L}_2$ **Norm of Actuator Position**
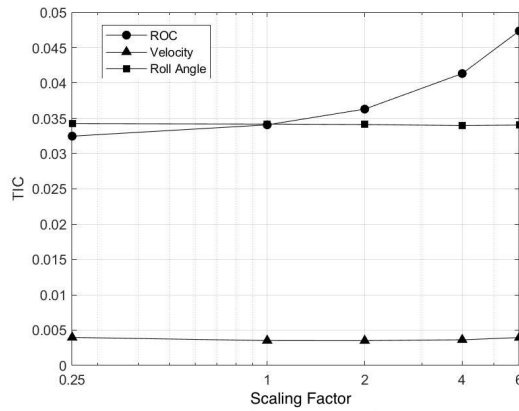
(c) **TIC Values**

Figure 33. Workload and Performance Metrics of M_q Scaled Climbing Spiral

for how well the aircraft performs the task, with cutoff points for Level 1 at a TIC of 0.15, Level 2 at 0.25, and Level 3 for any TIC values higher than 0.25. These numbers were chosen based on previous research by Kim [30] and are subject to modification as more data is gathered. The advantage of this plot is that it can identify what the aircraft designer needs to change when aircraft performance is unsatisfactory. If the TIC is acceptable but the ζ_{sp} is outside of the limits, then the bare airframe dynamics of the aircraft should be adjusted. If the bare airframe has good flying characteristics but the TIC is too high, then the controller needs to be modified to allow the aircraft to fly the mission task. Altering controller gains demonstrates the case of a high TIC

(a) $\omega_{sp}T_{\theta 2}$ **vs** ζ_{sp}

(b) **CAP vs** ζ_{sp}

(c) **TIC vs** ζ_{sp}

(d) $\mathcal{L}_2$ **Norm vs TIC ROC**
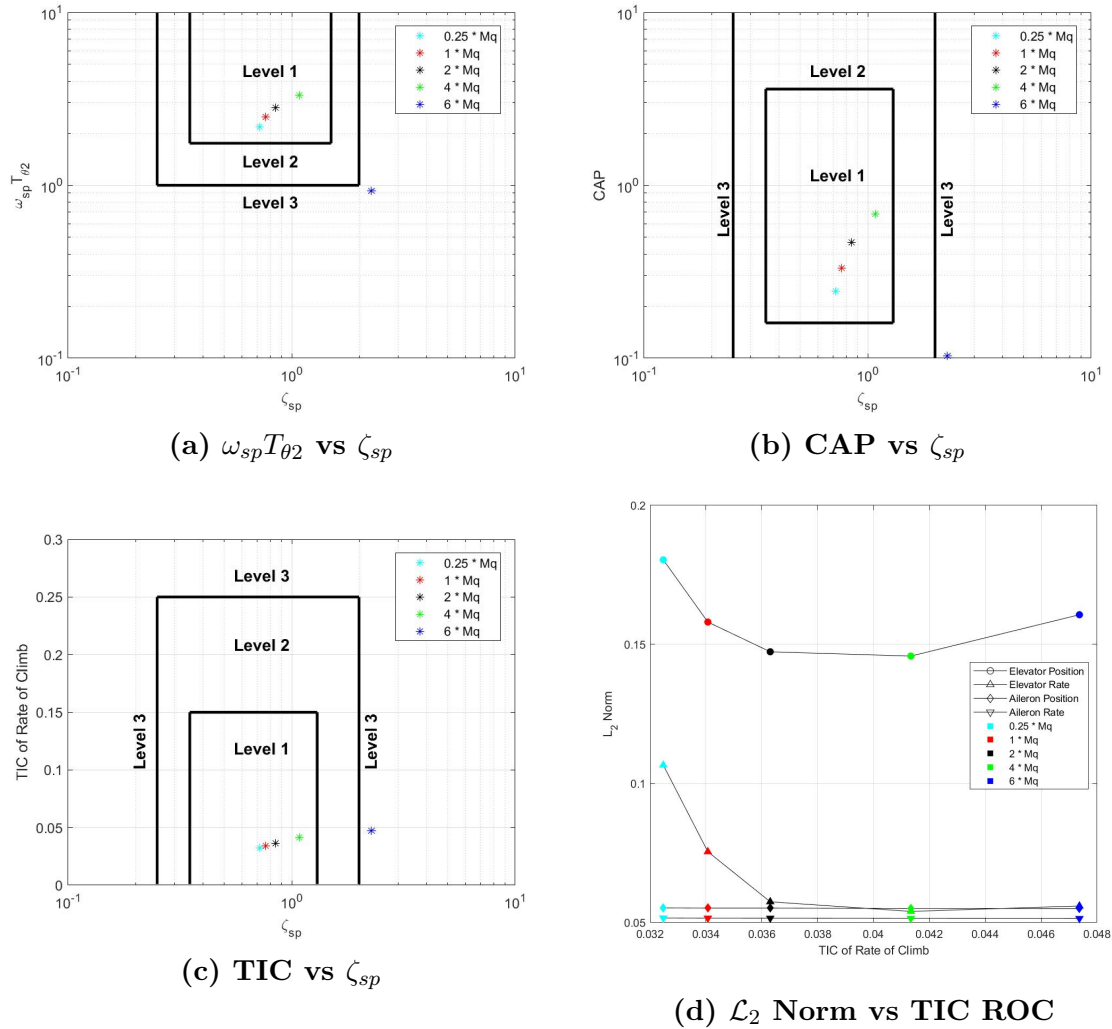
Figure 34. Flying Qualities Graphs of M_q Scaled Climbing Spiral

occurring with acceptable levels of ζ_{sp}.

In this particular case of scaling M_q, all values are within Level 1 limits with the exception of 6 x M_q, which has a ζ_{sp} of 1.63. Although the aircraft model exhibits acceptable performance of the maneuver, as indicated by a TIC value of around 0.05, the overdamped bare airframe will cause sluggish control. A more aggressive or more precise maneuver may not be possible with that bare airframe design.

Figure 34d was created in order to identify further trends in actuator positions and rates with parameter scaling. The colors depict which scaling factor was applied

for that data point, and the symbols represent either the aileron actuator or elevator actuator's $\mathcal{L}_2$ norm of rate or position. The plot provides a singular view of how scaling a specific stability and control parameter affects the workload of the actuators. It also gives perspective on how much more workload is being done and the corresponding performance at that workload. In this case of scaling M_q, the workload for the elevator actuator bottoms out at 2 x M_q to 4 x M_q. The low values for $\mathcal{L}_2$ norm of aileron actuator position and rate show that changes to M_q have no effect on aileron workload.

Figure 34d highlights a weakness of TIC. On the x-axis is TIC of ROC, which indicates Level 1 flying qualities for all scaled values of M_q. Yet the MIL-STD-1797 plots, which utilize the literal factor ζ_{sp}, indicate Level 3 flying qualities for 6 x M_q. Both are correct, as a ζ_{sp} of 1.63 is too high and Figure 32 shows aircraft performance is satisfactory during the climbing maneuver. But because the climbing turn is a benign maneuver, a high ζ_{sp} will not effect performance, and hence provide a low TIC value. The MIL-STD-1797 graphs are based on bare airframe literal factors and applicable in all flight phases, indicating that for maneuvers requiring more aggression or precision the aircraft will display Level 3 flying qualities at 6 x M_q. TIC, on the other hand, does not take bare airframe dynamics into account, and therefore satisfactory performance during a non-precision, non-aggressive maneuver, should not be extrapolated to precision or aggressive maneuvers. A designer can avoid this pitfall by utilizing the hybrid Figure 34c, which incorporates the both critical bare airframe literal factor ζ_{sp} and aircraft performance for that particular maneuver.

4.2.2.2 $M_{\delta e}$ Scaling.

The next parameter scaled was $M_{\delta e}$, the pitching moment due to elevator deflection, and was scaled by 0.25 x $M_{\delta e}$, 0.75 x $M_{\delta e}$, 1 x $M_{\delta e}$, 1.25 x $M_{\delta e}$, and 1.5 x $M_{\delta e}$.

Figure 35 depicts the resulting climbing turn while scaling $M_{\delta e}$.
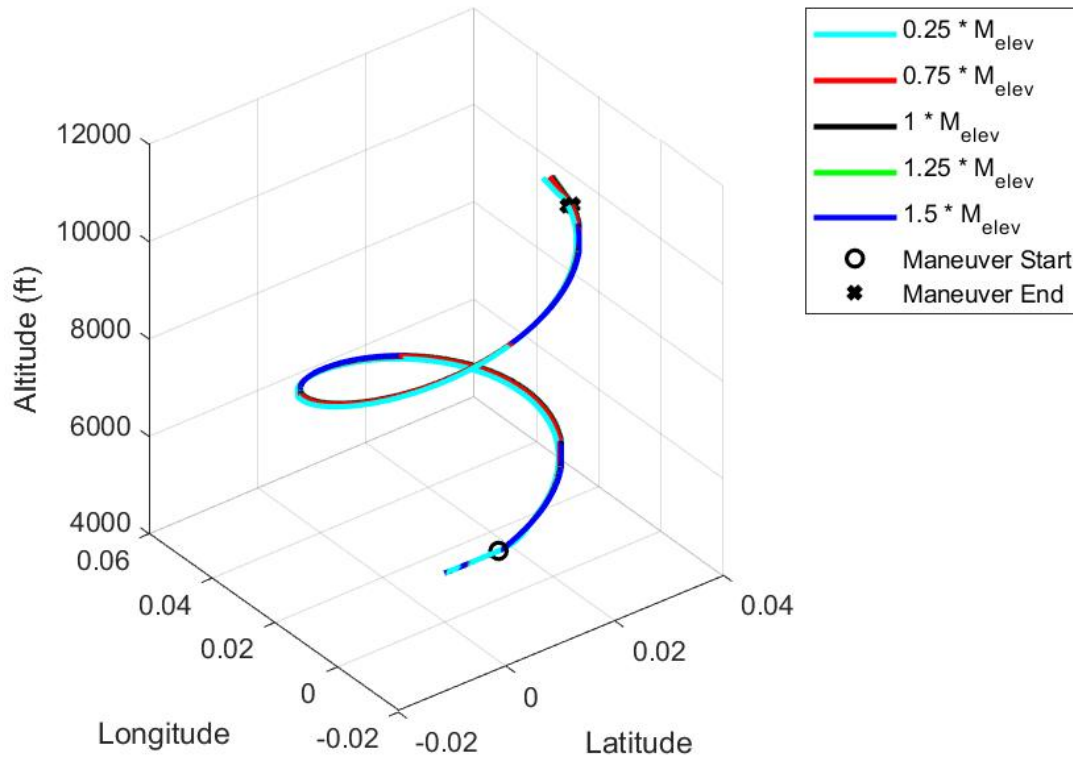
Figure 35. M_{δ_e} **Scaled Climbing Spiral Maneuver**

Figure 36a and Figure 36b show an interesting interaction between elevator actuator rates and positions as $M_{\delta e}$ is scaled. The $\mathcal{L}_2$ norm of elevator rate increases while the $\mathcal{L}_2$ norm of elevator position bottoms out at 0.75 x $M_{\delta e}$ and then steadily increases upward. The scaling of $M_{\delta e}$ essentially increases the effectiveness of the elevator, which explains the large drop off in $\mathcal{L}_2$ norm position between 0.25 x $M_{\delta e}$ and 0.75 x $M_{\delta e}$. TIC of ROC steadily decreases with increasing $M_{\delta e}$, but the changes are small. TIC of roll angle and TIC of velocity stay constant. In assessing these results, a designer could decrease elevator size by 25% (from 1 x $M_{\delta e}$ to 0.75 x $M_{\delta e}$) to limit the workload of the elevator while still maintaining adequate climbing turn performance.

The subfigures of Figure 37 all indicate Level 1 flying qualities for all values of
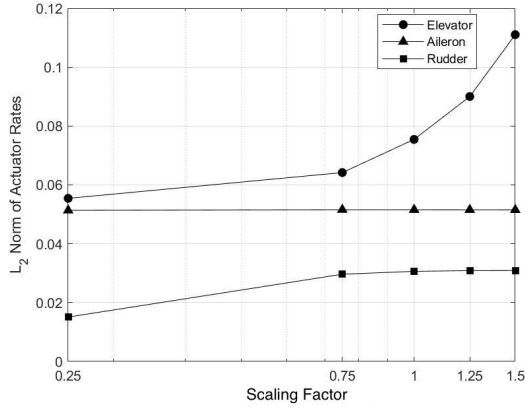
(a) $\mathcal{L}_2$ **Norm of Actuator Rate**
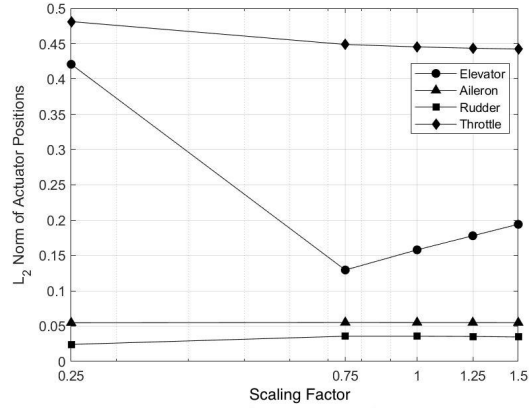
(b) $\mathcal{L}_2$ **Norm of Actuator Position**
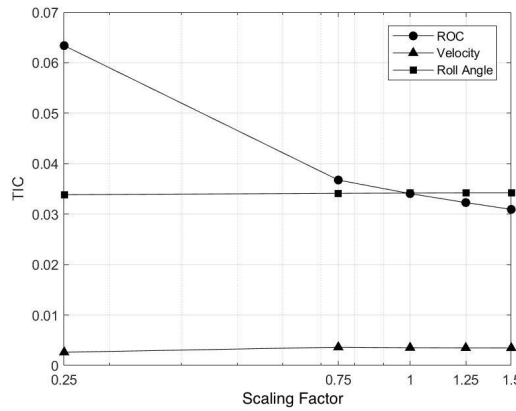
(c) **TIC Values**

Figure 36. Workload and Performance Metrics of $M_{\delta e}$ Scaled Climbing Spiral

$M_{\delta e}$. Figures 37a, 37b, and 37c all show a trends towards Level 2 flying qualities, but only on the graph of $\omega_{sp}T_{\theta 2}$ vs ζ_{sp} does 1.5 x $M_{\delta e}$ come close to that boundary. Figure 37d shows a high aileron actuator $\mathcal{L}_2$ norm at 0.25 x $M_{\delta e}$, but the TIC of ROC is relatively low regardless of scaling factor. The $\mathcal{L}_2$ norms of elevator actuator rate also remain low across the board, indicating once the proper deflection is achieved for the bank and climb, the controller only needs to make small changes to maintain good performance. Another point to note is the consistent low values for $\mathcal{L}_2$ norm of aileron actuator position and rate, indicating the changes to $M_{\delta e}$ have no effect on aileron workload and thus no cross-coupling effects were present.

(a) $\omega_{sp}T_{\theta 2}$ vs ζ_{sp}

(b) CAP vs ζ_{sp}

(c) TIC vs ζ_{sp}

(d) $\mathcal{L}_2$ Norm vs TIC ROC
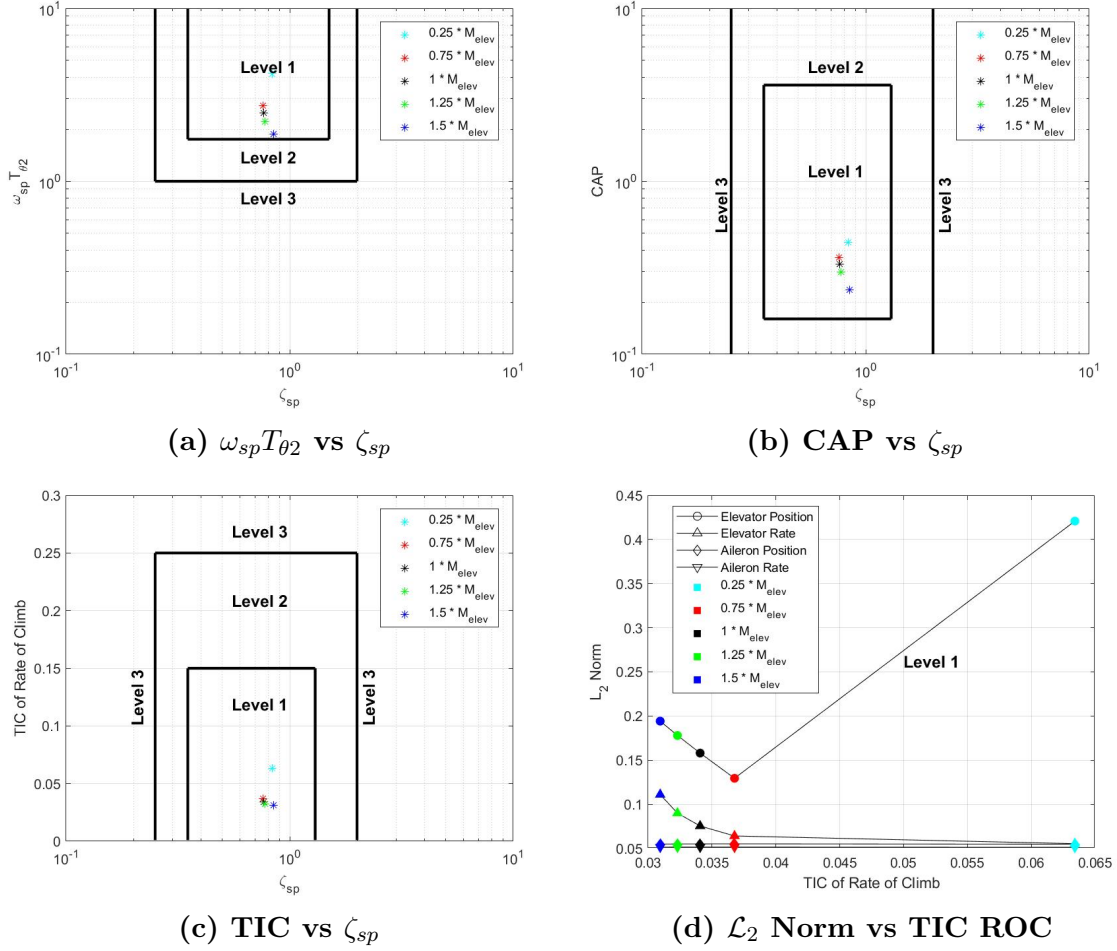
Figure 37. Flying Qualities Graphs of M_{δ_e} Scaled Climbing Spiral

4.2.2.3 L_p Scaling.

Next, the lateral stability parameter L_p representing the roll moment due to roll rate was scaled by 0.25 x L_p, 0.75 x L_p, 1 x L_p, 1.25 x L_p, and 1.50 x L_p. Figure 38 shows the resulting five aircraft courses plotted on a single graph. Due to the non-aggressive, non-precision nature of the maneuver, visual inspection of the five maneuvers appears to indicate similar results.

Despite the scaling of L_p, Figures 39a and 39b indicate the $\mathcal{L}_2$ norm of all actuator rates and positions stay relatively constant across the board. In addition, TIC values for ROC, velocity, and roll angle all remain nearly constant as well. This indicates
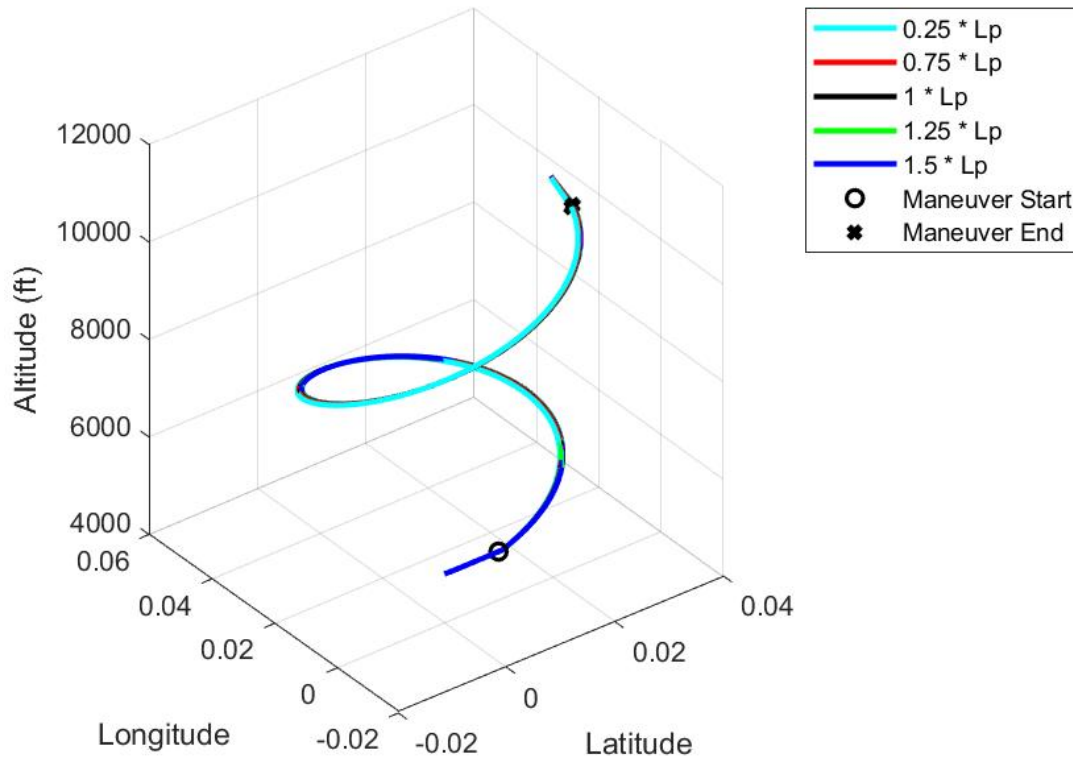
Figure 38. L_p **Scaled Climbing Spiral Maneuver**

that changes in L_p on the scales demonstrated appear to have little to no effect on the workload and performance of the LJ-25D in a climbing spiral maneuver.

4.2.2.4 $L_{\delta a}$ Scaling.

Finally, the lateral control parameter $L_{\delta a}$ was scaled by 0.5 x $L_{\delta a}$, 0.75 x $L_{\delta a}$, 1 x $L_{\delta a}$, 1.25 x $L_{\delta a}$, and 1.5 x $L_{\delta a}$. Figure 40 depicts the climbing maneuver with the scaled values of $L_{\delta a}$. Visual inspection of the graph indicates that there is a variation between each run, as the turns have a slightly wider radius with increasing $L_{\delta a}$. Whether or not that the wider turns are closer to the ideal bank angle of 30 degrees will have to be determined by the data.

Figure 41c shows that as $L_{\delta a}$ is scaled up, the TIC of roll angle decreases. Although
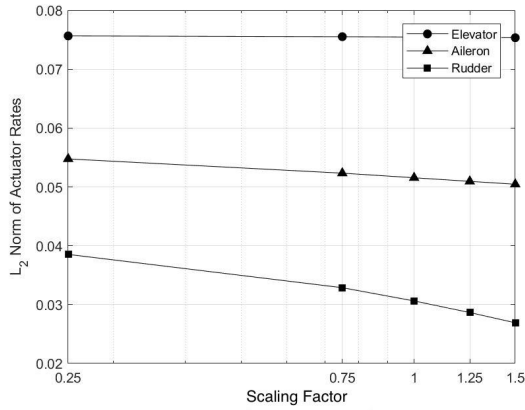
(a) $\mathcal{L}_2$ Norm of Actuator Rate
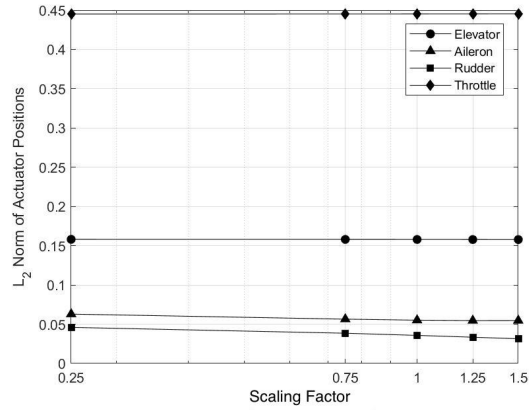
(b) $\mathcal{L}_2$ Norm of Actuator Position
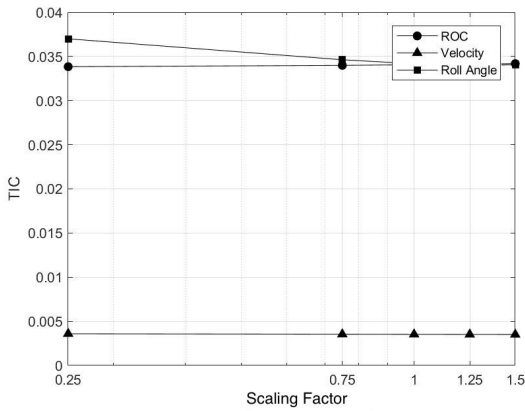
(c) TIC Values
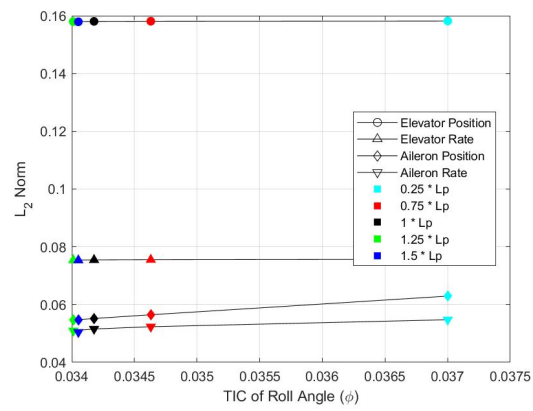
(d) $\mathcal{L}_2$ Norm vs TIC of Roll Angle

Figure 39. Workload and Performance Metrics of L_p Scaled Climbing Spiral

the difference in TIC of roll angle between 0.5 x $L_{\delta a}$ and 1.5 x $L_{\delta a}$ is only 0.01, this supports the notion that a larger control surface provides more control and can thus slightly increase aircraft turning performance in the climbing spiral maneuver. Figure 41d also affirms previous conclusions that larger control surfaces both decrease workload and increase turning performance. No improvements were seen in velocity tracking performance or ROC performance.
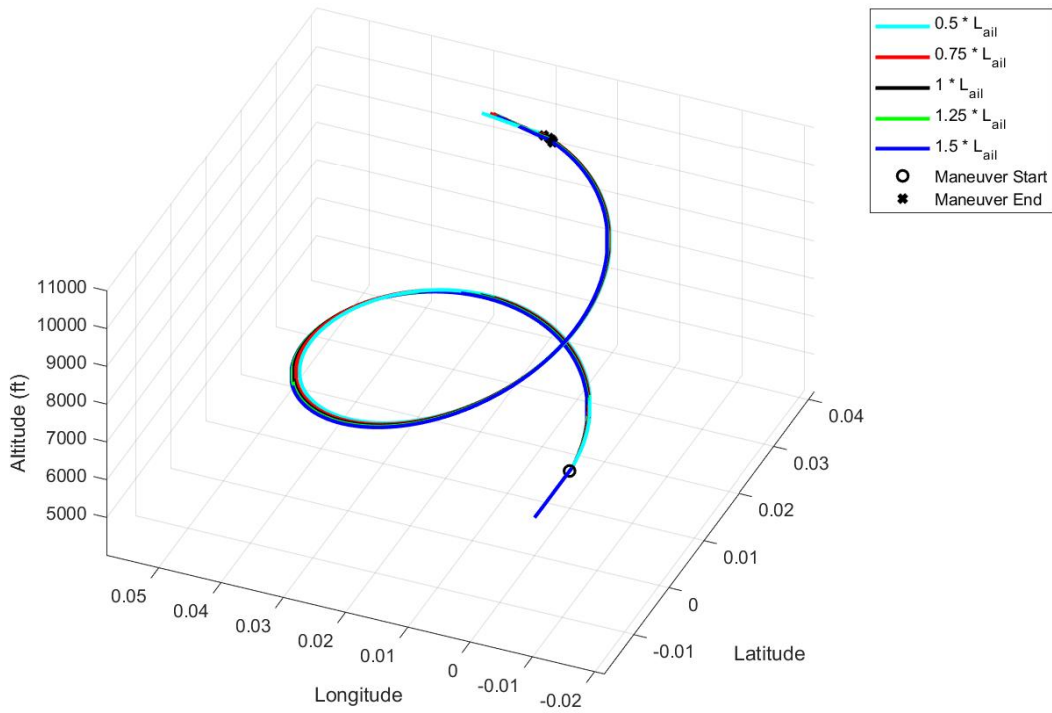
Figure 40. $L_{\delta a}$ **Scaled Climbing Spiral Maneuver**
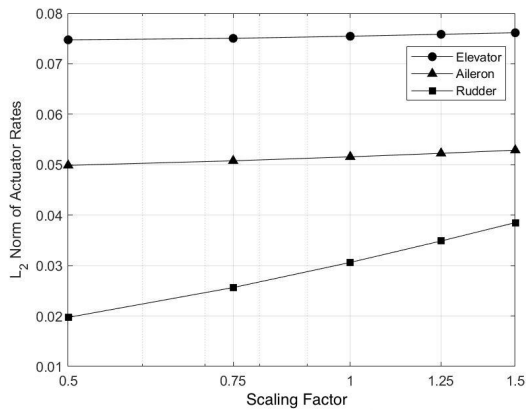
(a) $\mathcal{L}_2$ **Norm of Actuator Rate**

(b) $\mathcal{L}_2$ **Norm of Actuator Position**

(c) **TIC Values**

(d) $\mathcal{L}_2$ **Norm vs TIC of Roll Angle**

70
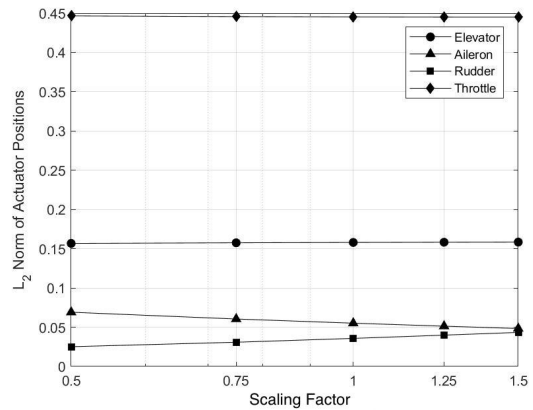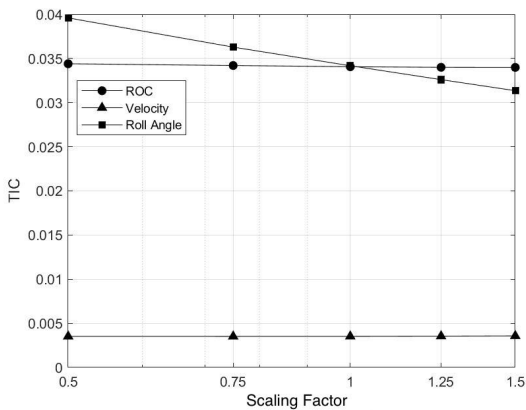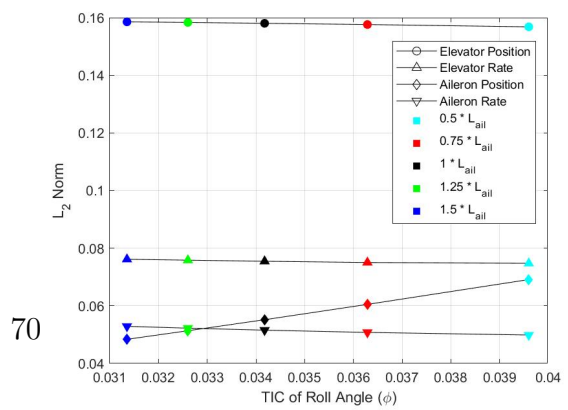
4.2.3   Longitudinal Controller Gain Scaling.

In addition to scaling stability and control parameters and observing their effects on performance and workload, controller gains were scaled to observe and compare the effects as well. For the climbing spiral maneuver, K_c, the proportional gain of the PID controller for rate of climb, was scaled according to Table 19. The high end value of 2.25 x K_c was chosen as it nears the limit of an uncontrollable aircraft.

Table 19. K_c **Scaling Factors for Climbing Turn**

Run Number	K_c Scaling Factor
1	0.25 x
2	0.5 x
3	1 x
4	2 x
5	2.25 x
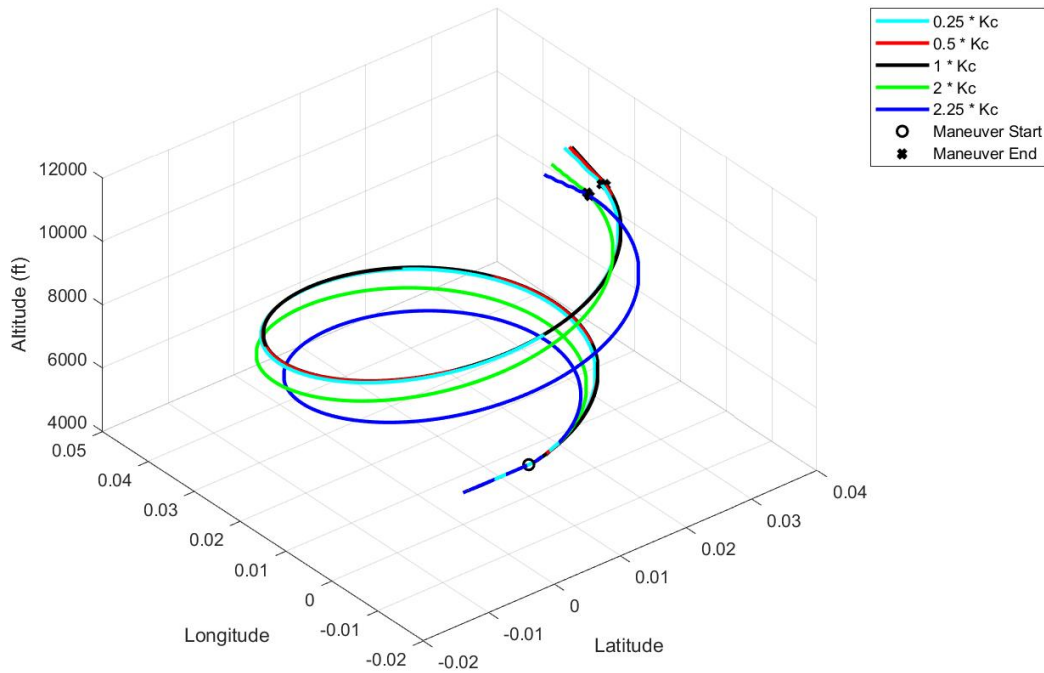
Figure 42. K_c **Scaled Climbing Spiral Maneuver**

Observing the visual tracks of the climbing spiral with K_c variations clearly in-

dicates varying performance levels, particularly at values of 2 x K_c and 2.25 x K_c. Figure 43a indicates that with changing the gains, the elevator actuator is more active at higher gains. Figure 43b shows elevator position also follows suit, and sees increases in workload at higher gain values. An interesting point is the change in throttle control, as the data indicates about a 20% throttle increase from the baseline 1 x K_c to the 2.25 x K_c run. In previous runs, throttle control stayed constant throughout the changes to all stability and control derivatives. Finally, Figure 43c indicates varying trends for the three TIC calculations. First, TIC ROC bottoms out at 1 x K_c, with higher values at both low and high gain changes. TIC velocity steadily increases with the scaling of K_c, indicating there were unforeseen consequences on the performance of the throttle controller. TIC roll angle remains constant throughout the maneuver.
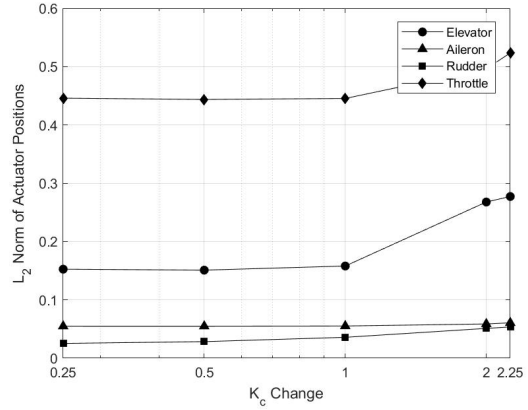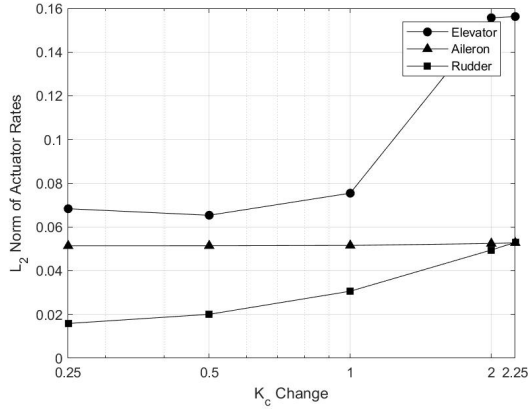
(a) $\mathcal{L}_2$ **Norm of Actuator Rate**

(b) $\mathcal{L}_2$ **Norm of Actuator Position**
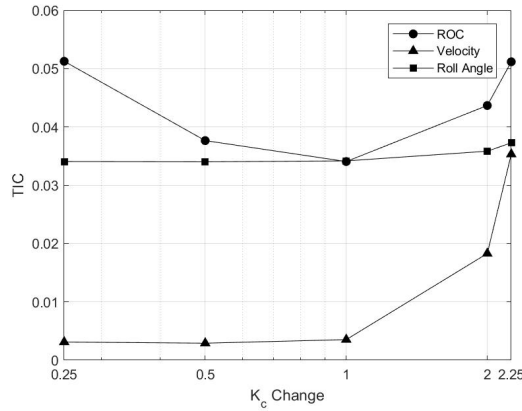
(c) **TIC Values**

Figure 43. Workload and Performance Metrics of K_c Scaled Climbing Spiral

Figures 44a and 44b show every point stacked on 2.25 x K_c because the bare airframe dynamics remain unchanged in this sequence. Figure 44c presents an interesting trend in TIC vs ζ_{sp} not previously observed. As K_c scales up, ζ_{sp} remains constant, but TIC of ROC increases. Therefore on a plot of TIC vs ζ_{sp}, large changes in TIC of ROC without an accompanying change in ζ_{sp} indicates to an aircraft designer that a change in the elevator controller is needed to increase aircraft performance. This idea will be further fortified with scaling of K_c during the side step maneuver.

(a) $\omega_{sp}T_{\theta2}$ vs ζ_{sp}

(b) CAP vs ζ_{sp}

(c) TIC vs ζ_{sp}

(d) $\mathcal{L}_2$ Norm vs TIC ROC
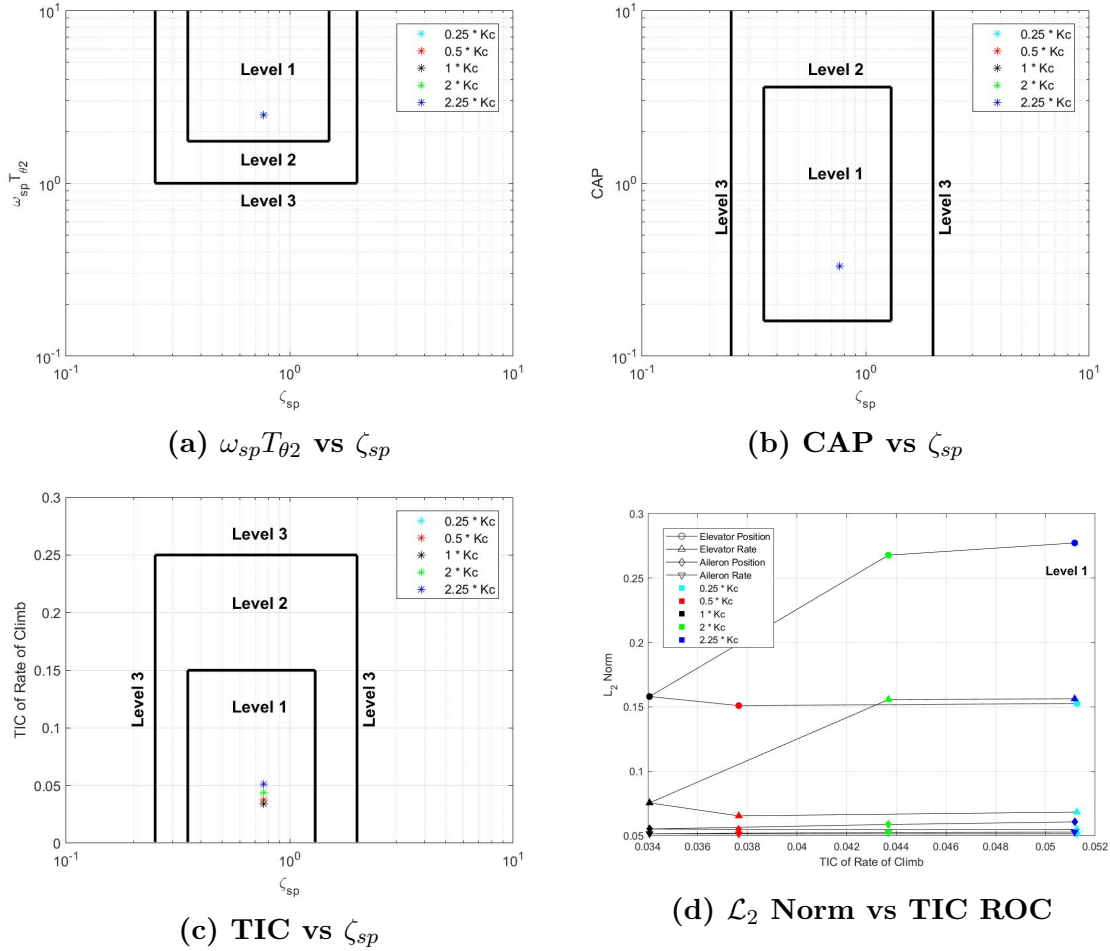
Figure 44. Flying Qualities Graphs of K_c Scaled Climbing Spiral

Lastly, Figure 44d shows another new trend in data, with the $\mathcal{L}_2$ norm of elevator position and rates showing a trade off between performance and workload. The highest performance, as indicated by the lowest TIC ROC value, is at 1 x K_c, but it is not the lowest workload. There is a slightly lower workload on 0.5 x K_c and 0.25 x K_c, but at the cost of a higher TIC. 2 x K_c and 2.25 x K_c are the worst cases, as workload increases and performance decreases. Therefore using Figure 44d, a designer could modify controller gains to weight aircraft performance or aircraft workload, as well as make a trade-off between the two.

4.3 Side Step Landing Analysis

The second maneuver assessed was the side step landing task. This precision, non-aggressive task requires both lateral and longitudinal tracking. Lateral tracking requires the use of aileron and rudder to center the aircraft on the runway and maintain proper heading, as well as elevator and throttle control to achieve a controlled descent and flare at the proper time.

4.3.1 Baseline Side Step Maneuver.

In order to properly gauge the results of scaling stability and control parameters, a baseline run was conducted to achieve datum values for workload and performance. The target parameters were 140 KIAS, 750 FPM descent rate, gear down and flaps at 10 degrees, as described in Section 3.2.2.2. Figures 45a and 45b show a perspective and top-down view, respectively, of the baseline side step maneuver.
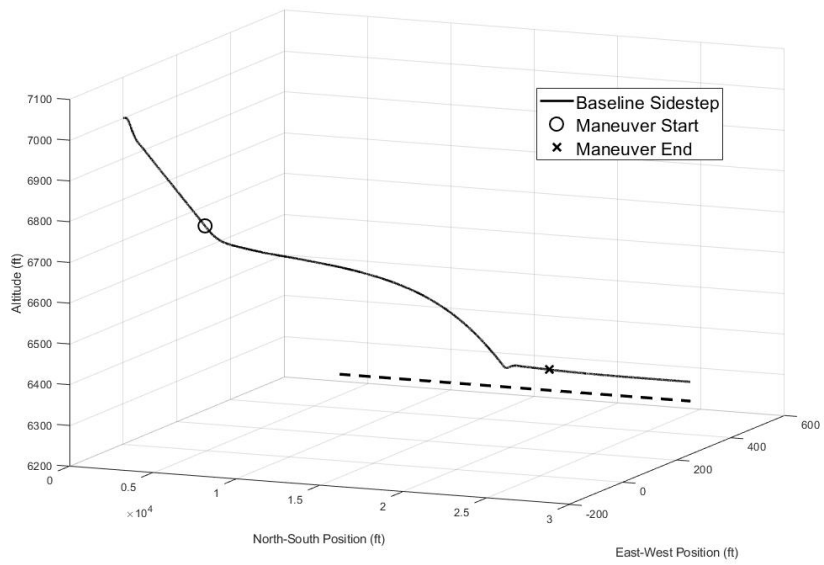
(a) Perspective View
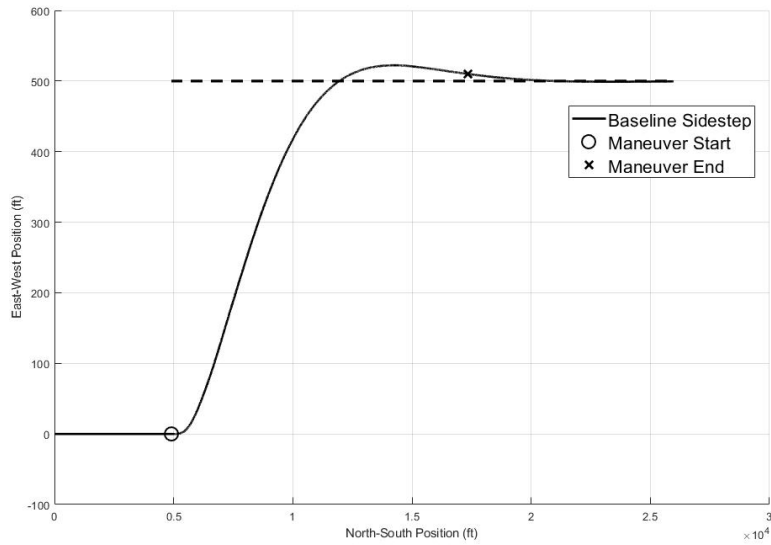
(b) Top-down View

Figure 45. Baseline Side Step Maneuver

4.3.2   Stability Parameter Scaling.

As part of the analysis of the side step maneuver, the stability and control param-
eters M_q, $M_{\delta e}$, L_p, and $L_{\delta a}$ were scaled according to their values in Section 4.1.1. The

simulations were utilized to calculate $\mathcal{L}_2$ norm and TIC values, and then assessed via MIL-STD-1797 and newly developed criteria.

4.3.2.1 M_q Scaling.

The first scaled parameter was M_q, representing the pitching moment due to pitch rate, and was scaled by 0.25 x M_q, 1 x M_q, 2 x M_q, 4 x M_q, and 6 x M_q. Figure 46 shows the resulting five aircraft tracks. The black circle represents the maneuver start point for all runs, where all $\mathcal{L}_2$ norm and TIC calculations begin, and each colored X in the figure represents where each individual run ended, and thus all $\mathcal{L}_2$ norm and TIC calculations stop. The finality criterion was determined according to parameters explained in Section 3.2.2.2.
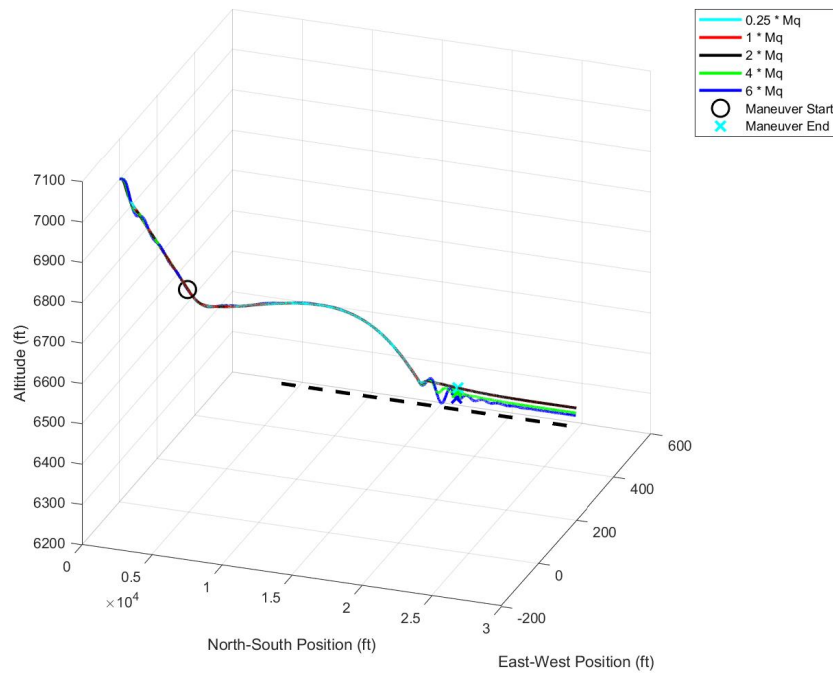
(a) Perspective View
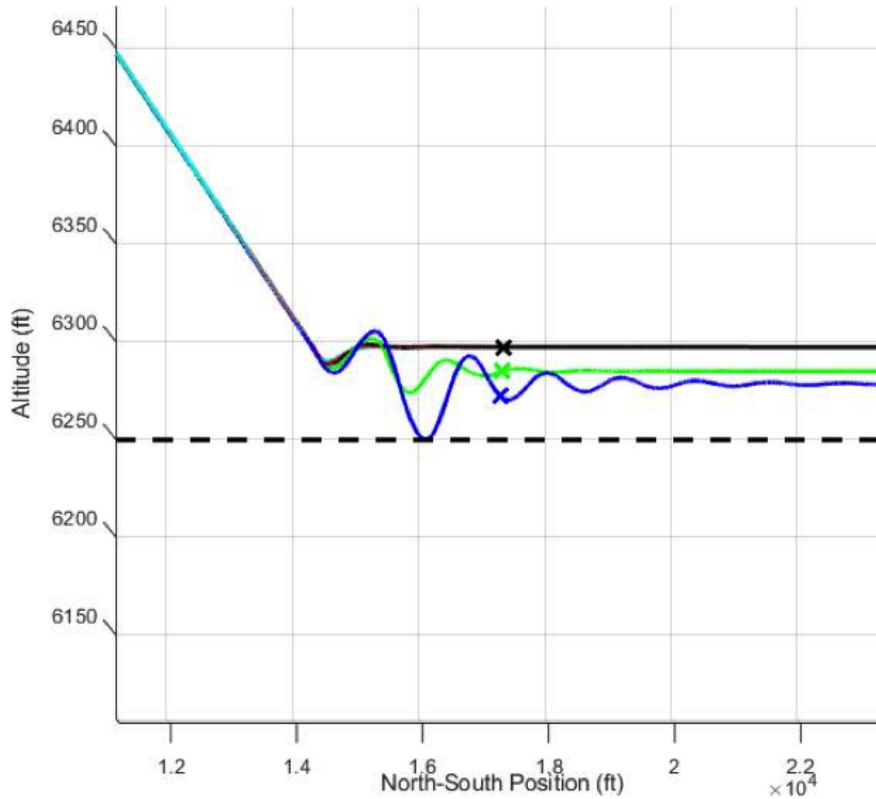
(b) Side View

Figure 46. M_q **Scaled Side Step Maneuver**

Figure 47 shows the workload and performance of the LJ-25D during the side step maneuver. First, $\mathcal{L}_2$ norms for aileron and rudder remain unaffected with changes to M_q. Elevator workload varies non-linearly, as evidenced by the elevator curves in both Figure 47a and Figure 47b. There is a local minimum at 2 x M_q for $\mathcal{L}_2$ norm of elevator rate, but despite this valley, $\mathcal{L}_2$ norm of elevator position always grows as M_q increases. This matches the trend with TIC of ROC, which steadily increases with increasing M_q. TIC of velocity stays at nearly zero for all runs, indicating good velocity tracking at all values of M_q. For the side step maneuver no TIC of roll angle is calculated because lateral distance was utilized as the command input. To avoid an overly complex controller, only one tracking input was made to the aileron controller. The results in Figure 47 present the aircraft designer with the ability to alter M_q

78

between 0.25 x to 2 x the current values with minimal effect on ROC performance.

(a) $\mathcal{L}_2$ Norm of Actuator Rate

(b) $\mathcal{L}_2$ Norm of Actuator Position

(c) TIC Values
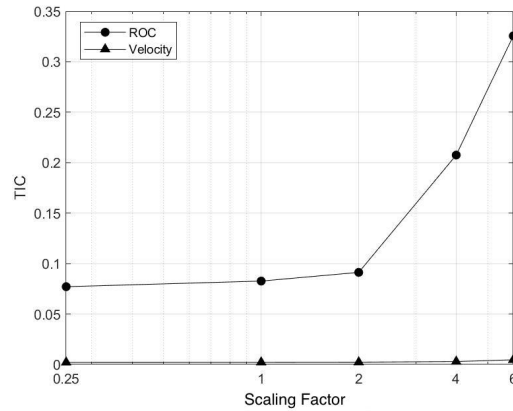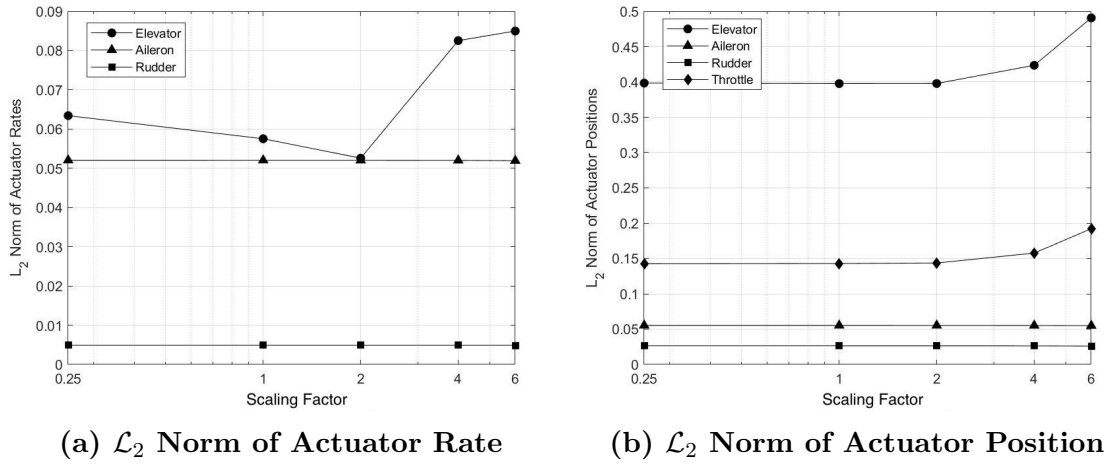
Figure 47. Workload and Performance Metrics of M_q Scaled Side Step

MIL-STD-1797 charts present a similar conclusion that longitudinal flying perfor-
mance steadily decreases with increasing M_q. Figures 48a and 48b have 4 x M_q and
6 x M_q well beyond Level 2 flying qualities limits. Figures 48c and 48d concur with
conclusions of the MIL-STD-1797 criteria. The values for 0.25 x M_q, 1 x M_q, and 2
x M_q all remain well within the Level 1 flying qualities boundaries, while 4 x M_q and
6 x M_q stray outside to Level 3. Figure 48c indicates that 4 x M_q is unsatisfactory
based on the ζ_{sp} limits and 6 x M_q is unsatisfactory due to both TIC of ROC and
ζ_{sp}. Figure 48d shows that based on $\mathcal{L}_2$ norm values and TIC values, the aircraft is

on the verge of Level 3 flying qualities at high values of M_q. The results of scaling M_q during the side step maneuver shows that mathematical tools such TIC and $\mathcal{L}_2$ norm can provide an alternative classification of flying qualities levels to the classical literal factors in MIL-STD-1797.

(a) $\omega_{sp}T_{\theta 2}$ vs ζ_{sp}

(b) CAP vs ζ_{sp}

(c) TIC vs ζ_{sp}

(d) $\mathcal{L}_2$ Norm vs TIC ROC
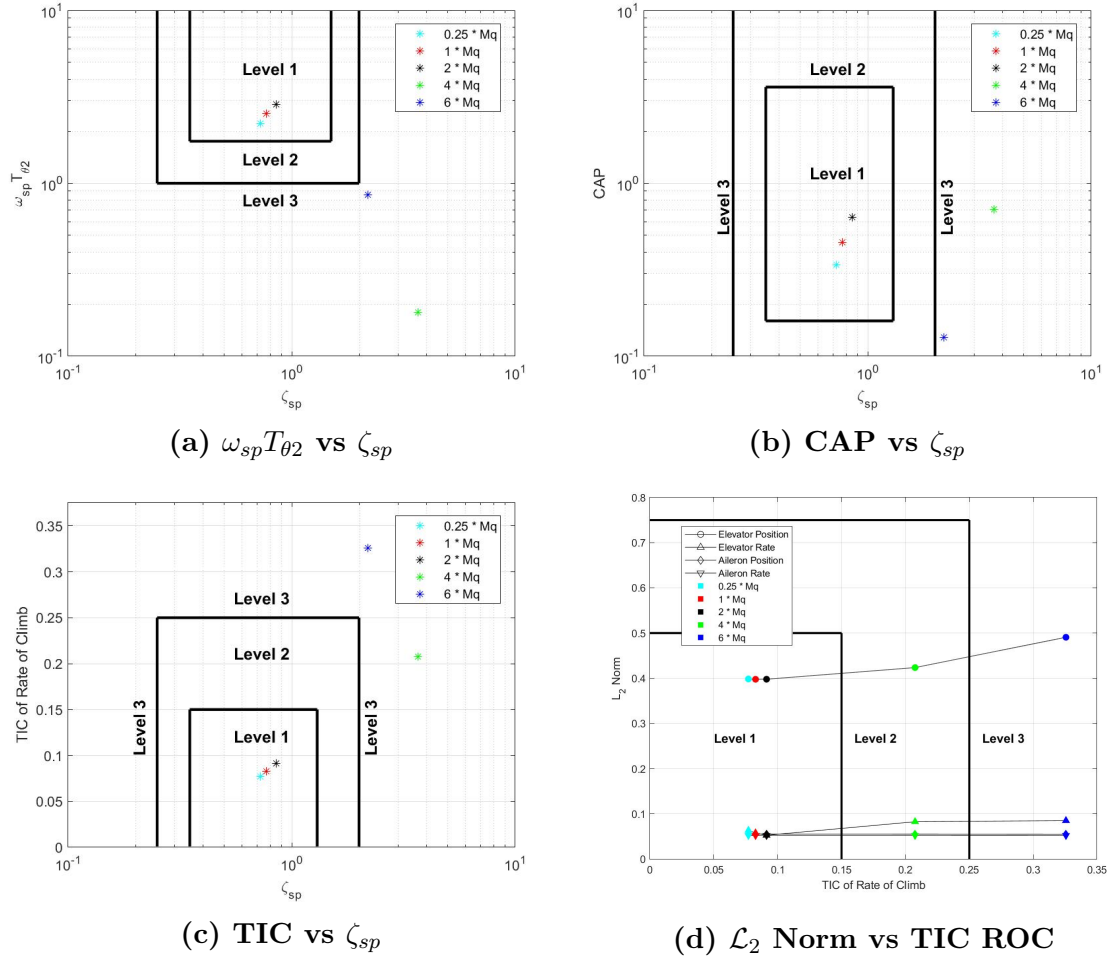
Figure 48. Flying Qualities Graphs of M_q Scaled Side Step

4.3.2.2 $M_{\delta e}$ Scaling.

The next parameter assessed during the side step maneuver was $M_{\delta e}$, scaled by 0.25 x $M_{\delta e}$, 0.75 x $M_{\delta e}$, 1 x $M_{\delta e}$, 1.25 x $M_{\delta e}$, and 1.5 x $M_{\delta e}$. Figure 49 depicts the side step maneuver while scaling $M_{\delta e}$.
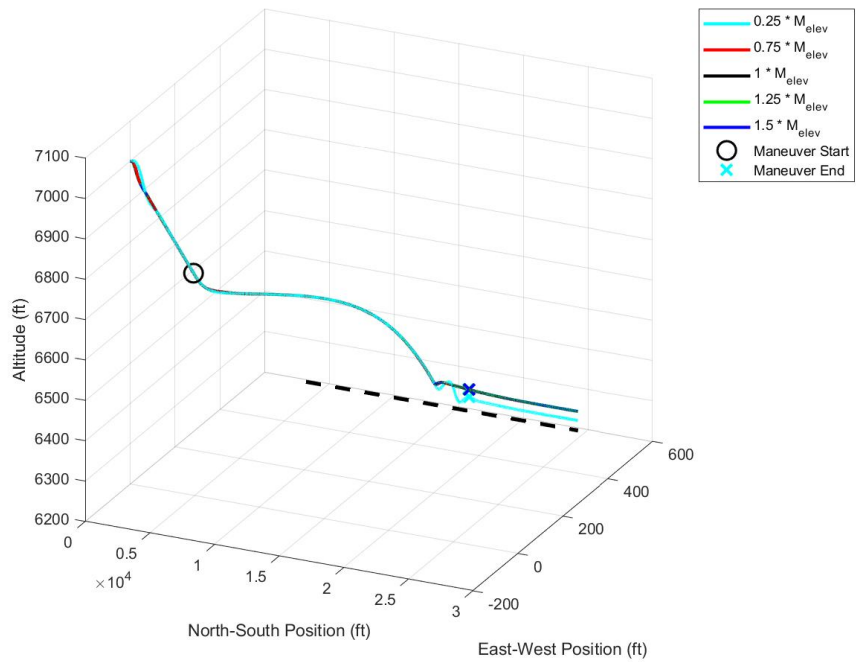
(a) Perspective View
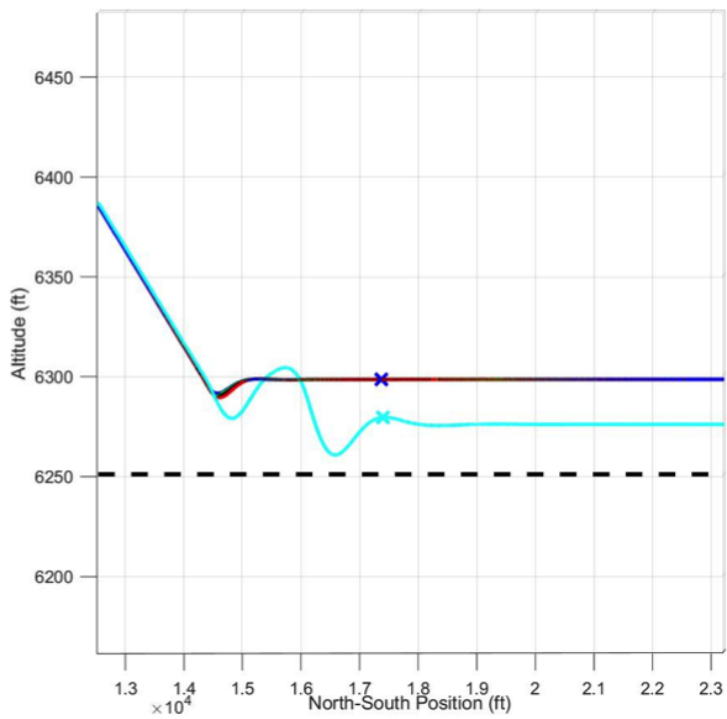
(b) Side View

Figure 49. M_{δ_e} Scaled Side Step Maneuver

81

0.75 x $M_{\delta e}$ to 1.5 x $M_{\delta e}$ all have similar path performance throughout the maneuver, but 0.25 x $M_{\delta e}$ has noticeably more overshoot and steady-state error as compared to the other runs. This is confirmed in the data shown in Figure 50c, which indicates a large drop off in TIC from 0.25 x $M_{\delta e}$ to 0.75 x $M_{\delta e}$. A similar trend is depicted in Figures 50a and 50b, which exhibit a minimum workload at 0.75 x $M_{\delta e}$. Workload then increases from 0.75 x $M_{\delta e}$ to 1.5 x $M_{\delta e}$, with a slight increase in performance as well. The trends would give an aircraft designer the option to increase performance slightly at the expense of a higher elevator actuator workload.
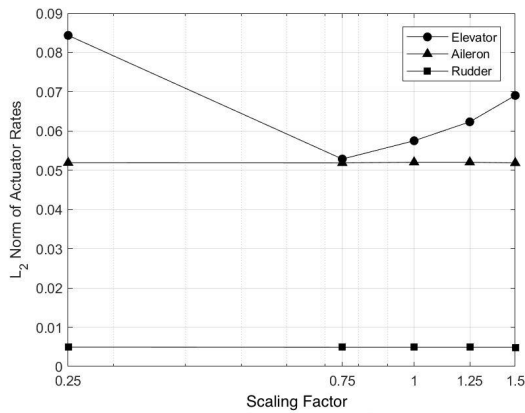
(a) $\mathcal{L}_2$ **Norm of Actuator Rate** (b) $\mathcal{L}_2$ **Norm of Actuator Position**
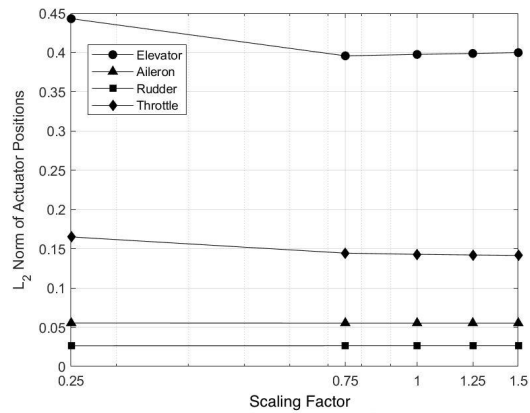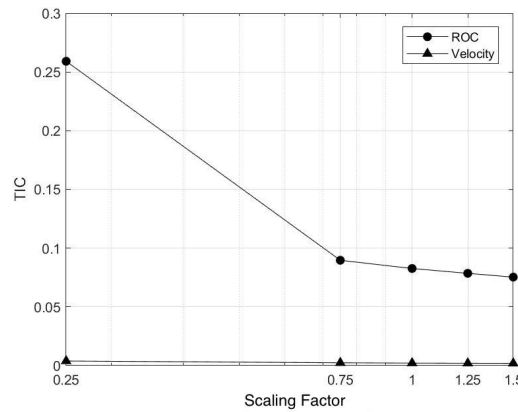
(c) **TIC Values**

Figure 50. Workload and Performance Metrics of $M_{\delta e}$ Scaled Side Step

The subfigures of Figure 51 show an interesting dynamic when comparing the

MIL-STD-1797 results to the developed graphs. 0.25 x $M_{\delta e}$, which is Level 1 in Figures 51a and 51b, is Level 3 in Figure 51d due to the high TIC value for ROC. The opposite is true for 1.5 x $M_{\delta e}$, in which Figures 51a and 51b identify the point as Level 3, with a ζ_{sp} of 6.7, but Figure 51d indicates the configuration is Level 1. Figure 51c, which combines aspects of the MIL-STD-1797 literal factors and the TIC performance metric, correctly identifies both 0.25 x $M_{\delta e}$ and 1.5 x $M_{\delta e}$ as Level 3. This further supports the notion of classifying UAV handling qualities using aspects of the literal factors criteria in MIL-STD-1797 and new criterion such as TIC.

(a) $\omega_{sp}T_{\theta 2}$ vs ζ_{sp}

(b) CAP vs ζ_{sp}

(c) TIC vs ζ_{sp}

(d) $\mathcal{L}_2$ Norm vs TIC ROC
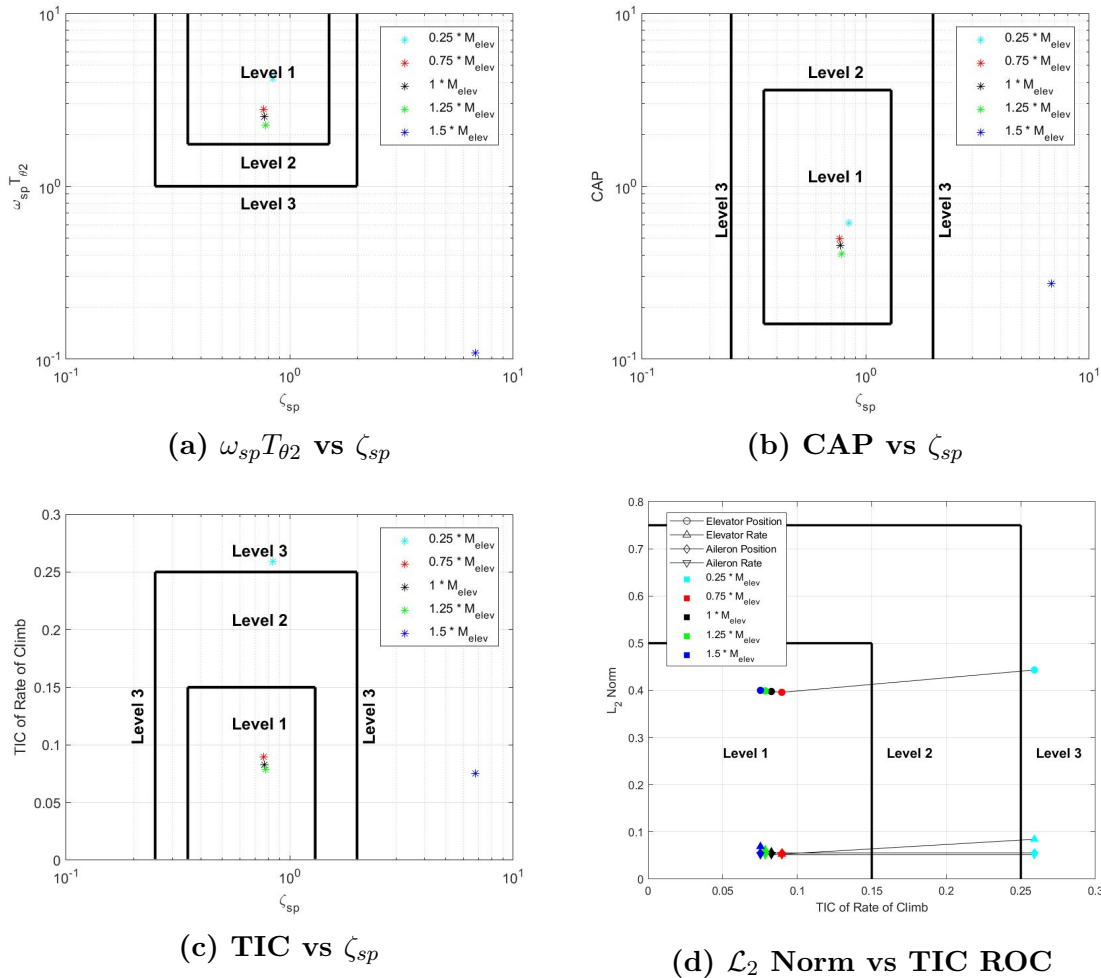
Figure 51. Flying Qualities Graphs of $M_{\delta e}$ Scaled Side Step

4.3.2.3 L_p Scaling.

The lateral stability parameter L_p representing the roll moment due to roll rate was scaled by 0.25 x L_p, 0.75 x L_p, 1 x L_p, 1.25 x L_p, and 1.50 x L_p. Figure 52 shows the resulting aircraft tracks. When observing the top-down view shown in Figure 52b, its clear the 0.25 x L_p has degraded performance when approaching the runway, and continues on a limit cycle of approximately $\pm$ 10 feet when centered on the runway.
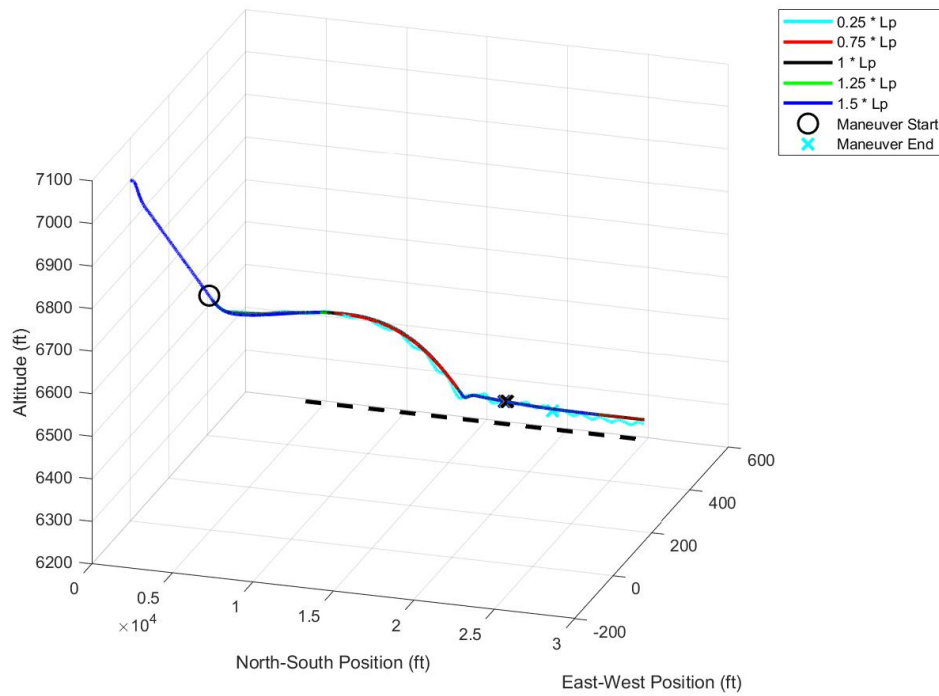
(a) Perspective View
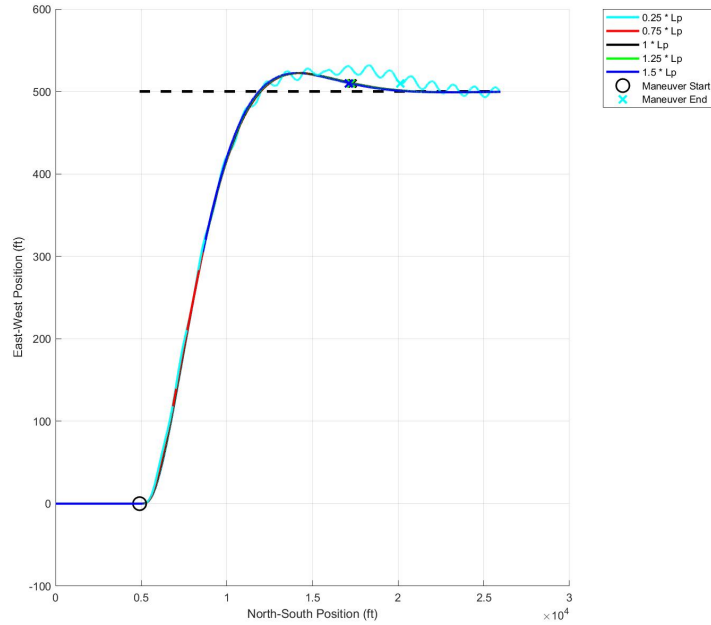
(b) Top-down View

Figure 52. L_p **Scaled Side Step Maneuver**

The poor performance of 0.25 x L_p evident in Figure 52 manifests itself in the $\mathcal{L}_2$ norm of aileron actuator position and rate. The high $\mathcal{L}_2$ norm values for aileron in Figures 53a and 53b for 0.25 x L_p drop off at 0.75 x L_p, where the $\mathcal{L}_2$ norm and TIC of ROC values remain relatively constant for the remainder of the scaling. Figure 53c indicates that the poor performance and high aileron workload put 0.25 x L_p into Level 2 flying qualities, informing the aircraft designer changes should be made. Another interesting point is that thus far cross-coupling effects between longitudinal and lateral have been negligible. Here, the lateral parameter L_p is effecting a longitudinal performance metric, TIC of ROC.
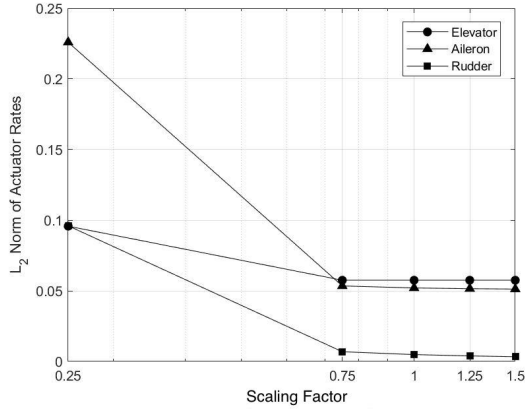
(a) $\mathcal{L}_2$ **Norm of Actuator Rate**
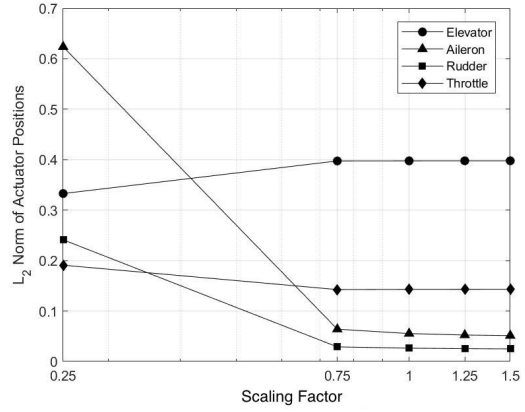
(b) $\mathcal{L}_2$ **Norm of Actuator Position**
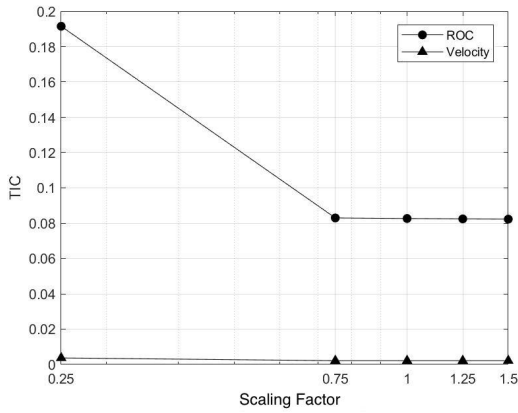
(c) **TIC Values**
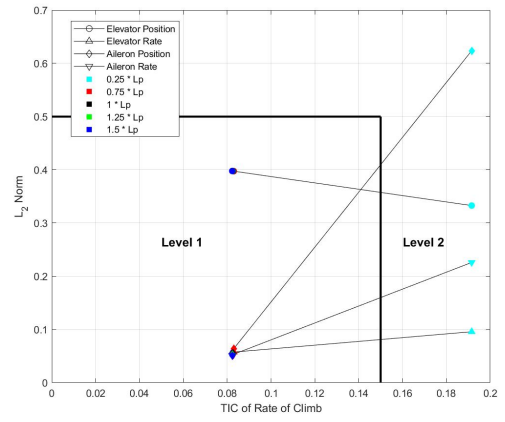
(d) $\mathcal{L}_2$ **Norm vs TIC of Roll Angle**

Figure 53. Workload and Performance Metrics of L_p Scaled Side Step Maneuver

4.3.2.4 $L_{\delta a}$ **Scaling.**

Lastly, the control parameter $L_{\delta a}$ was scaled by 0.5 x $L_{\delta a}$, 0.75 x $L_{\delta a}$, 1 x $L_{\delta a}$, 1.25 x $L_{\delta a}$, and 1.5 x $L_{\delta a}$. Figure 54 depicts the side step maneuver from a perspective view and a top-down view. First glance indicates there is satisfactory performance for all scaled values, with the exception of slightly increasing lateral overshoot as $L_{\delta a}$ is increased.

86
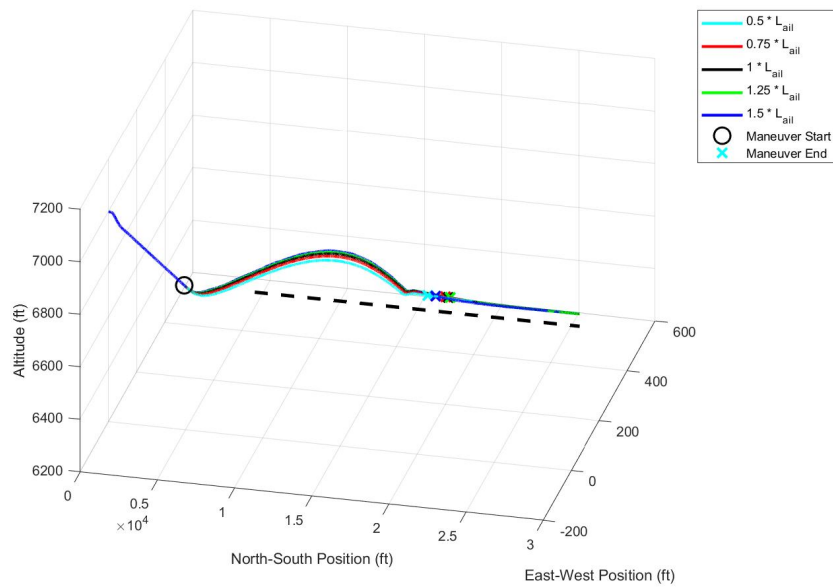
(a) Perspective View
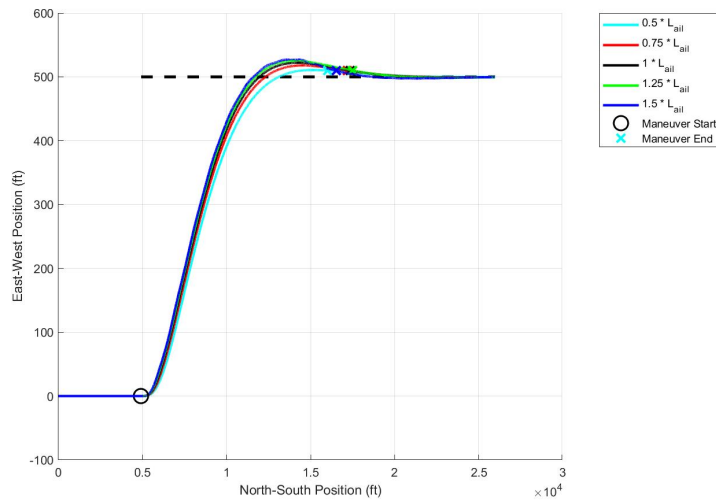
(b) Top-down View

Figure 54. L_{δ_a} **Scaled Side Step Maneuver**

Figures 55a and 55b show that the workload continually increases a small amount for rudder and aileron as L_{δ_a} is scaled up. Figure 55c indicates that the TIC values for both ROC and velocity stay relatively constant despite the changes to $L_{\delta a}$. Overall, the scaling to $L_{\delta a}$ negligibly changed aircraft performance and workload during the

side step landing maneuver.
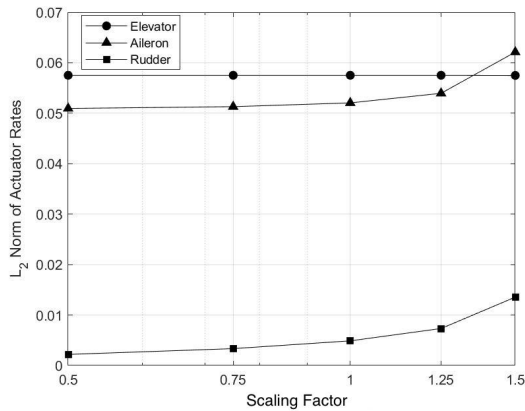
(a) $\mathcal{L}_2$ Norm of Actuator Rate
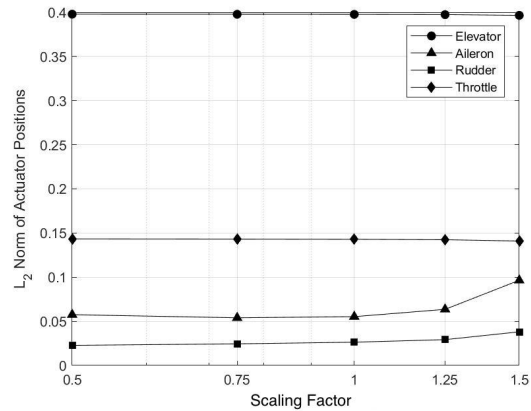
(b) $\mathcal{L}_2$ Norm of Actuator Position
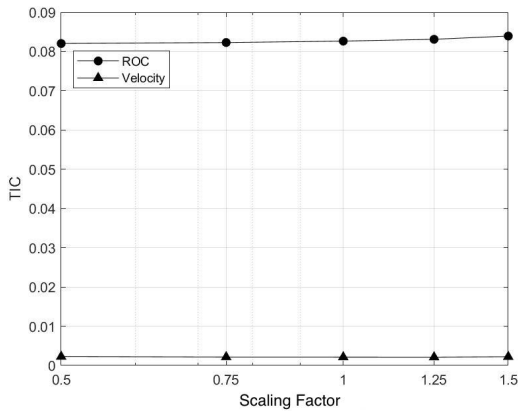
(c) TIC Values
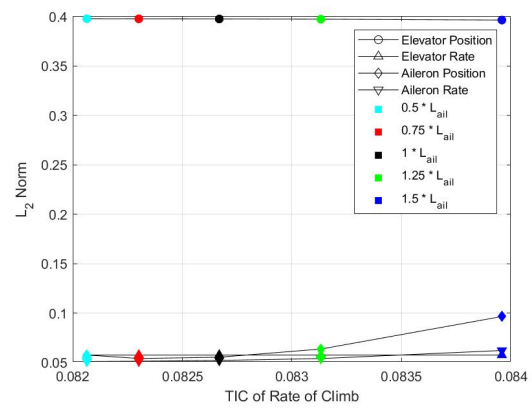
(d) $\mathcal{L}_2$ Norm vs TIC of Roll Angle

Figure 55. Workload and Performance Metrics of $L_{\delta a}$ Scaled Side Step Maneuver

4.3.3   Lateral Controller Gain Scaling.

In addition to scaling the stability and control parameters, the gains on the lateral controller were also scaled. K_c, the gain on the lead compensator tracking the side step distance, was scaled by the values shown in Table 20. The values were chosen to represent a system that started overdamped and steadily transitioned to being underdamped. The same aircraft workload and performance parameters of $\mathcal{L}_2$ norm and TIC were then calculated for each maneuver and an analysis was completed. Figure 56 shows the resulting tracks of the K_c scaled side step maneuvers.

88

Table 20. K_c **Scaling Factors for Side Step Maneuver**

Run Number	K_c Scaling Factor
1	0.5 x
2	1 x
3	2 x
4	3.5 x
5	4.5 x
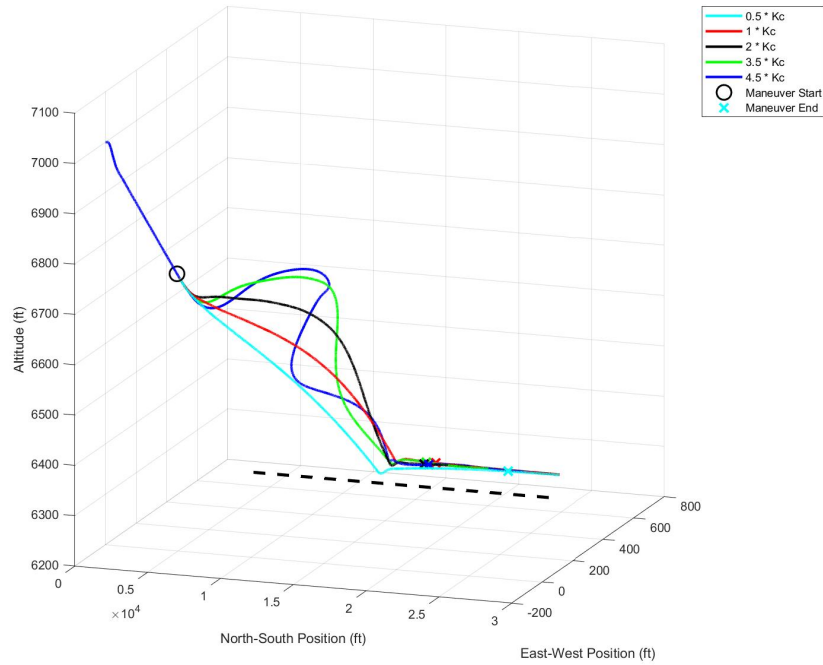
(a) Perspective View
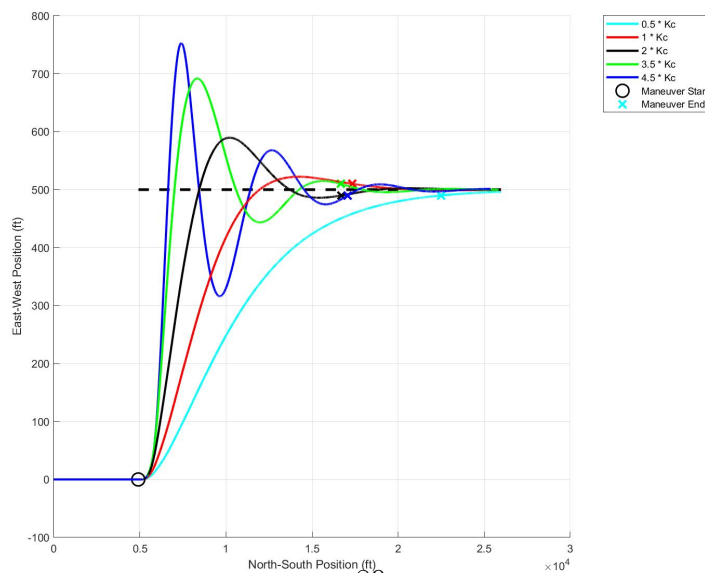
(b) Top-down View

Figure 56. K_c **Scaled Side Step Maneuver**

Observing the top-down view in Figure 56b indicates that 0.5 x K_c is clearly overdamped, while 2 x K_c and 3.5 x K_c are underdamped and 4.5 x K_c is on the verge of instability. The graphs in Figures 57a and 57b show that workload is steadily increasing for all control surfaces as K_c increases. TIC value of rate of climb also steadily climbs, which is the second instance during the side step maneuver that a change to a lateral parameter affected longitudinal performance.
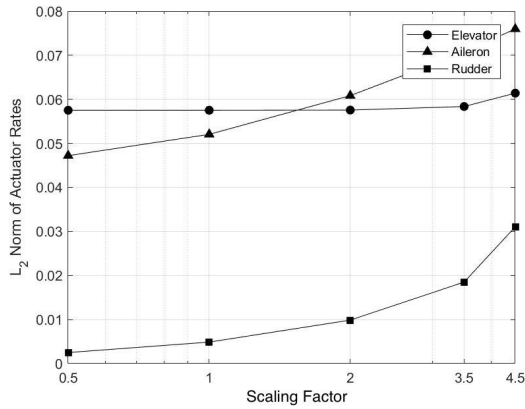
(a) $\mathcal{L}_2$ **Norm of Actuator Rate**
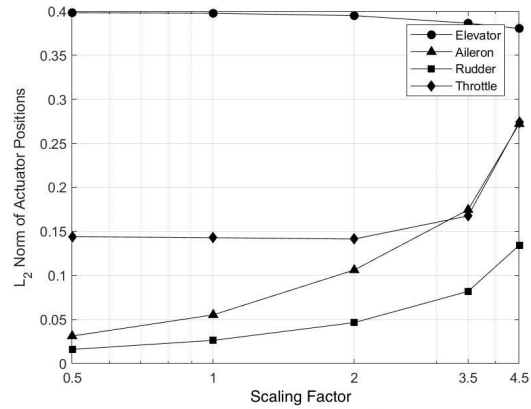
(b) $\mathcal{L}_2$ **Norm of Actuator Position**
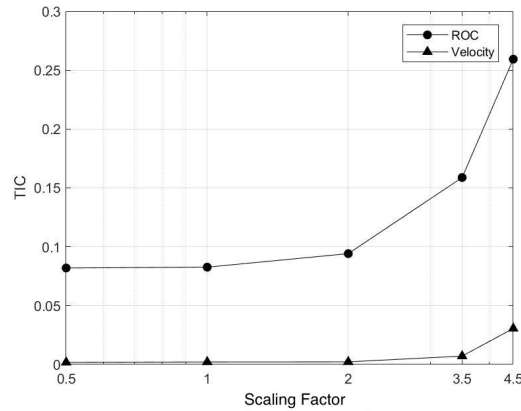
(c) **TIC Values**

Figure 57. Workload and Performance Metrics of K_c Scaled Side Step

The flying qualities graphs in Figure 58 indicate a similar trend to the K_c scaling results in the climbing turn. Since the bare airframe is unchanged, the MIL-STD-1797 graphs in Figures 58a and 58b are each five points stacked on each other in the Level

1 category. Figure 58c shows that as K_c increases, TIC also increases to the point where the aircraft is considered Level 2 at 3.5 x K_c and then Level 3 at 4.5 x K_c. A large TIC value accompanied by a ζ_{sp} value within Level 1 boundaries indicates to an aircraft designer that the bare airframe design is adequate but changes to the controller need to be made to improve the aircraft performance.

(a) $\omega_{sp}T_{\theta2}$ vs ζ_{sp}

(b) CAP vs ζ_{sp}

(c) TIC vs ζ_{sp}

(d) $\mathcal{L}_2$ Norm vs TIC ROC
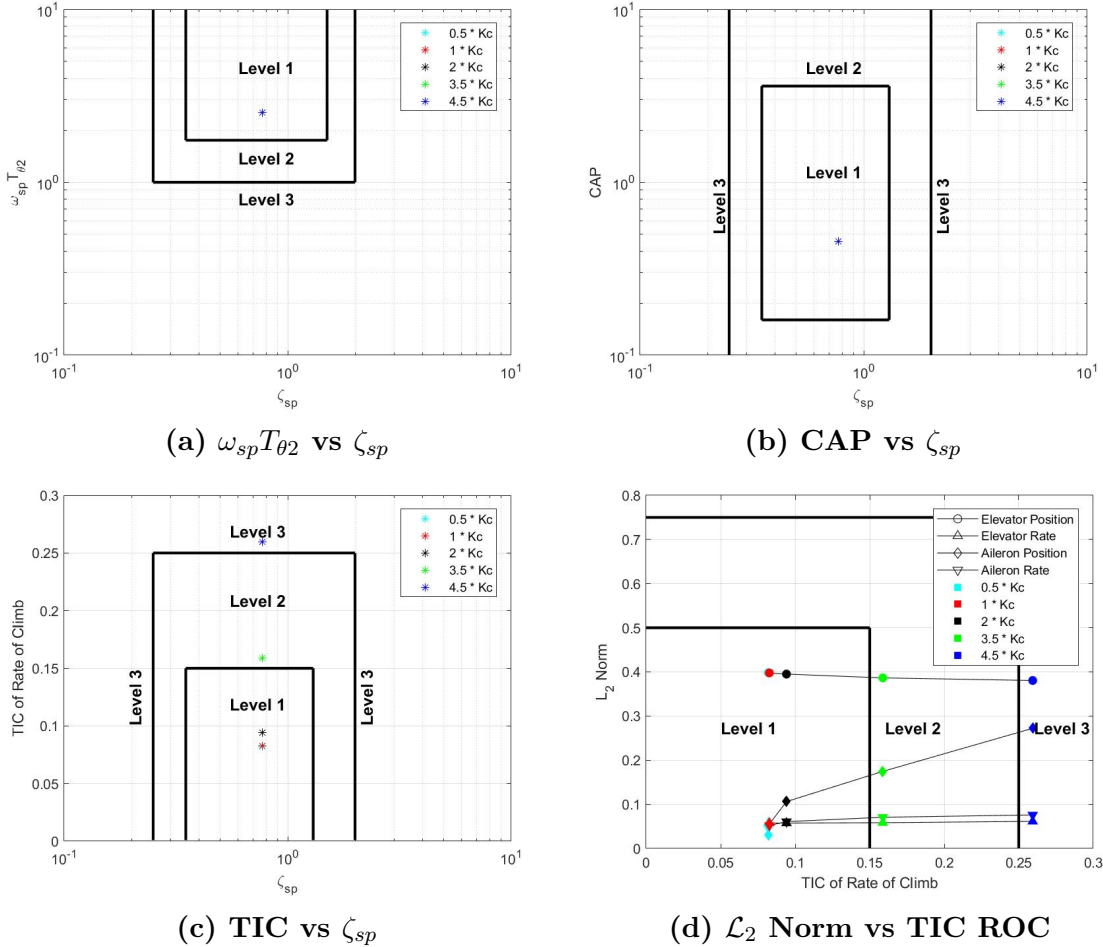
Figure 58. Flying Qualities Graphs of K_c Scaled Side Step

4.3.4 Cross-Coupling Effects.

As previously stated, cross-coupling occurred in both the L_p and K_c scaling during the side step maneuver. The cross-coupling manifesting itself in the side step and not the climbing turn indicates that the side step's precision nature reveals otherwise

unknown flying qualities issues, information important to an aircraft designer. The cross-coupling discovery reinforces the importance of a robust test plan when assessing UAV flying qualities, including all maneuvers related to the operational mission of the aircraft.

4.4   Aerial Refueling Analysis

The final maneuver assessed was the precision, non-aggressive aerial refueling task. This task requires precision control to simultaneously track a specified altitude and a specified bank angle while maintaining a constant velocity.

4.4.1   Baseline Aerial Refueling.

Before scaling any stability and control derivatives, a baseline analysis of the aerial refueling maneuver was completed to achieve a datum for workload and performance of the unscaled bare airframe with the controller in the loop. The same aircraft nominals were used for the baseline maneuver and the subsequent scaled parameter maneuvers: 5000 ft, 200 KTAS, with gear up and flaps up. Both the desired aircraft roll angle and altitude were set to the same sum-of-sines function based on research by Hamidani and discussed in Section 3.3.1.2. The sum-of-sines tracking portion lasted 30 seconds, began 10 seconds into the simulation, and terminated with 10 seconds remaining. The dashed lines seen in Figure 59a show the tracking input to the controllers and the red lines show the resulting aircraft track.

From inspecting the altitude tracking portion, there is steady-state error and overshoot evident from the first 10 seconds and last 10 seconds of the maneuver, respectively. The first 10 seconds indicate a steady-state error of about 10 feet, and the last 10 seconds show about a 10 foot overshoot of the desired altitude. To mitigate this, the performance and workload metrics were calculated only in the 30 second band of

(a) **Altitude Tracking**   (b) **Roll Angle Tracking**
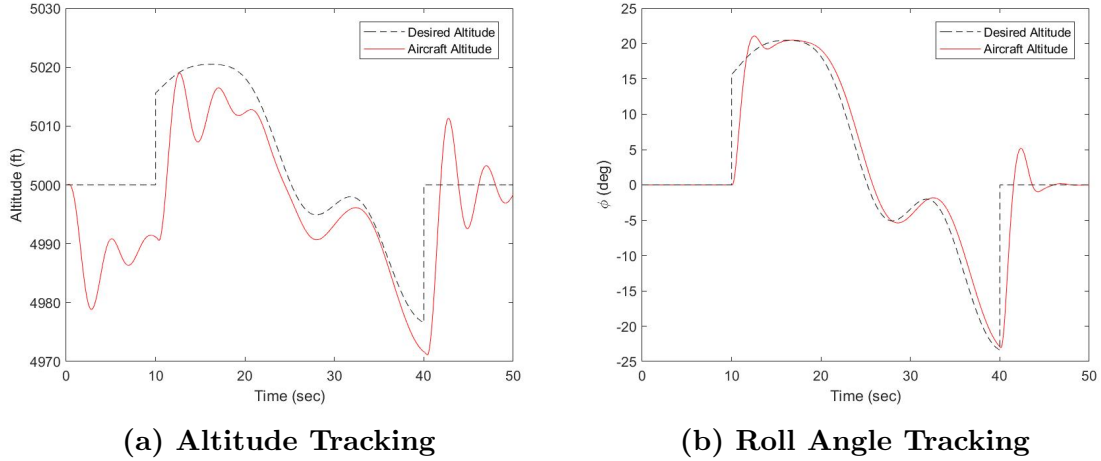
Figure 59. Baseline Aerial Refueling Tracking

tracking the sum-of-sines input. Since the same controller was used throughout the scaling of all parameters, the changes in performance and workload can be attributed to changes in the bare airframe dynamics, and not controller performance. In assessing bank angle tracking, Figure 59b indicates excellent performance throughout the maneuver, only showing a slight delay in control and minor overshoot after each step input.

An assessment was also done of the workload and performance of the aircraft during the baseline maneuver using $\mathcal{L}_2$ norm and TIC. Figures 60a and 60b show a very active elevator actuator as compared to both the rudder and aileron. This matches the data shown in Figures 59a and 59b, which shows the aircraft struggled to track altitude as compared to roll angle. But the interesting point comes in Figure 60c, which shows TIC for roll angle having the highest value by a large margin, with TIC for altitude and velocity only a fraction of that amount.

The unusually low TIC values of altitude arise due to the large trim value of altitude. The TIC calculation sees a 10 foot altitude tracking error as minuscule when compared to the trim altitude of 5,000 feet. A small one or two degree bank angle error is magnified due to the target angles being less than 25 degrees. Therefore,

the relativity in size between the trim value and target value directly correlates to the magnitude of the TIC value. Although the magnitudes of TIC change, the trends observed during stability and control parameter scaling remain preserved. In the case of altitude for the aerial refueling maneuver, the subsequent performance plots and cutoffs for Level 1, 2, and 3 flying qualities have to be adjusted accordingly.

(a) $\mathcal{L}_2$ Norm of Actuator Rate

(b) $\mathcal{L}_2$ Norm of Actuator Position

(c) TIC Values
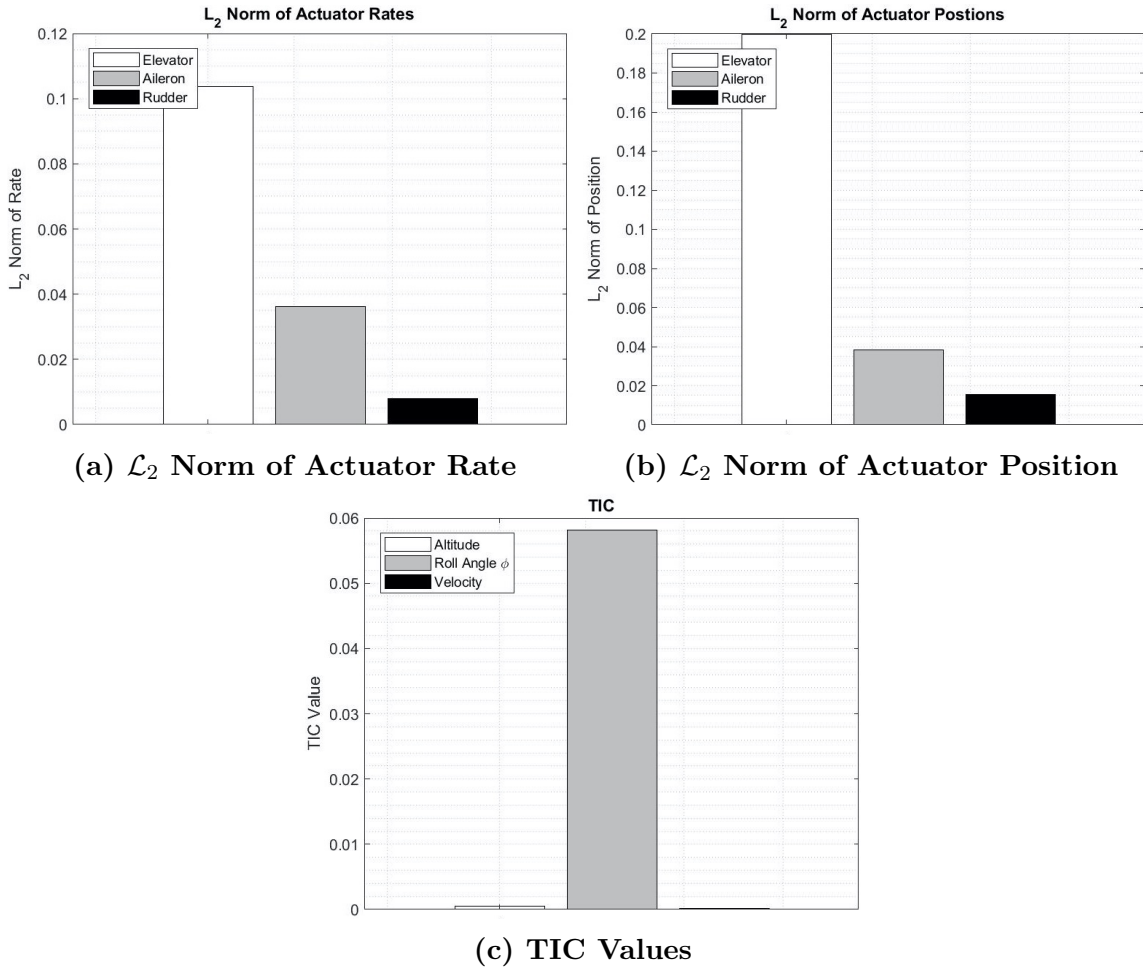
Figure 60. Baseline Aerial Refueling Tracking

4.4.2 Stability Parameter Scaling.

To assess how the stability and control parameters affected aircraft workload and performance during the aerial refueling task, the four stability and control parameters M_q, $M_{\delta e}$, L_p, and $L_{\delta a}$ were scaled according to their values in Section 4.1.1.

4.4.2.1 M_q Scaling.

First, M_q was scaled by 0.25 x M_q, 1 x M_q, 2 x M_q, 4 x M_q, and 6 x M_q. Figure 61 shows the resulting five aircraft tracks for altitude and roll angle.

(a) Altitude Tracking
(b) Roll Angle Tracking
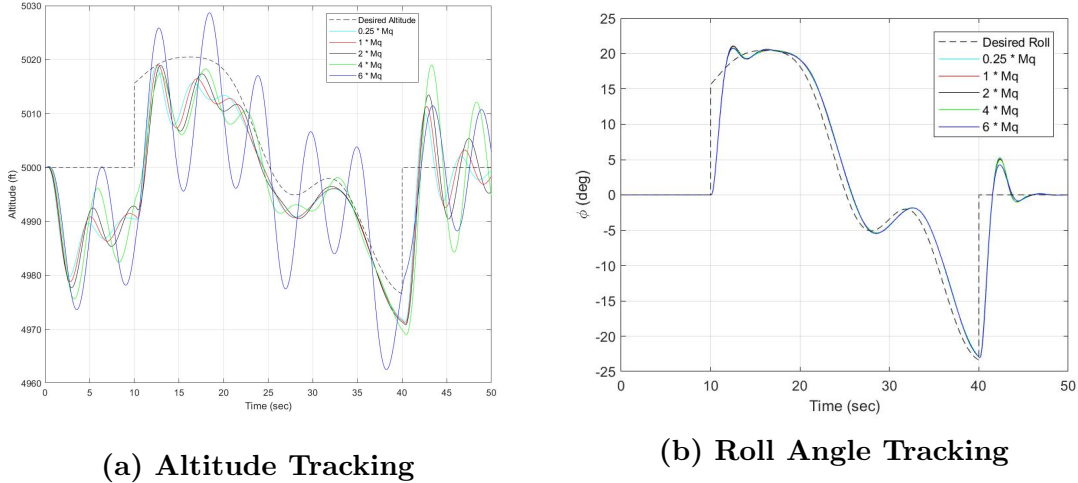
Figure 61. M_q **Scaled Aerial Refueling Tracking**

When assessing the initial results, its clear that scaling in M_q has only an effect on altitude tracking, as the roll angles plotted in Figure 61b are nearly identical. Looking at Figure 61a shows clear variations in performance as M_q is scaled up. 0.25 x M_q through 2 x M_q show similar tracking performance, while 4 x M_q and 6 x M_q have discernibly more overshoot and oscillations, with 6 x M_q reaching limit cycle oscillation throughout the maneuver. The graphs shown in Figure 62 confirm that as M_q is scaled up, $\mathcal{L}_2$ norm of elevator position steadily increases, as does TIC of altitude. This indicates that the aircraft is both doing more work and performing worse. TIC of velocity continually decreases until 6 x M_q, at which point it spikes, indicating that changes in M_q also have an effect on throttle control. Figure 62d shows that TIC of roll angle is changing, but a trivial amount, as indicated by the y-axis values.
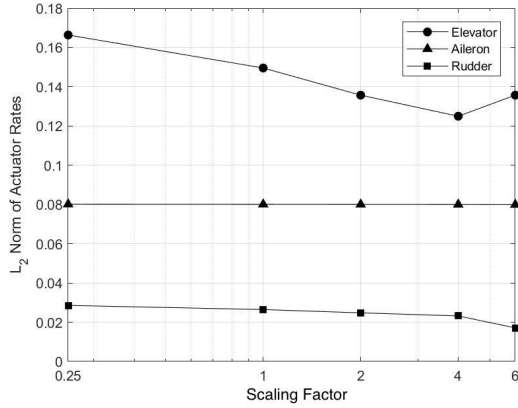
(a) $\mathcal{L}_2$ **Norm of Actuator Rate**
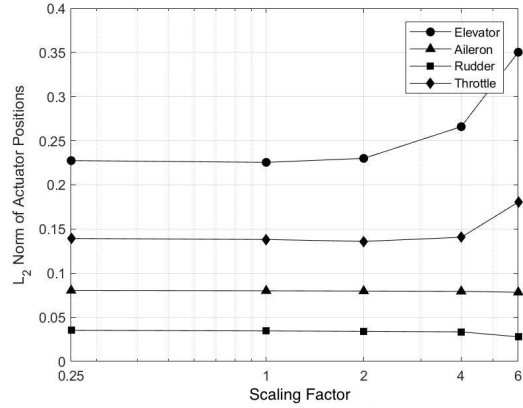
(b) $\mathcal{L}_2$ **Norm of Actuator Position**
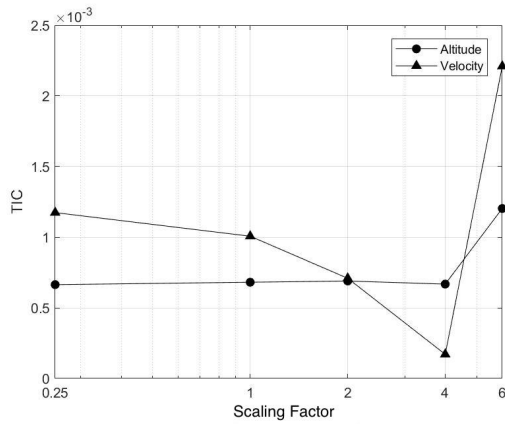
(c) **Altitude and Velocity TIC Values**
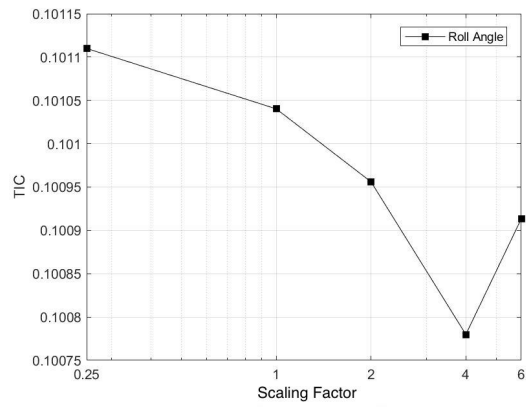
(d) **Roll Angle TIC Values**

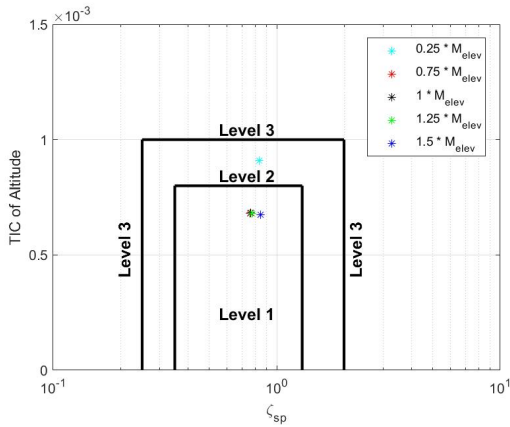**Figure 62.** M_q **Scaled Aerial Refueling Tracking**

The MIL-STD-1797 plots and newly developed criteria plots of Figure 63 agree that unsatisfactory flying qualities exist at 6 x M_q. Its location on Figure 63c shows that it falls outside both the ζ_{sp} Level 3 limit and the TIC Level 3 limit, indicating to the aircraft designer the possibility that both the controller and the bare airframe need to be modified. In addition, 0.25 x M_q, 1 x M_q, 2 x M_q, and 4 x M_q are closely grouped within Level 1, but as stated earlier, the Level 2 and Level 3 boundaries are flexible, as the values set for those boundaries are rough estimates based on aircraft responses. With more research and subsequent data, the boundaries can be adjusted to better match the aircraft's response.

(a) $\omega_{sp}T_{\theta 2}$ vs ζ_{sp}

(b) CAP vs ζ_{sp}

(c) TIC vs ζ_{sp}

(d) $\mathcal{L}_2$ Norm vs TIC Altitude
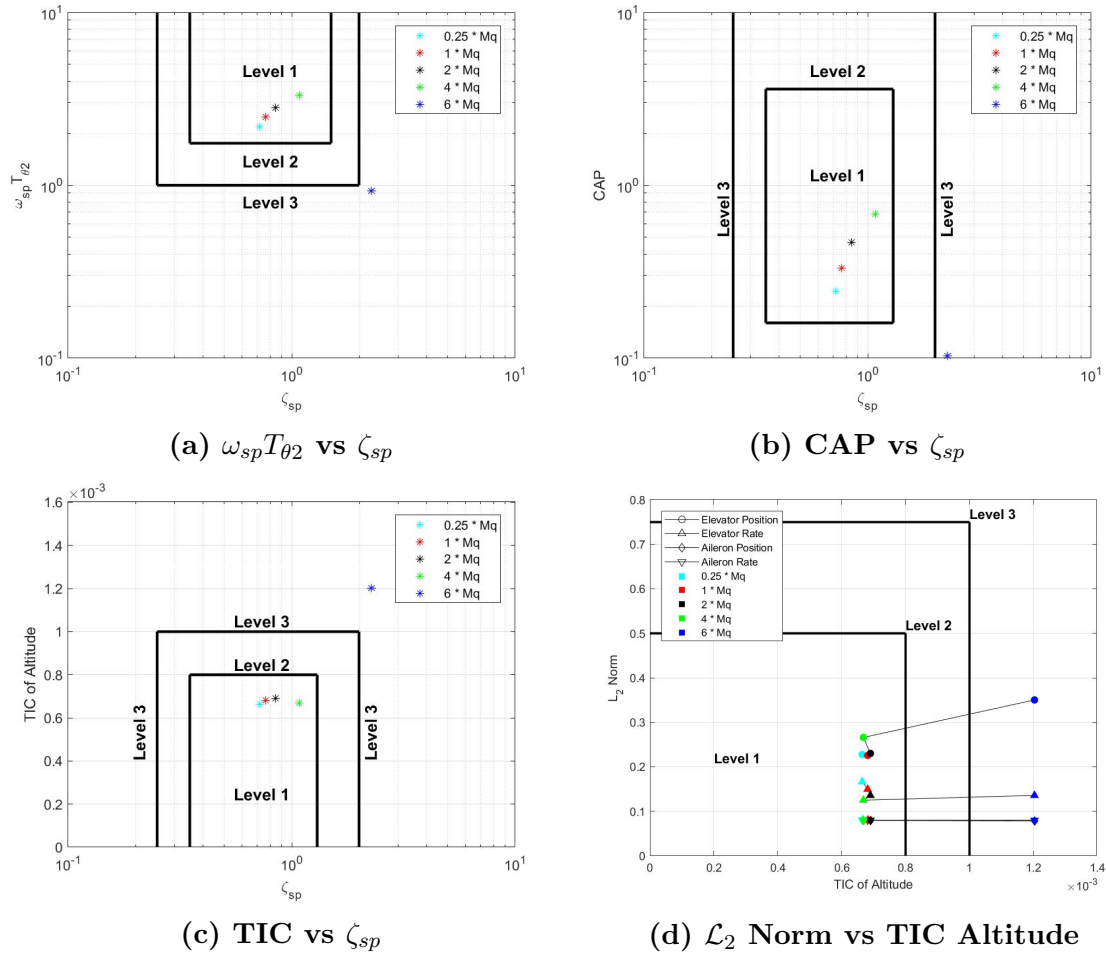
Figure 63. Flying Qualities Graphs of M_q Scaled Aerial Refueling

4.4.2.2 $M_{\delta e}$ Scaling.

The second scaled maneuver assessed during the aerial refueling task was $M_{\delta e}$, the pitching moment due to elevator deflection. $M_{\delta e}$ was scaled by 0.25 x $M_{\delta e}$, 0.75 x $M_{\delta e}$, 1 x $M_{\delta e}$, 1.25 x $M_{\delta e}$, and 1.5 x $M_{\delta e}$. Figure 64 depicts the resulting aerial refueling plots.
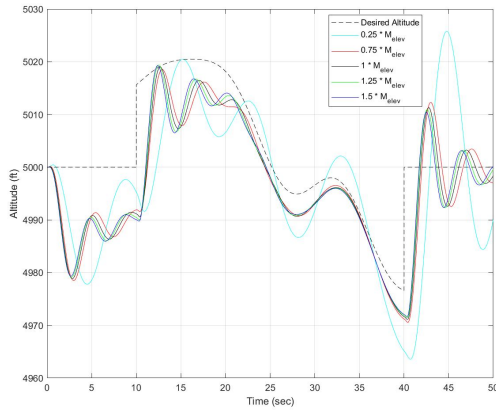
(a) Altitude Tracking
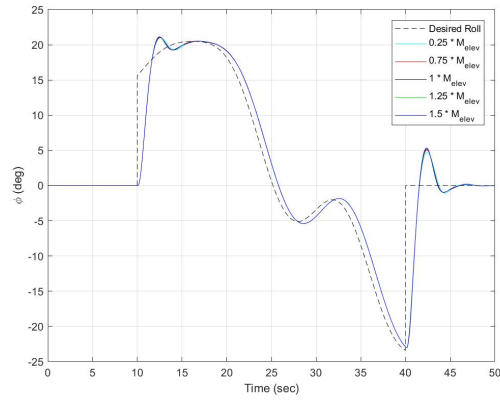
(b) Roll Angle Tracking

Figure 64. $M_{\delta e}$ **Scaled Aerial Refueling Tracking**

The changes to $M_{\delta e}$ show similar results as the climbing spiral and side step maneuver. A smaller value of $M_{\delta e}$ causes the aircraft to be sluggish in pitch, indicating less control. A higher $M_{\delta e}$ increases the aircraft's responsiveness in pitch and thus improves both rise time and overshoot performance. Figure 65b shows a sharp decrease in workload required to accomplish the task from 0.25 x $M_{\delta e}$ to 0.75 x $M_{\delta e}$, but then a slight increase from 0.75 x $M_{\delta e}$ to 1.5 x $M_{\delta e}$. These trends coincide with a TIC of altitude that steadily decreases with increasing $M_{\delta e}$. From the graphs, an aircraft designer could choose to minimize elevator workload or maximize performance based on changes to $M_{\delta e}$.
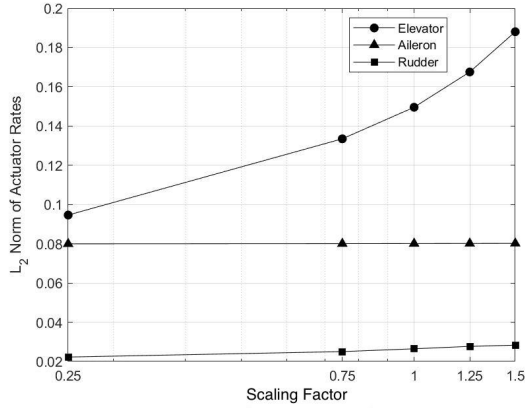
(a) $\mathcal{L}_2$ **Norm of Actuator Rate**
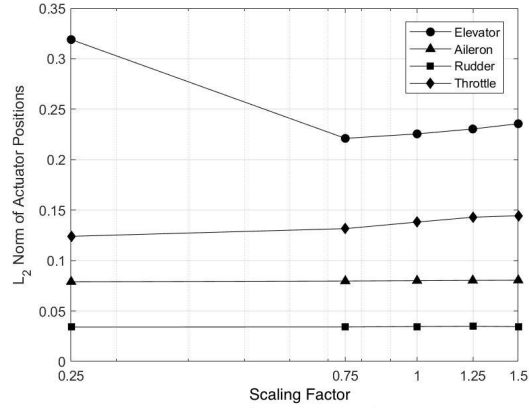
(b) $\mathcal{L}_2$ **Norm of Actuator Position**
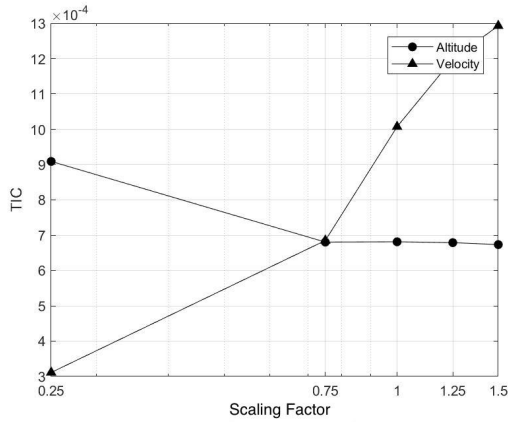
(c) **Altitude and Velocity TIC Values**
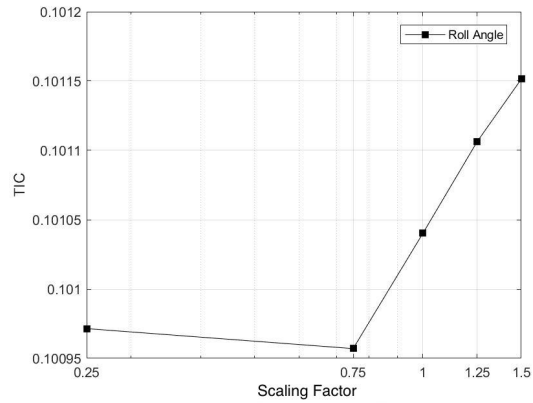
(d) **Roll Angle TIC Values**

Figure 65. $M_{\delta e}$ **Scaled Aerial Refueling Tracking**

The MIL-STD-1797 graphs in Figures 66a and 66b primarily indicate that the aircraft has Level 1 flying qualities throughout the scaling of $M_{\delta e}$. In contrast, the 0.25 x $M_{\delta e}$ exceeds the Level 1 flying qualities limit, based on the TIC of altitude limit set at 0.8 x 10^{-3}. As previously stated, these TIC limits are floating until more data is available. But referencing Figure 64a indicates that the tracking performance of 0.25 x $M_{\delta e}$ has larger delays and overshoots in comparison to the other five runs. In this case, the developed criteria of flying qualities more accurately categorizes the aircraft response than the classical methods used in MIL-STD-1797.

(a) $\omega_{sp}T_{\theta 2}$ **vs** ζ_{sp}

(b) **CAP vs** ζ_{sp}

(c) **TIC vs** ζ_{sp}
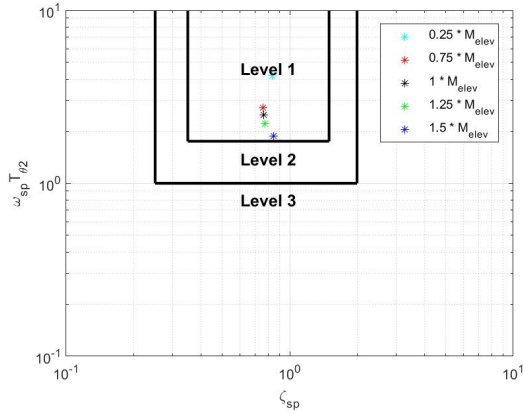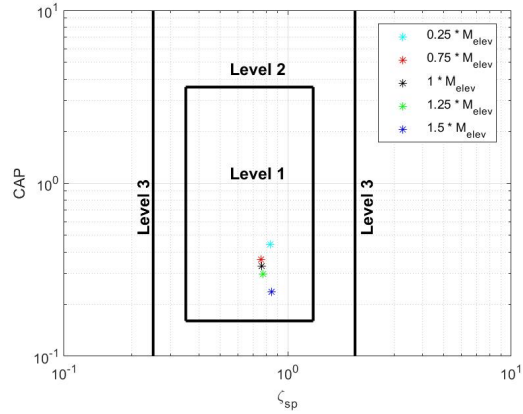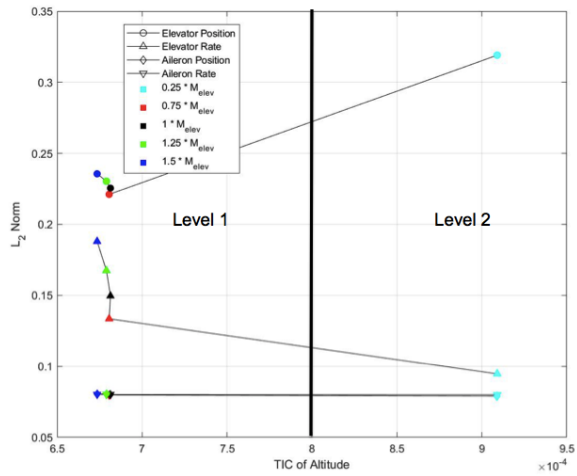
(d) $\mathcal{L}_2$ **Norm vs TIC Altitude**

Figure 66. Flying Qualities Graphs of $M_{\delta e}$ Scaled Aerial Refueling

4.4.2.3 L_p Scaling.

Third, the lateral stability parameter L_p representing the roll moment due to roll rate was scaled by 0.25 x L_p, 0.75 x L_p, 1 x L_p, 1.25 x L_p, and 1.50 x L_p. Figures 67a and 67b show the resulting five aircraft courses.
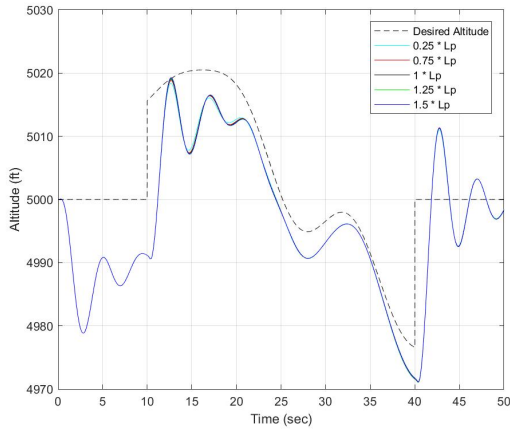
(a) Altitude Tracking
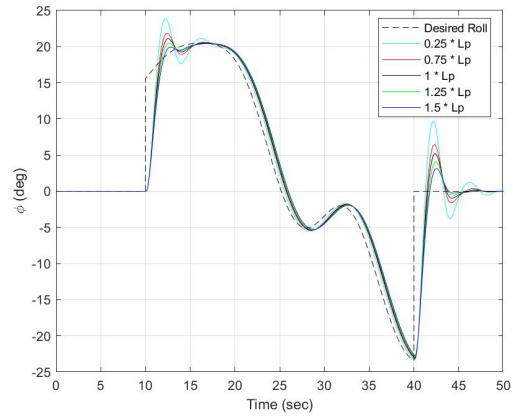
(b) Roll Angle Tracking
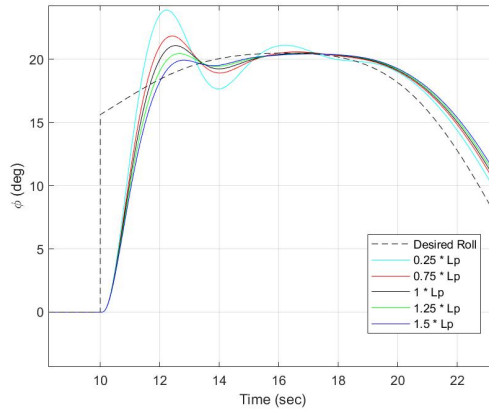
(c) Initial Roll Angle Capture

Figure 67. L_p **Scaled Aerial Refueling Tracking**

First glance indicates the decoupled nature of the longitudinal and lateral stability and control parameters during the aerial refueling maneuver, as altering L_p has nearly no effect on the altitude tracking performance of the aircraft. Figure 67c is an zoomed-in view at the first step input of the roll angle tracking. Roll tracking shows larger overshoot as L_p decreases, along with a slower rise time, indicating a trade-off that a higher value of L_p decreases overshoot and increases rise time.
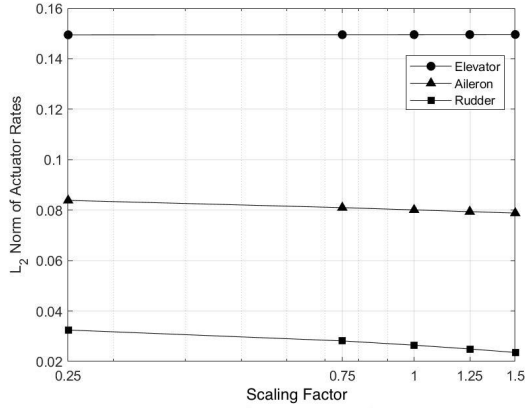
(a) $\mathcal{L}_2$ **Norm of Actuator Rate**
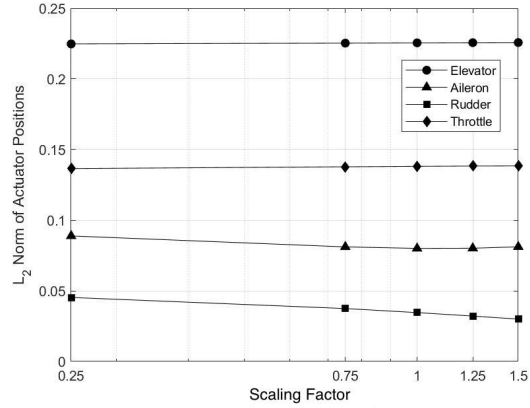
(b) $\mathcal{L}_2$ **Norm of Actuator Position**
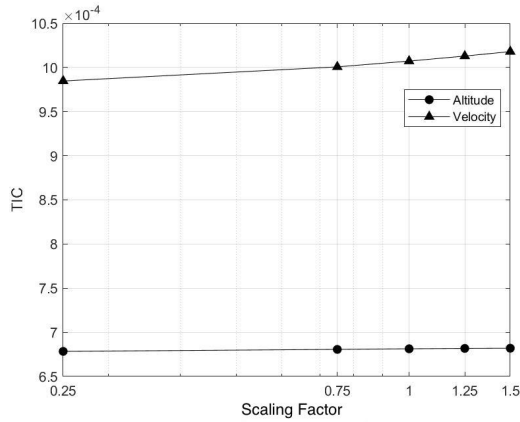
(c) **Altitude and Velocity TIC Values**
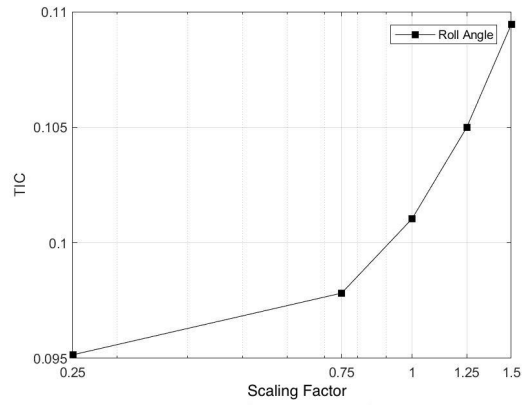
(d) **Roll Angle TIC Values**

Figure 68. L_p **Scaled Aerial Refueling Tracking**

Figure 68d shows that as L_p increases, roll tracking performance decreases. This appears counterintuitive, as 0.25 x L_p clearly has the largest overshoot, indicating poor performance in the transient response. But upon closer inspection of Figure 67b, 0.25 x L_p has the best steady-state tracking performance, which over the 30 second interval equates to the lowest TIC of roll angle. When assessing $\mathcal{L}_2$ norm vs TIC of roll angle, Figure 69 shows little change in TIC over the course of scaling L_p, with all five runs tightly packed well within the Level 1 flying qualities boundaries, indicated by the bold black lines on the top and right of the plot. Since changing L_p has little effect on the workload and performance during the aerial refueling maneuver,

102

an aircraft designer could then use L_p as a free variable to meet other requirements.
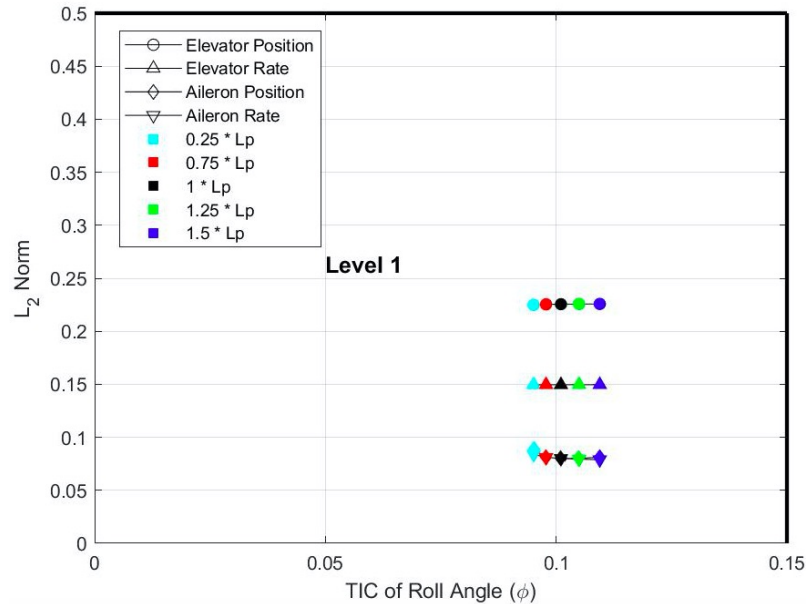
Figure 69. $\mathcal{L}_2$ Norm vs TIC of Roll Angle

4.4.2.4 $L_{\delta a}$ Scaling.

Lastly, the lateral control parameter $L_{\delta a}$ was scaled by 0.5 x $L_{\delta a}$, 0.75 x $L_{\delta a}$, 1 x $L_{\delta a}$, 1.25 x $L_{\delta a}$, and 1.5 x $L_{\delta a}$. Figure 70 depicts the track of the aircraft in altitude and roll angle. Figures 70b and 70c indicate a lower overshoot and faster rise time with increasing $L_{\delta a}$. This matches with previous results during the climbing spiral and side step maneuver, as changing the size of the control surface and maintaining the same actuator performance will provide more control authority.
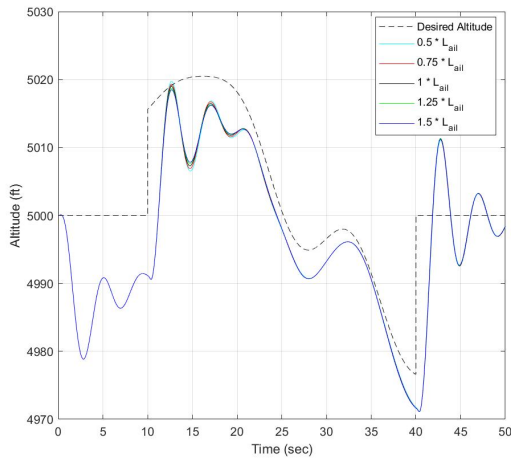
(a) Altitude Tracking
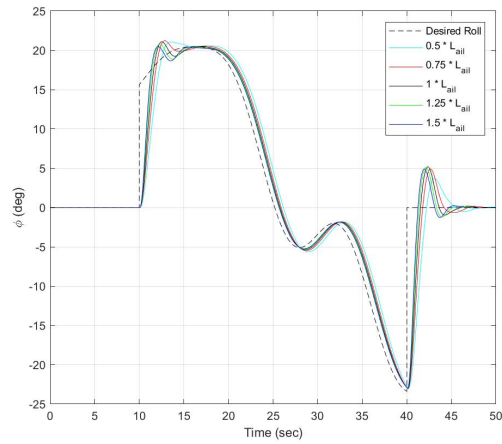
(b) Roll Angle Tracking
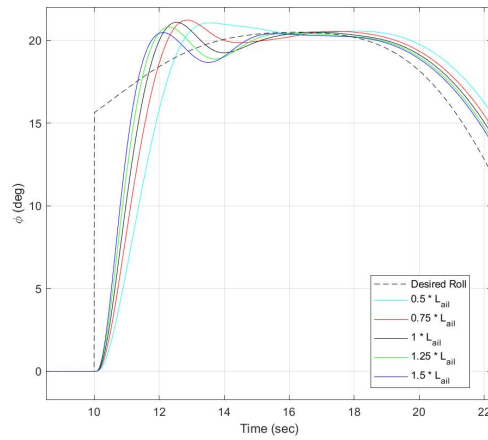
(c) Roll Angle Tracking

Figure 70. $L_{\delta a}$ **Scaled Aerial Refueling Tracking**

Figure 71c confirms that increasing $L_{\delta a}$ both decreases workload, as evidenced by the decreasing $\mathcal{L}_2$ norm of the aileron position. Figure 71d shows that performance increases as well, with TIC of roll angle starting above 0.13 and decreasing to below 0.09 over the course of scaling $L_{\delta a}$. TIC of velocity and altitude remains largely unchanged.
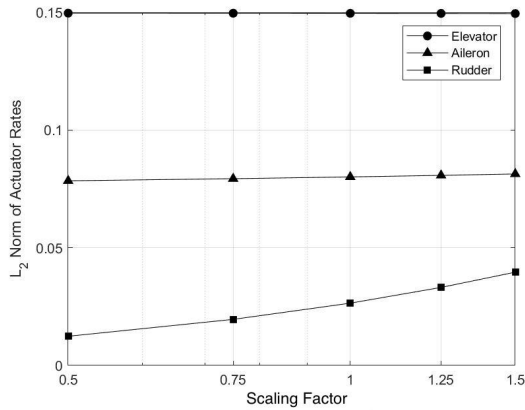
(a) $\mathcal{L}_2$ **Norm of Actuator Rate**
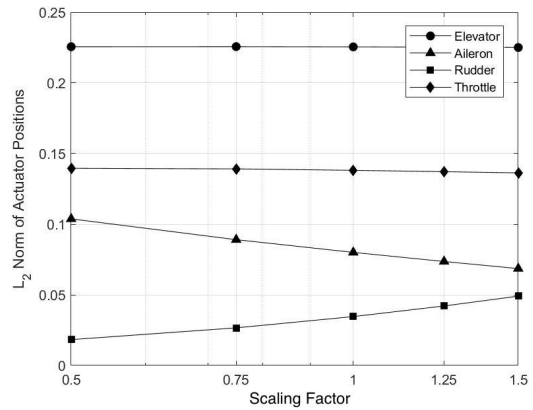
(b) $\mathcal{L}_2$ **Norm of Actuator Position**
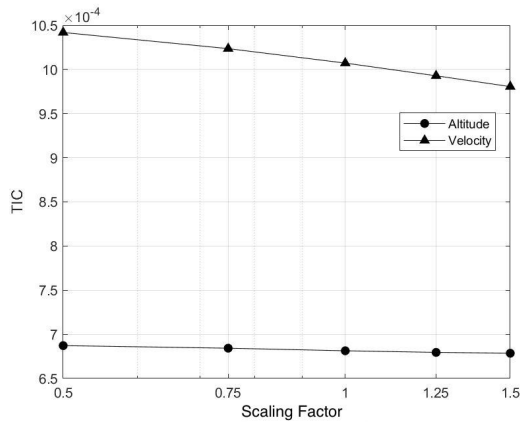
(c) **Altitude and Velocity TIC Values**
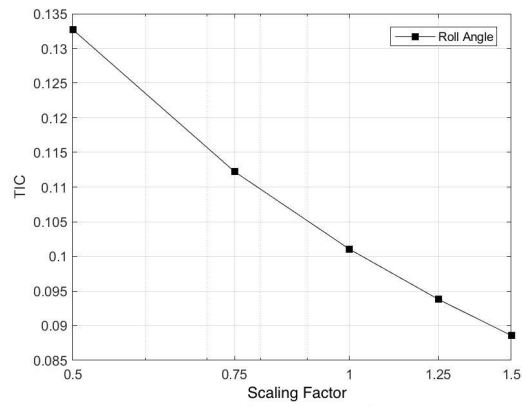
(d) **Roll Angle TIC Values**

Figure 71. L_{δ_a} **Scaled Aerial Refueling Tracking**

Figure 72 shows that all tested values of L_{δ_a} are within the Level 1 boundaries. A trend suggests that increasing L_{δ_a} draws the aircraft further away from the Level 1 to Level 2 boundary, shown as the bold outlines on the top and right side of the figure. The presented results would provide an aircraft designer with information on how small an aileron could be made without compromising significant performance during a precision, non-aggressive task.
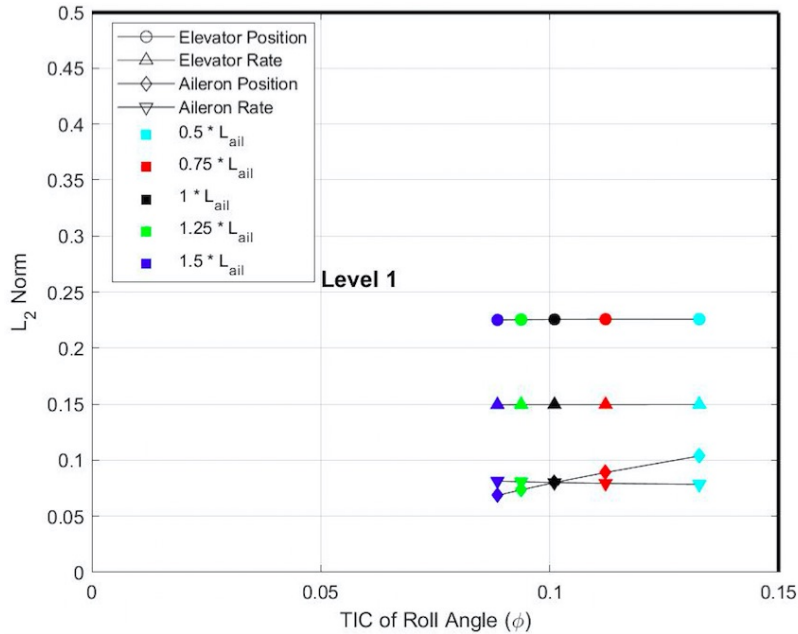
Figure 72. $\mathcal{L}_2$ **Norm vs TIC of Roll Angle**

4.4.3 Deficiency Identification in UAV Flying Qualities.

Trends identified in Figure 48c indicated poor performance at 6 x M_q was due to a large ζ_{sp} value, and thus a bare airframe issue. Trends from Figure 58c indicated that gain increase correlated to poor performance, and thus a controller design issue. Combining the results from these two graphs, an aircraft designer who just simulated a maneuver could plot results on a graph of TIC vs ζ_{sp} and determine what is causing the deficiencies of the aircraft. Figure 73 identifies to the aircraft designer if the aircraft has a controller issue, a bare airframe issue, or both.
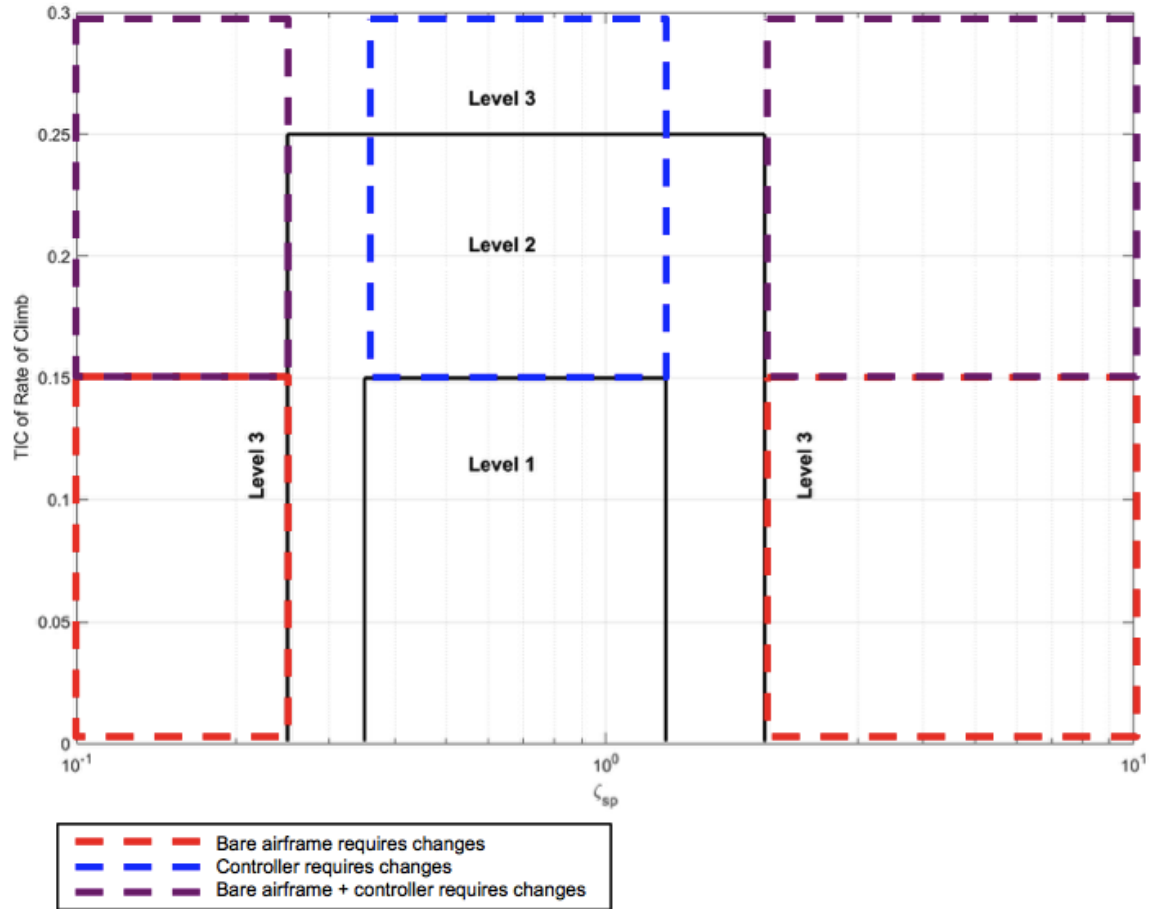
Figure 73. TIC vs ζ_{sp} Deficiency Overlay

Figure 73 has the same bold black lines plotted on it to show Level 1, Level 2, and Level 3 flying qualities, with the addition of red, blue, and purple dotted lines overlaid. The red dotted lines are areas where ζ_{sp} is either too large or too small, and thus data points in those areas would indicate a bare airframe issue. The blue dotted lines indicate areas of poor performance caused by the controller, and thus to improve the performance a controller redesign is required. Finally, the purple lines indicate areas where both the controller and bare airframe are causing issues, and thus both may require redesign. A graph such as Figure 73 provides critical information to an aircraft designer pertaining to the deficiencies of the aircraft and how to improve them.

4.4.4 Adjusting TIC of Altitude for Flight Test.

In Section 4.4.1, it was explained that TIC of altitude had orders of magnitude smaller values than TIC of bank angle. This was due to the baseline altitude being a large number, and the deviation from that proportionally much smaller, therefore indicating a nearly insubstantial error when using the TIC calculation. For the aerial refueling analysis completed in this thesis, altitude was held to a constant 5,000 feet for stability and control parameter scaling. As previously stated, holding altitude constant preserves the trends present between the scaling factors.

The issue arises when changing the datum altitude for completing the same aerial refueling task at different altitudes. To demonstrate, the same baseline profile was completed at altitudes of 5,000 feet, 10,000 feet, and 15,000 feet, and then plotted as a net altitude change on the same plot. Only the altitude at which the maneuver was completed was changed between runs. The multi-sine input was held constant, along with the aircraft velocity. Figure 74 shows the resulting aircraft altitude tracking plots.

The plot indicates nearly identical performance at each altitude, with the exceptions that as altitude increases, there is a small increase in overshoot and a slight decrease in steady-state error. Yet, TIC calculations indicate something different. Table 21 shows that as altitude increases, there is also a significant increase in performance. According to the traditional TIC calculation, the aircraft saw a 50% increase in performance at 10,000 feet over the 5,000 foot run and a 67% increase in performance at 15,000 feet over the 5,000 foot run. Clearly this is a mathematical effect and not an indicator of performance, and therefore an adjustment to TIC was developed for the altitude calculation.
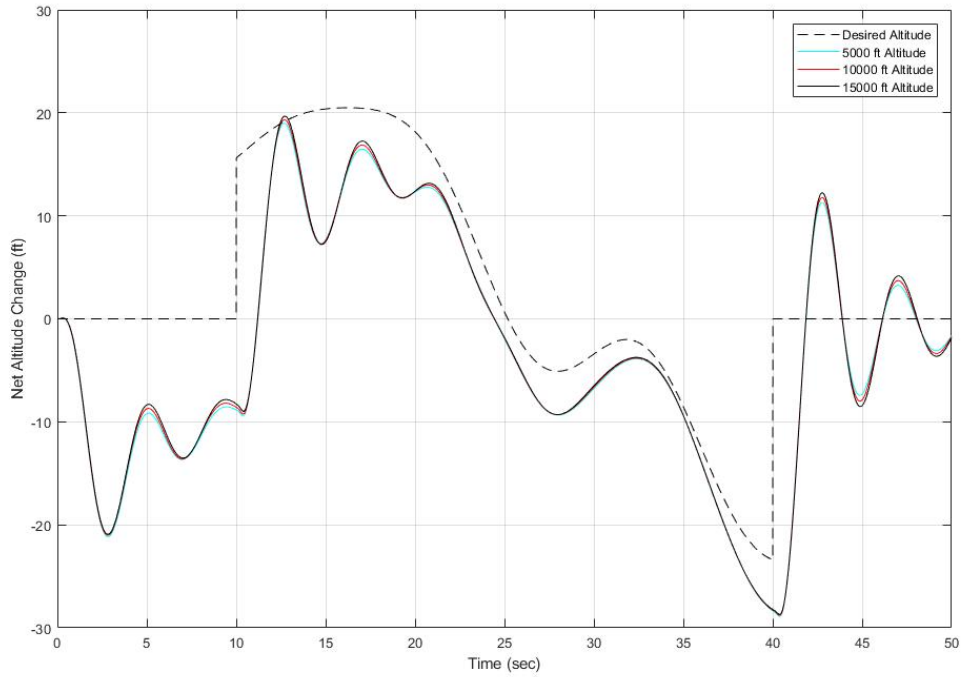
Figure 74. Baseline Aerial Refueling Tracking

Table 21. TIC Calculations for Aerial Refueling Altitude Comparison

Altitude (ft)	TIC Value	Percent of Performance Increase
5,000	0.000681	-
10,000	0.000338	50.3
15,000	0.000223	67.1

Adjusted TIC uses a datum altitude to scale down all results to that altitude. In the case of this analysis, the 10,000 foot and 15,000 foot altitudes were scaled down to 5,000 feet by subtracted 5,000 feet and 10,000 feet, respectively, from every data point in the matrix. Now, TIC of altitude can be evaluated on the same scale and subsequent performance issues can be identified without the confounded mathematical effects of TIC. The simple change maintains the same magnitude of TIC across several altitudes while preserving the correct trends of TIC changing across altitudes.

109

The aerial refueling task was then completed at the same three altitudes, this time calculating adjusted TIC instead of the original TIC calculation. Table 22 shows the results of using the normalized TIC calculation. These results indicate a much more realistic increase in performance: a 0.77% increase at 10,000 feet over the 5,000 foot run, and 1.54% increase at 15,000 feet over the 5,000 foot run.

Table 22. Adjusted Input TIC Calculations for Aerial Refueling Altitude Comparison

Altitude (ft)	Adjusted Input TIC Value	Percent of Performance Increase
5,000	0.000681	-
10,000	0.000676	0.77
15,000	0.000671	1.54

The Air Force Test Pilot School plans to do similar aircraft performance tests to compare simulation results from this thesis to actual flight test data. The runs conducted in the aerial refueling simulations hold altitude and velocity constant, and therefore the large scaling issues seen with TIC between altitude would not be present. But in actual flight test, a certain altitude may not be available to complete the maneuver, and if a higher or lower altitude is chosen, TIC will incorrectly indicate large increases or decreases in performance. Adjusted input TIC may be employed in flight test in order to provide the flexibility of completing the aerial refueling task at a large range of altitudes.

4.5   Chapter Summary

Results of the bare airframe analysis were presented to establish the baseline aircraft parameters. Bode plots of the HOS and LOES were compared and from those literal factors were derived. This process was repeated for both the longitudinal axis and lateral-directional axis. Next, stability and control parameters were scaled to modify the existing bare airframe. The resulting literal factors of each stability and control scaled bare airframe were then presented. Then, the analysis of the climbing

spiral was completed for each parameter. Workload and performance comparisons were made utilizing $\mathcal{L}_2$ norm and TIC as well as several flying qualities graphs. After, the same previous steps were completed for the side step maneuver and the aerial refueling maneuver. Results point to utilizing a combination of classical aircraft literal factors, such as ζ_{sp} and CAP, with newly developed mathematical techniques, such as $\mathcal{L}_2$ norm and TIC, to assess the workload of the flight controller and performance during the maneuver.

V. Conclusions and Recommendations

5.1 Conclusions

The primary objective of this research was to provide data on flying qualities assessments in an effort to expand the research of UAV flying qualities. The research completed indicated that the Simulink model of the LJ-25D is an excellent platform for simulating various precision and non-precision maneuvers as well as assessing workload and performance metrics. In summary, the objectives of this research were as follows:

1. Evaluate the flying qualities of an unmanned LJ-25D through various precision and non-precision maneuvers.

2. Identify trends between stability and control parameter scaling, workload and performance metrics, and classical control literal factors.

Each of the three maneuvers completed provided valuable data pertaining to the trends of flying qualities. First, the non-precision, non-aggressive climbing turn identified the importance of retaining some of the original literal factors from MIL-STD-1797 in the assessment of UAVs. During the scaling of M_q, TIC indicated that all scaled values would provide Level 1 flying qualities, while MIL-STD-1797 predicted that 6 x M_q would have Level 3 flying qualities due to the high ζ_{sp}. All scaled values of M_q performed adequately during the climbing turn, but did not during another maneuver: the aerial refueling task. The result points to the importance of ζ_{sp} across all maneuvers, and that its inclusion in a future UAV flying qualities standard is vital.

The scaling $M_{\delta e}$ during the aerial refueling task showed positive results for using TIC to predict flying qualities levels. 0.25 x $M_{\delta e}$ had large overshoots and poor steady-state tracking performance during the maneuver, indicative of Level 2 or Level 3 flying qualities. MIL-STD-1797 predicted 0.25 x $M_{\delta e}$ as Level 1 flyinq qualities, while TIC

112

indicated Level 2. This particular case shows the merit of using TIC in the assessment of flying qualities over some classical control literal factors. The side step maneuver also presented surprising results when assessing the effects of scaling $M_{\delta e}$. The results indicate that neither MIL-STD-1797 nor $\mathcal{L}_2$ norm and TIC correctly classify all the scaled values. Combining aspects of the two into a graph of TIC vs. ζ_{sp} creates a resultant plot that correctly categorizes each instance of $M_{\delta e}$. This result further solidifies the notion that new metrics and classical literal factors should both be used in the development of a UAV flying qualities standard.

The identification of trends between the scaling of stability and control parameters and resultant workload and performance metrics provides an aircraft designer with trade-offs during the design phase. Several important trends were discovered in the assessment of the LJ-25D which if presented to the aircraft design team in the early phases of the program would provide a valuable trade space between aircraft performance and workload. One example is the scaling of $M_{\delta e}$ during the aerial refueling task. Between 0.75 x $M_{\delta e}$ and 1.5 x $M_{\delta e}$, the workload and performance metrics during the task are nearly identical. But at 0.25 x $M_{\delta e}$, the performance encounters a large decrease to Level 2. That information indicates to a design team to keep the limits of $M_{\delta e}$ between 0.75 x and 1.5 x its current value or risk significantly decreasing performance during the aerial refueling task. This was also true for $M_{\delta e}$ during the side step maneuver, which showed that scaling $M_{\delta e}$ below 0.75 x caused a significant decrease in performance. The sharp drop off in performance indicates to the designer the lower performance limit of $M_{\delta e}$, also correlated to the size of the elevator. Similar trends were present in the scaling of $L_{\delta a}$ during the aerial refueling task. As $L_{\delta a}$ increased, the aileron effectively became larger while holding actuator dynamics constant, which both increased performance and decreased workload. Additionally, scaling some parameters indicated no change in workload and performance during

113

the maneuver. For example, scaling L_p during aerial refueling made only minuscule changes to how the aircraft performed during task. That information relays to the aircraft designer that L_p is a free variable, and can be modified within the scaled boundaries without hindering aircraft performance.

The scaling of K_c during the climbing spiral maneuver and the side step maneuver point out the dual nature of UAV flying handling qualities. Small changes to the controller gain significantly changed the performance of the aircraft, but important literal factors such as ζ_{sp} remained unchanged with these gain changes and indicated the aircraft was well within limits of Level 1 flying qualities predicted by MIL-STD-1797. The results indicate that an aircraft with satisfactory bare airframe dynamics will perform unsatisfactorily when paired with poorly designed controller. The highly augmented flight control systems of modern UAVs play a key role in UAV flying qualities and should be accounted for in a UAV flying qualities standard.

The inclusion of the precision, non-aggressive side step maneuver also reinforced the notion of a diverse flying qualities assessment. For example, cross-coupling was present only during L_p scaling and K_c scaling of the side step maneuver, as scaling L_p and K_c both significantly degraded the longitudinal rate of climb tracking performance. This cross-coupling discovery highlights the need for a robust test plan that includes all operational maneuvers in order to assess a UAVs flying qualities.

One point that was present in previous research by Kim [30] but not seen in the assessment of the LJ-25D was position or rate saturation of actuators. The precision, non-aggressive tasks showed varying trends in workload. Little can be stated on the effects of position and rate saturation on performance since the demonstrated maneuvers were non-aggressive in nature and never fully exercised the actuators to their limits.

5.2 Future Research Recommendation

The Simulink LJ-25D model proved useful in providing a new understanding on how scaling stability and control parameters affects aircraft workload and performance. With that, there are still further discoveries to be made in pursuit of UAV flying qualities using the LJ-25D model.

In this research, the primary focus was altering the open-loop bare airframe dynamics while maintaining the same flight controller. But the flight controller is another piece of the puzzle which can be further investigated. Including the controller in the open-loop analysis will provide more information on how a controller can overcome poor bare airframe dynamics by assessing workload and performance in various maneuvers. Studying how changes in controller design affect in workload and performance could uncover new trends leading to better controller designs for the task at hand.

Further research could be conducted in developing a better performance measure based on TIC. As previously stated, TIC works well for comparing performance at the same aircraft nominals. Yet when changing those nominals between runs, such as altitude, TIC becomes scaled which skews the performance results. Developing a TIC that mitigates the variances of aircraft nominals and provide a more robust performance metric that could be used across any altitude, airspeed, or specified nominal. Additionally, researchers could investigate the use of the capability machine index as a way of measuring performance of the aircraft. Capability machine index measures how well a machine performs in relation to given tolerance limits [39]. This would allow the engineer to specify a tolerance and measure how well the aircraft maintains that tolerance throughout the maneuver.

The last recommendation is to perform more maneuvers with the LJ-25D model. Specifically, a precision, aggressive maneuver would provide more workload and per-

formance data to verify the trends identified in the precision, non-aggressive and non-precision, non-aggressive maneuvers. It would also furnish more data points to be utilized in the development of thumb print plots in setting Level 1, Level 2, and Level 3 flying qualities limits.

A planned follow-on of this research is to perform the same maneuvers in the CALSPAN LJ-25D at the USAF Test Pilot School, Edwards AFB, California. In an effort to collect more data on the role pilots play in rating flying qualities, the author recommend three overarching sets of test points. In the first, a pilot in the seat will fly each maneuver with varying stability and control parameters and provide Cooper-Harper ratings. This will provide a baseline level of Cooper-Harper ratings at each scaled stability and control parameter. Next, a pilot in the remote facility will fly each scaled stability and control parameter and attempt to rate each maneuver. Last, a controller either adapted from this research, developed by CALSPAN, or developed by the USAF test pilot school will fly each maneuver at each scaled stability and control parameter.

Each pilot will fly a maneuver at a chosen scaled stability and control parameter. It is important to randomize both the stability and control derivative and the magnitude of the scaling. As such, all 20 runs for each maneuver in which a pilot is flying should be randomly ordered, thus removing any indications to the pilots of trends in an increase or decrease in performance over the course of the test. During the test, pilots will provide Cooper-Harper ratings to obtain information on their perceived workload during each maneuver. The $\mathcal{L}_2$ norm of actuator deflections and rates will also be recorded. TIC will be calculated to determine the pilot performance during each maneuver. Adjusted input TIC, as described in Section 4.4.4, may also be utilized for calculating TIC during the aerial refueling task. The desired value input to the pilot will be $\tilde{x}$ and the actual aircraft track will be x. With this large set of

data, comparisons can be made between the pilot-in-the-seat, the remote pilot, the controller in the aircraft, and the simulation results from this thesis. The Level 1, Level 2, and Level 3 limits on the developed flying qualities graphs of TIC vs ζ_{sp} and $\mathcal{L}_2$ norm vs TIC can be compared and adjusted based on pilots' Cooper-Harper ratings of the aircraft during that maneuver. These resulting graphs from flight test can be compared to the simulation graphs and aid in developing new thumb print plots which more accurately predict UAV flying qualities.

5.3 Summary

In conclusion, the LJ-25D Simulink model has provided invaluable information on identifying trends between scaled aircraft stability and control parameters and aircraft workload and performance. The three maneuvers conducted each offer another data point in the growing database of UAV flying qualities. Neither the MIL-STD-1797 standards or developed $\mathcal{L}_2$ norm and TIC metrics alone accurately predict UAV flying qualities at every data point. Instead, a combination of the two utilized in a thumb print plot more accurately predict UAV performance over precision, non-aggressive and non-precision, non-aggressive maneuvers. By using the LJ-25D model, comparisons from simulations can be made to flight test and bridge the gap between theoretical flying qualities performance metrics and measured flight test performance metrics.

Appendix A. LOES Bode Plots

This appendix contains data from the LOES development of the LJ-25D. The Bode plot overlays of LOES and HOS are a graphical depiction verifying LOES fidelity. The boundaries described by MIL-STD-1797, displayed in black, mathematically confirm a LOES as acceptable at all frequencies.
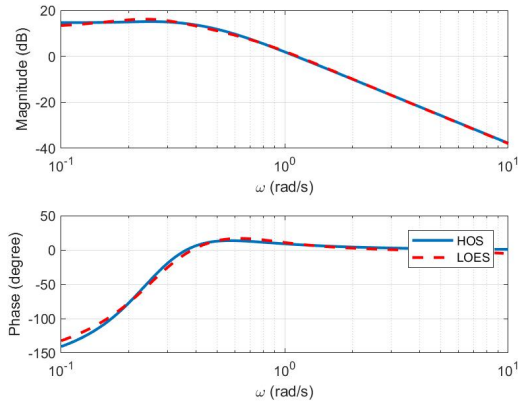
(a) M_q x 0.25 Bode Plot
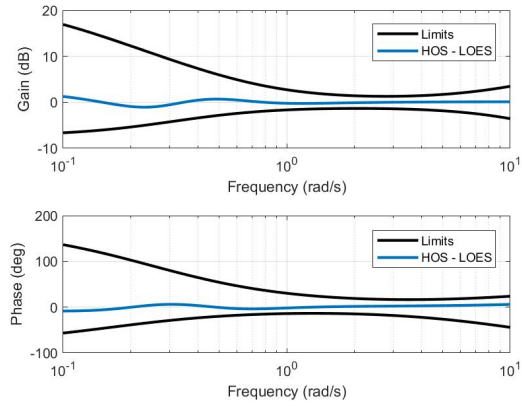
(b) M_q x 0.25 Envelope Plot

(c) M_q x 1 Bode Plot

(d) M_q x 1 Envelope Plot

118
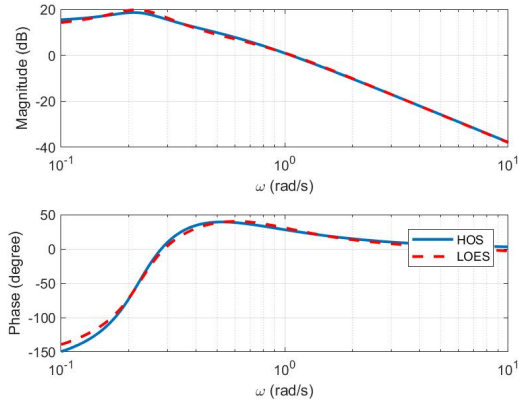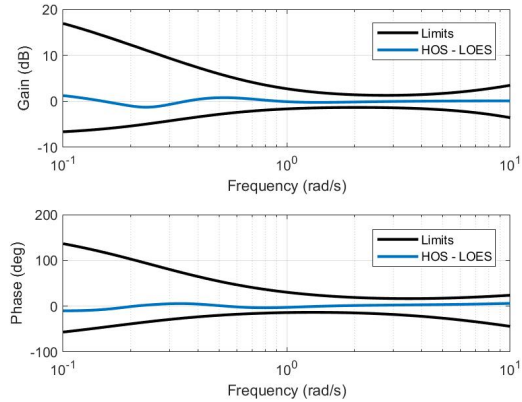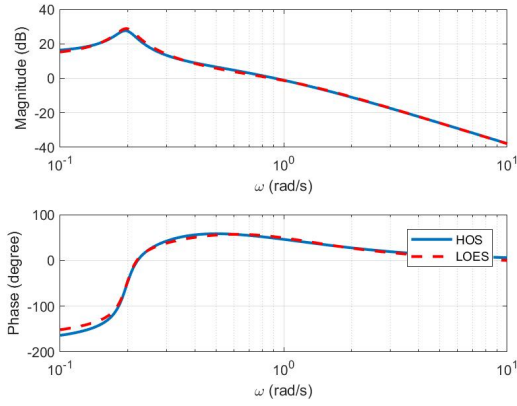
(e) M_q **x 2 Bode Plot**
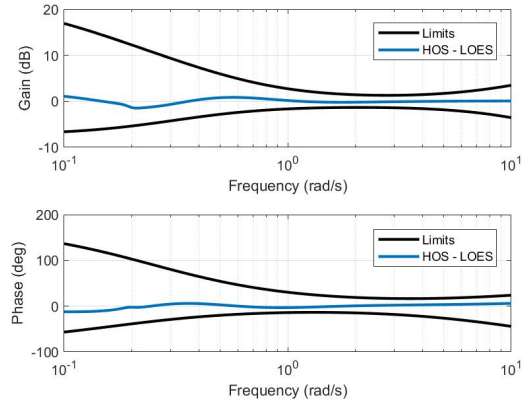
(f) M_q **x 2 Envelope Plot**
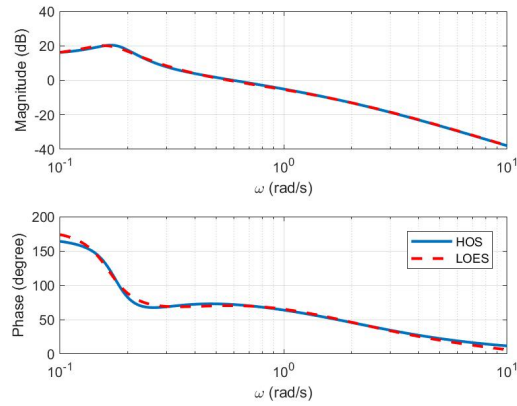
(g) M_q **x 4 Bode Plot**
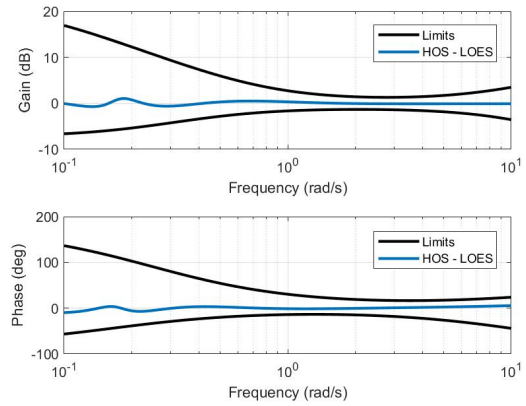
(h) M_q **x 4 Envelope Plot**
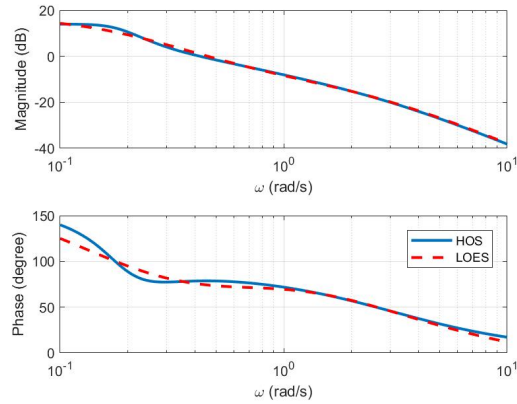
(i) M_q **x 6 Bode Plot**
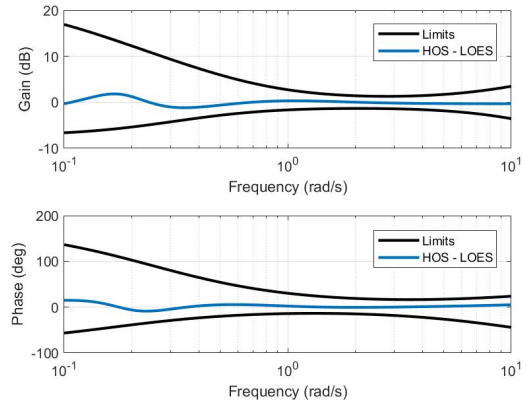
(j) M_q **x 6 Envelope Plot**

Figure 75. M_q **Scaling Bode Plots**
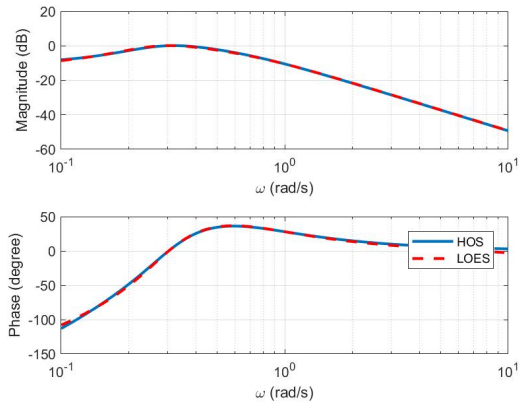
(a) M_{elev} **x 0.25 Bode Plot**
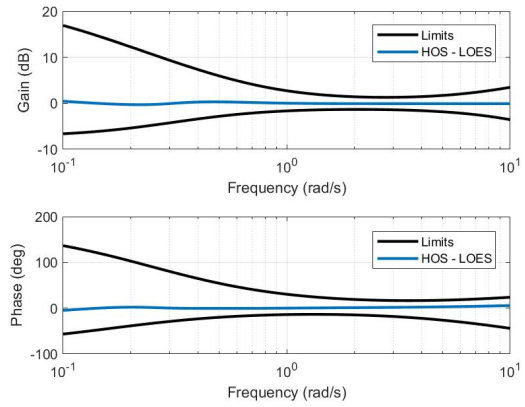
(b) M_{elev} **x 0.25 Envelope Plot**
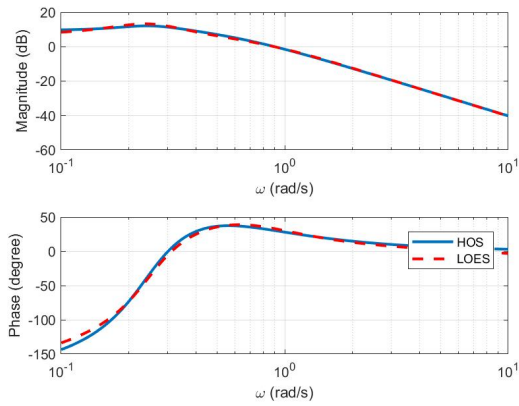
(c) M_{elev} **x 0.75 Bode Plot**
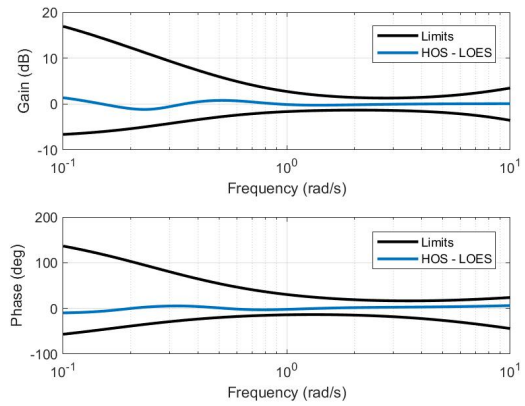
(d) M_{elev} **x 0.75 Envelope Plot**
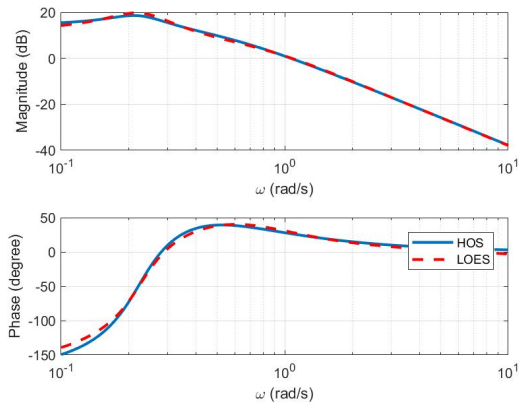
(e) M_{elev} **x 1 Bode Plot**
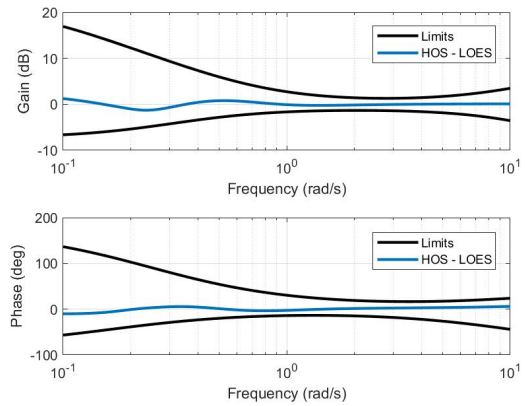
(f) M_{elev} **x 1 Envelope Plot**
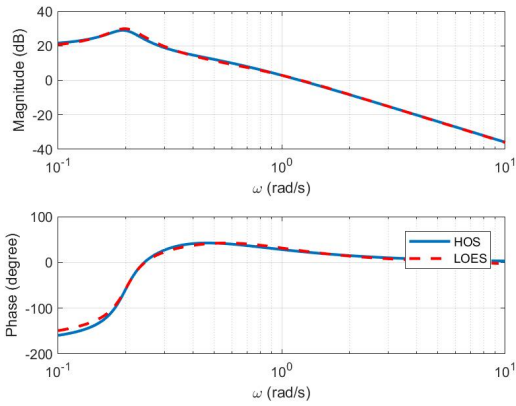
(g) M_{elev} **x 1.25 Bode Plot**
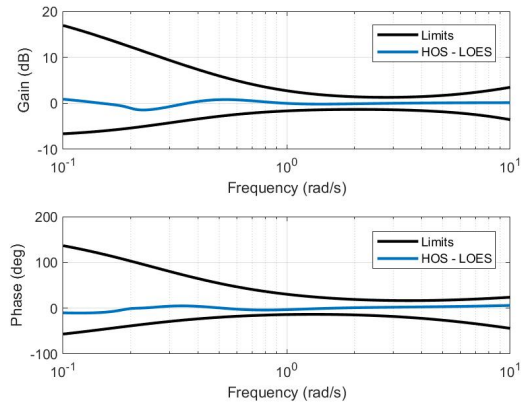
(h) M_{elev} **x 1.25 Envelope Plot**
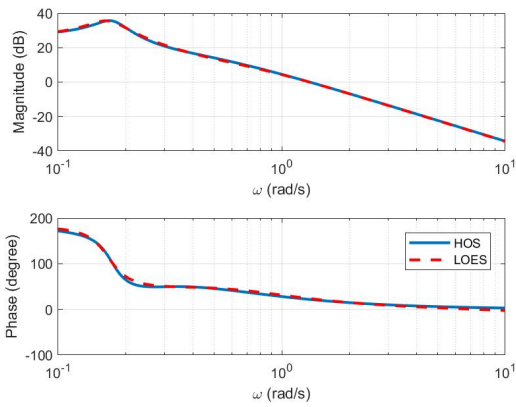
(i) M_{elev} **x 1.5 Bode Plot**
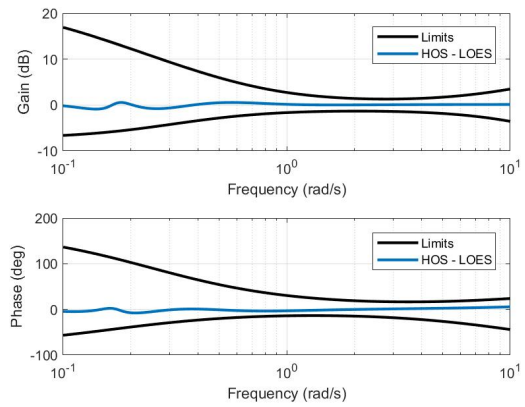
(j) M_{elev} **x 1.5 Envelope Plot**

Figure 76. M_{elev} **Scaling Bode Plots**
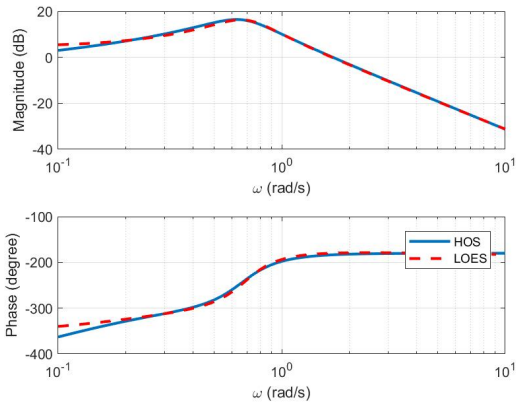
(a) L_p x 0.25 Bode Plot
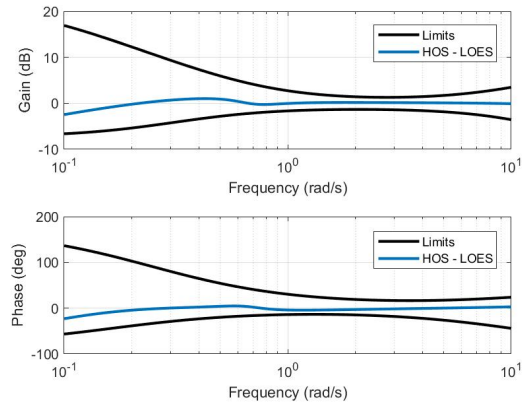
(b) L_p x 0.25 Envelope Plot
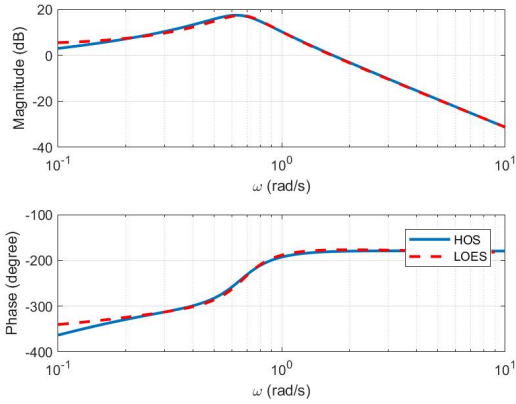
(c) L_p x 0.75 Bode Plot
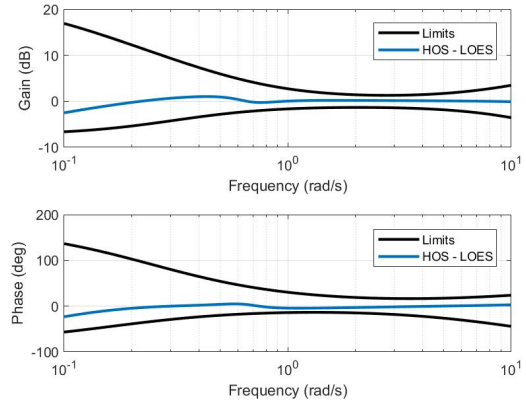
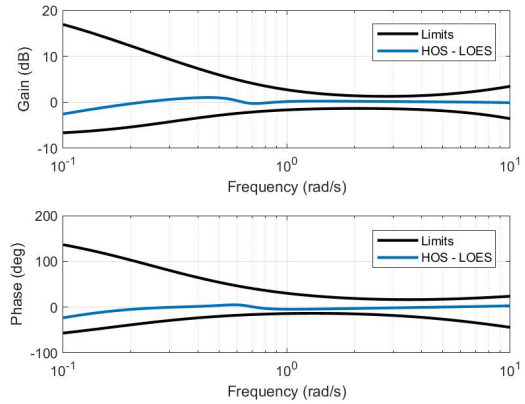(d) L_p x 0.75 Envelope Plot
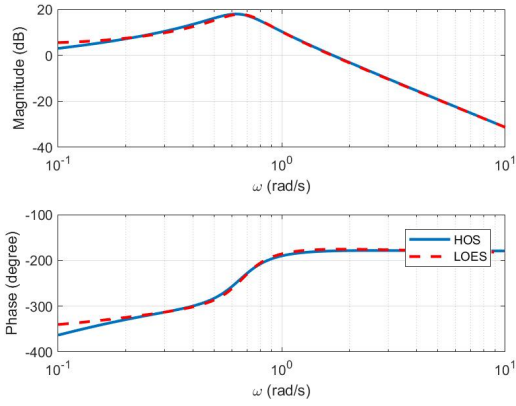
(e) L_p x 1 Bode Plot
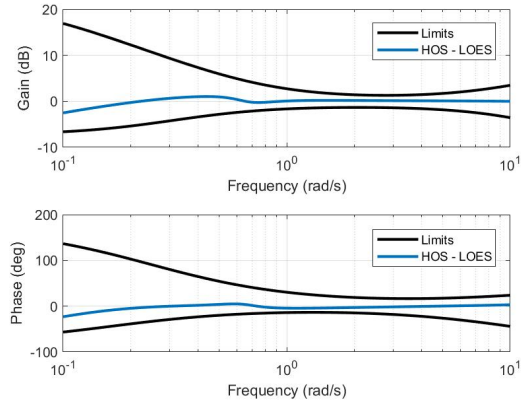
(f) L_p x 1 Envelope Plot
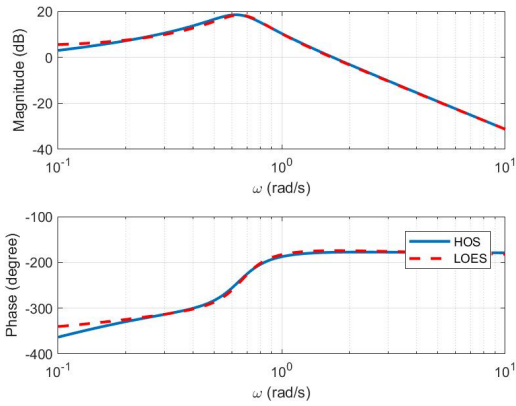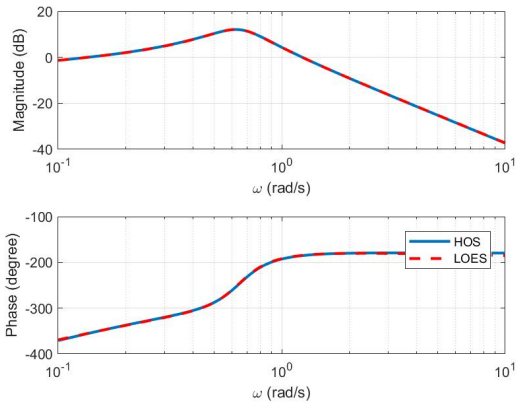
(g) L_p x 1.25 Bode Plot
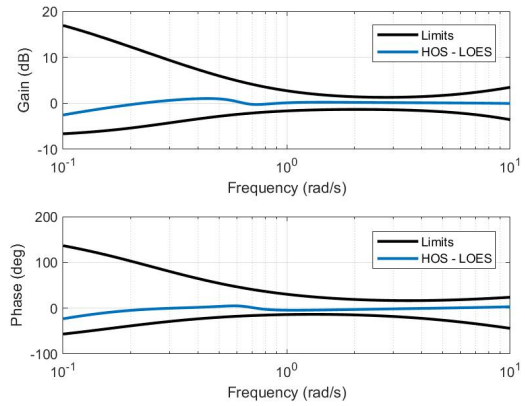
(h) L_p x 1.25 Envelope Plot
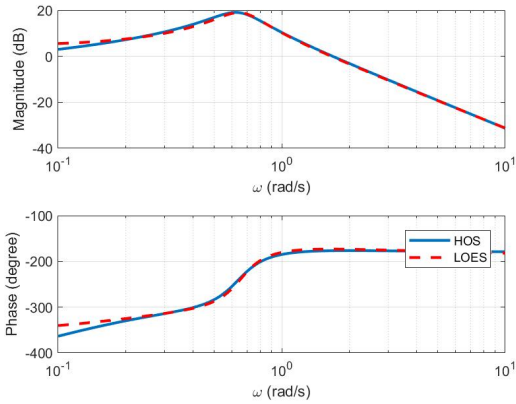
(i) L_p x 1.5 Bode Plot

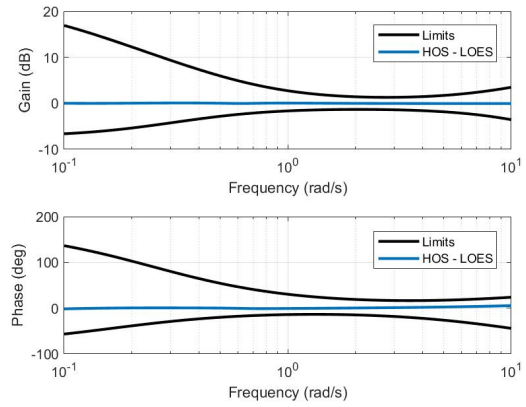(j) L_p x 1.5 Envelope Plot

Figure 77. L_p Scaling Bode Plots

(a) L_{ail} **x 0.5 Bode Plot**

(b) L_{ail} **x 0.5 Envelope Plot**
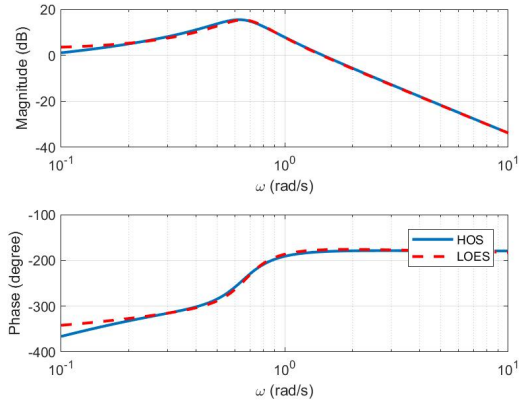
(c) L_{ail} **x 0.75 Bode Plot**
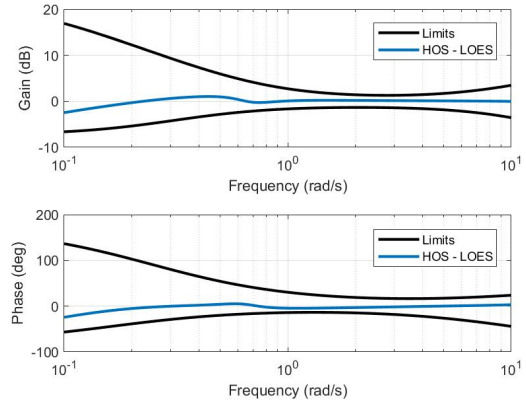
(d) L_{ail} **x 0.75 Envelope Plot**
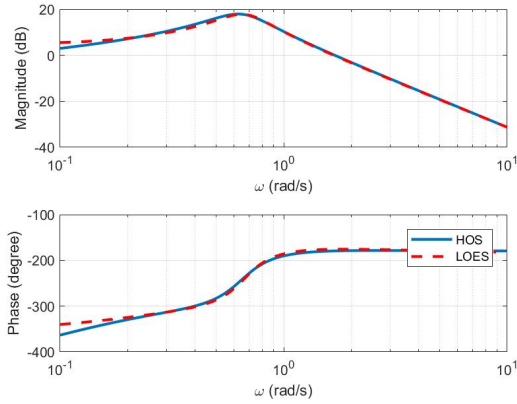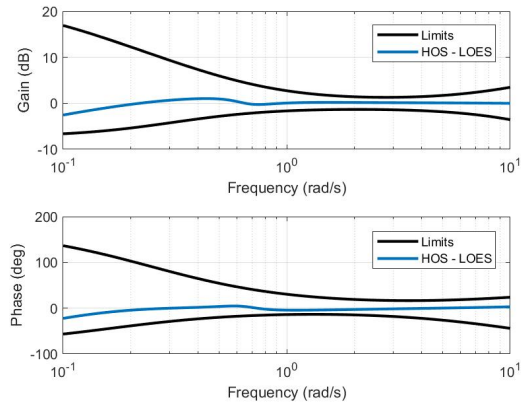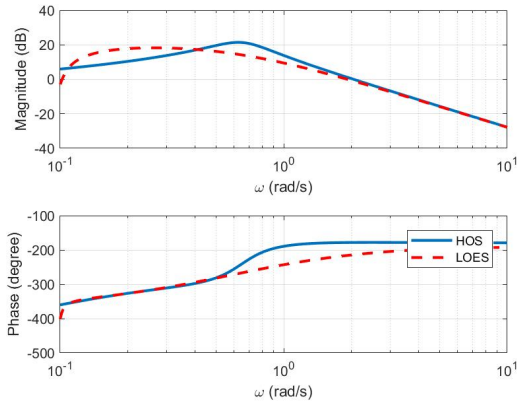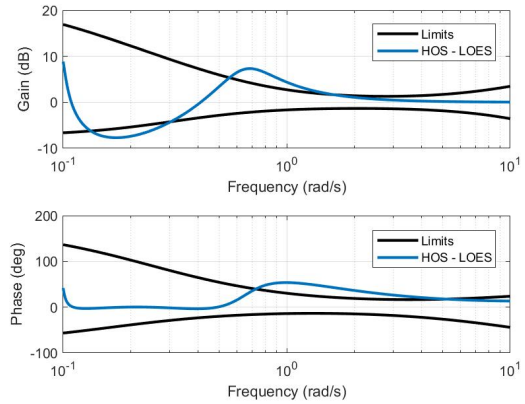
(e) L_{ail} x 1 Bode Plot
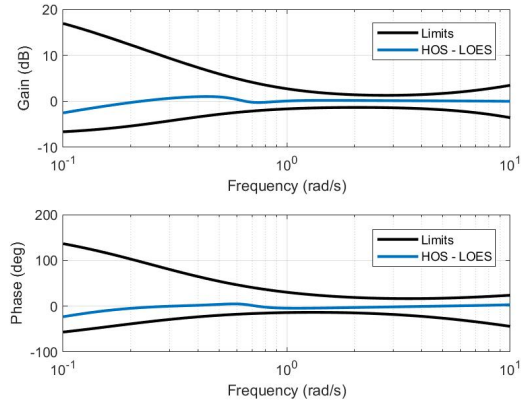
(f) L_{ail} x 1 Envelope Plot
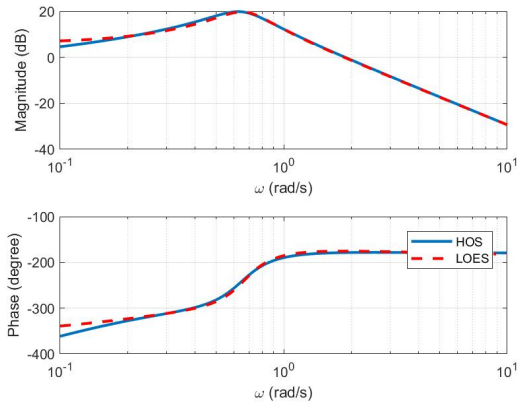
(g) L_{ail} x 1.25 Bode Plot

(h) L_{ail} x 1.25 Envelope Plot

(i) L_{ail} x 1.5 Bode Plot

(j) L_{ail} x 1.5 Envelope Plot

Figure 78. L_{ail} Scaling Bode Plots

Bibliography

1. "Stinson Reliant". *Wikipedia*, 1935. URL `https://en.wikipedia.org/wiki/Stinson_Reliant`.

2. *Flying Qualities of Piloted V/STOL Aircraft.* Technical Report MIL-F-83300, Department of Defense, 1970.

3. *Flying Qualities of Piloted Airplanes.* Technical Report MIL-F-8785C, Department of Defense, 1980.

4. *USAF Test Pilot School Flying Qualities Textbook.* Edwards AFB, California, 1986.

5. *Flying Qualities of Piloted Aircraft.* Interface Standard MIL-STD-1797A, NOTICE 1, Department of Defense, 1995.

6. "Lockheed NT-33A". *National Museum of the Air Force Fact Sheet*, 2016. URL `https://www.nationalmuseum.af.mil/Visit/Museum-Exhibits/Fact-Sheets/Display/Article/195773/lockheed-nt-33a/`.

7. Allen, James. *Advertisement and Specification for a Heavier-than-Air Flying Machine.* Washington D.C., 1907. URL `https://www.libraries.wright.edu/special/wrightbrothers/packet/signal`.

8. Berger, Tom, Mark Tischler, Steven G. Hagerott, M Christopher Cotting, William R. Gray, James Gresham, Justin George, Kyle Krogh, Alessandro D'Argenio, and Justin Howland. "Development and Validation of a Flight-Identified Full-Envelope Business Jet Simulation Model Using a Stitching Architecture". *AIAA Modeling and Simulation Technologies Conference*, 2017.

9. Bihrle, William. *A Handling Qualitites Theory for Precise Flight Path Control.* Air Force Flight Dynamics Laboratory, Wright Patterson AFB, Ohio, 1966.

10. Bilstein, Roger E. *Flight Patterns: Trends of Aeronautical Development In the United States, 1918-1929.* University of Georgia Press, Athens, GA, 2008.

11. Bischoff, D. E. *The Control Anticipation Parameter for Augmented Aircraft.* Technical Report NADC-81186-60, Naval Air Development Center, Warminster, PA, 1981.

12. Bryan, G. H. *Stability in Aviation.* MacMillan, London, 1911.

13. Caughey, David A. "Introduction to Aircraft Stability and Control". *Sibley School of Mechanical & Aerospace Engineering, Cornell University*, 2011. URL `https://courses.cit.cornell.edu/mae5070/Caughey_2011_04.pdf`.

14. Chalk, C. R. *Study for a Fighter Total In-Flight Simulator.* Calspan Flight Research Memorandum 566, 1982.

15. Clapper, J. R., J. J. Young, J. E. Grimes, S.C. Payton, S. Stackley, and D. Popps. "FY 2009-2034 Unmanned Systems Integrated Roadmap". *Department of Defense: Office of the Secretary of Defense Unmanned Systems Roadmap*, 92–93, 2009.

16. Cooper, G. E. and R. P. Harper. "The Use of Pilot Ratings in the Evaluation of Aircraft Handling Qualities". *Advisory Group for Aerospace Research and Development*, 1–56, 1969.

17. Cotting, M Christopher. *Evolution of Flying Qualities Analysis: Problems for a New Generation of Aircraft.* Dissertation, Virginia Polytechnic Institute and State University, 2010.

18. Cotting, M Christopher. "UAV Performance Rating Scale Based on the Cooper-Harper Piloted Rating Scale". *49th AIAA Aerospace Sciences Meeting including the New Horizons Forum and Aerospace Exposition*, 2011.

19. Daniel, Larry, Barry Baskett, Samuek Crews, and William Smith. *Aeronautical Design Standard Performance Specification Handling Qualities Requirements for Military Rotorcraft.* Technical Report ADS-33E, United States Army Aviation and Missile Command, Redstone Aresenal, Alabama, 2000.

20. Dorobantu, Andrei, Peter Seiler, and Gary Balas. "Validating Uncertain Aircraft Simulation Models using Flight Test Data". *AIAA Atmospheric Fligth Mechanics Conference*, 2013.

21. Ehrhard, Thomas P. "Air Force UAVs: The Secret History". *The Mitchell Institute for Airpower Studies*, 89, 2010.

22. Federal Aviation Administration. *Airworthiness Standards: Transport Category Airplanes*, volume 14 CFR § 2. FAA, 2018.

23. Greene, Kara M. *Toward a Flying Qualities Standard for Unmanned Aircraft.* Dissertation, Air Force Instidue of Technology, 2017.

24. Greene, Kara M and Donald L Kunz. "Quickness Criteria for Large Unmanned Aircraft in Non-Precision , Aggressive and Non-Aggressive Maneuvers". *AIAA Atmospheric Flight Mechanics Conference*, 2015.

25. Greene, Kara M., Donald L. Kunz, and M Christopher Cotting. "Toward a Flying Qualities Standard for Unmanned Aircraft". *AIAA Atmospheric Flight Mechanics Conference*, 2014.

26. Hamidani, Ali M. *Evaluating the Autonomous Flying Qualities of a Simulated Variable Stability Aircraft.* Thesis, Air Force Institute of Technology, 2017.

27. Hodgkinson, John. *Aircraft Handling Qualities.* Blackwell Science, Oxford, 1999.

28. Johansen, I. *Autopilot Design for Unmanned Aerial Vehicles.* Thesis, Norwegian University of Science and Technology, Norway, 2012.

29. Key, David L. *Generation of a Military Specification for Flying Qualities of Piloted V/STOL Aircraft.* Technical Report AFFDL-TR-71-23, Cornell Aeronautical Laboratory, 1971.

30. Kim, Joshua P. *Evaluation of Unmanned Aircraft Flying Qualities Using JSBSim.* Thesis, Air Force Institute of Technology, 2016.

31. Klyde, D. and D. Mitchell. *Handling Quality Demonstration Maneuvers for Fixed-Wing Aircraft.* Technical Report WL-TR-97-3100, Systems Technology, Inc., Oct 1997.

32. Leggett, David B. "Lecture Notes in Flying Qualities", July 2018.

33. Leone, Dario. "The Fighter Jet that can Fly as a Cargo Plane: the F-16 VISTA". *The Aviationist*, 2013. URL `https://theaviationist.com/2013/09/10/vista-f-16/`.

34. Mathworks. "Simulink Overview", 2018. URL `https://www.mathworks.com/products/simulink.html`.

35. McFarland, M. W. *The Papers of Wilbur and Orville Wright.* McGraw-Hill, New York, 1st edition, 1953.

36. Miller, T. "F-16 Vista". *Aviation Photo Digest*, 2015. URL `http://aviationphotodigest.com/history-is-made-at-edwards-afb`.

37. Mitchell, David G., David B. Doman, David L. Key, David H. Klyde, David B. Leggett, David J. Moorhouse, David H. Mason, David L. Raney, and David K.

Schmidt. "Evolution, Revolution, and Challenges of Handling Qualities". *Journal of Guidance, Control, and Dynamics*, 27:12–28, 2004.

38. National Research Council. *Review of NASA's Aerospace Technology Enterprise: An Assessment of NASA's Aeronautics Technology Programs*. National Academies Press, 2004.

39. Nielson, Michael. "Statistical Process Control". URL `http://www.statisticalprocesscontrol.info/glossary.html`.

40. Philips, W. Hewitt. *Journey in Aeronautical Research: A Career at NASA Langley Research Center*. NASA History Division of Policy and Plans and Office of Space Science, Washington, DC, 1998. URL `https://history.nasa.gov/monograph12/ch4.htm`.

41. Prosser, C.F. and C. D. Wiler. *RPV Flying Qualities Design Criteria*. Technical Report AFFDL-TR-76-125, Rockwell International Corporation, 1976.

42. Reisinger, Don. "Here's How Many Lives Drones Have Saved Since 2013". *Fortune*, 2017. URL `http://fortune.com/2017/03/14/drones-save-lives/`.

43. Sarno, K.J. and C.D. Wickens. "The role of multiple resources in predicting timesharing efficiency". *The International Journal of Aviation Psychology*, 107–130, 1995.

44. Soulé, H. A. *Preliminary Investigation of the Flying Qualities of Airplanes*. Technical Report NACA TR-700, National Advisory Committee for Aeronautics, Langley, VA, 1940.

45. Stevens, Brian L and Frank L Lewis. *Aircraft Control and Simulation*. John Wiley & Sons, Inc, Hoboken, New Jersey, 2nd edition, 2003.

46. Suckow, Elizabeth. "NACA Overview". *NASA History Program Office*, 2009. URL `https://history.nasa.gov/naca/overview.html`.

47. Theil, H. *Economic Forecasts and Policy*. North-Holland Publishing Company, 1970.

48. Trueman, C. N. "Aircraft and World War One". *The History Learning Site*, 2015. URL `https://www.historylearningsite.co.uk/world-war-one/aerial-warfare-and-world-war-one/aircraft-and-world-war-one/`.

49. Weiner, Robert and Tom Sherman. "Drones spare troops, have powerful impact". *San Diego Tribune*, 2014. URL `http://www.sandiegouniontribune.com/opinion/commentary/sdut-drones-troops-impact-2014oct09-story.html`.

50. Williams, Warren and Michael Harris. "The Challenges of Flight-Testing Unmanned Air Vehicles". *Systems Engineering, Test & Evaluation Conference*, 2002.

51. Winnefeld, J.a. and F. Kendall. "Unmanned Systems integrated roadmap: FY 2011-2036". *Department of Defense*, 1–74, 2010.

52. Yechout, Thomas R., Steven L. Morris, David E. Bossert, and Wayne F. Hallgren. *Introduction to Aircraft Flight Mechanics*. American Institute of Aeronautics and Astronautics, Reston, VA, 2003.

REPORT DOCUMENTATION PAGE

Form Approved
OMB No. 0704–0188

1. REPORT DATE *(DD–MM–YYYY)*	2. REPORT TYPE	3. DATES COVERED *(From — To)*
22–03–2019	Master's Thesis	Sept 2017 — Mar 2019

4. TITLE AND SUBTITLE

Evaluation of Unmanned Aircraft Flying Qualities
Using A Stitched Learjet Model

5a. CONTRACT NUMBER

5b. GRANT NUMBER

5c. PROGRAM ELEMENT NUMBER

6. AUTHOR(S)

Callaghan, Patrick M., Capt, USAF

5d. PROJECT NUMBER

5e. TASK NUMBER

5f. WORK UNIT NUMBER

7. PERFORMING ORGANIZATION NAME(S) AND ADDRESS(ES)

Air Force Institute of Technology
Graduate School of Engineering and Management (AFIT/EN)
2950 Hobson Way
WPAFB OH 45433-7765

8. PERFORMING ORGANIZATION REPORT NUMBER

AFIT-ENY-MS-19-M-206

9. SPONSORING / MONITORING AGENCY NAME(S) AND ADDRESS(ES)

Department of Aeronautics and Astronautics
2950 Hobson Way
WPAFB OH 45433-7765
DSN 271-0690, COMM 937-255-3636
Email: patrick.callaghan@afit.edu

10. SPONSOR/MONITOR'S ACRONYM(S)

AFRL/RQ

11. SPONSOR/MONITOR'S REPORT NUMBER(S)

12. DISTRIBUTION / AVAILABILITY STATEMENT

DISTRIBUTION STATEMENT A:
APPROVED FOR PUBLIC RELEASE; DISTRIBUTION UNLIMITED.

13. SUPPLEMENTARY NOTES

This material is declared a work of the U.S. Government and is not subject to copyright protection in the United States

14. ABSTRACT MIL-STD-1797 lists flying qualities for UAVs as TBD, and the standards for manned fixed wing are inadequate when applied to UAVs. In an effort to expand the database of UAV flying qualities, an analysis was completed on a Simulink model of an LJ-25D developed from Calspans Variable Stability System aircraft at the United States Test Pilot School. Three maneuvers were simulated: (1) a non-precision, non-aggressive climbing spiral, (2) a precision, non-aggressive side step landing, and (3) a precision, non-aggressive aerial refueling task. These maneuvers were chosen to evaluate the performance and workload of the aircraft as four stability and control parameters were scaled. The data were utilized in identifying trends between the scaled stability and control parameters and resulting workload and performance metrics. Thumbprint plots were generated to identify Level 1, Level 2, and Level 3 flying qualities and compared to MIL-STD-1797 plots. Results point to utilizing a combination of classical aircraft literal factors, such as ζ_{sp} and CAP, with newly developed mathematical techniques, such as L_2 norm and TIC, to assess the workload of the flight controller and performance during the maneuver.

15. SUBJECT TERMS

Flying Qualities, UAVs, Flight Dynamics Model, Maneuver Performance, Flight Control System, Workload, Theil's Inequality Coefficient

16. SECURITY CLASSIFICATION OF:			17. LIMITATION OF ABSTRACT	18. NUMBER OF PAGES	19a. NAME OF RESPONSIBLE PERSON
a. REPORT	b. ABSTRACT	c. THIS PAGE			Dr. D. Kunz, AFIT/ENY
U	U	U	UU	149	19b. TELEPHONE NUMBER *(include area code)* (937) 255-3636, x4547; donald.kunz@afit.edu

Standard Form 298 (Rev. 8–98)
Prescribed by ANSI Std. Z39.18